

SEVERE PLASTIC DEFORMATION OF
AGE HARDENABLE ALUMINUM ALLOYS

A THESIS SUBMITTED TO
THE GRADUATE SCHOOL OF NATURAL AND APPLIED SCIENCES
OF
MIDDLE EAST TECHNICAL UNIVERSITY

BY

EVREN TAN

IN PARTIAL FULFILLMENT OF THE REQUIREMENTS
FOR
THE DEGREE OF DOCTOR OF PHILOSOPHY
IN
METALLURGICAL AND MATERIALS ENGINEERING

SEPTEMBER 2012

Approval of the thesis:

SEVERE PLASTIC DEFORMATION OF AGE HARDENABLE ALUMINUM ALLOYS

submitted by **EVREN TAN** in partial fulfillment of the requirements for the degree of **Doctor of Philosophy in Metallurgical and Materials Engineering Department, Middle East Technical University** by,

Prof. Dr. Canan Özgen _____
Dean, Graduate School of **Natural and Applied Sciences**

Prof. Dr. Cemil Hakan Gür _____
Head of Department, **Metallurgical & Materials Engineering**

Prof. Dr. Bilgehan Ögel _____
Supervisor, **Metallurgical & Materials Eng. Dept., METU**

Prof. Dr. Cemil Hakan Gür _____
Co-Supervisor, **Metallurgical & Materials Eng. Dept., METU**

Examining Committee Members:

Prof. Dr. Tayfur Öztürk _____
Metallurgical & Materials Engineering Dept., METU

Prof. Dr. Bilgehan Ögel _____
Metallurgical & Materials Engineering Dept., METU

Prof. Dr. Rıza Gürbüz _____
Metallurgical & Materials Engineering Dept., METU

Prof. Dr. Haluk Darendeliler _____
Mechanical Engineering Dept., METU

Assist. Prof. Dr. Ziya Esen _____
Materials Science and Eng. Dept., Çankaya University

Date: _____ **14 / 09 / 2012**

I hereby declare that all information in this document has been obtained and presented in accordance with academic rules and ethical conduct. I also declare that, as required by these rules and conduct, I have fully cited and referenced all material and results that are not original to this work.

Name, Last name : Evren TAN

Signature :

ABSTRACT

SEVERE PLASTIC DEFORMATION OF AGE HARDENABLE ALUMINUM ALLOYS

Tan, Evren

Ph.D., Department of Metallurgical and Materials Engineering

Supervisor : Prof. Dr. Bilgehan Ögel

Co-Supervisor: Prof.Dr. Cemil Hakan Gür

September 2012, 130 pages

Industrial products of high-strength Al-alloys are currently manufactured by thermo-mechanical processes, which are only applicable in the integrated plants requiring high investment cost. Moreover, reduction of the average grain size not less than 10 μm and re-adjustment of process parameters for each alloy type is evaluated as disadvantage. Therefore, recently there have been many research studies for development of alternative manufacturing techniques for aluminum alloys. Research activities have shown that it is possible to improve the strength of Al-alloys remarkably by severe plastic deformation which results in ultra-fine grain size.

This study aims to design and manufacture the laboratory scale set-ups for severe plastic deformation of aluminum alloys, and to characterize the severely deformed samples. The stages of the study are summarized below:

First, for optimization of die design and investigation of parameters affecting the deformation finite element modeling simulations were performed. The effects of process parameters (die geometry, friction coefficient) and material properties (strain hardening, strain-rate sensitivity) were investigated.

Next, Equal Channel Angular Pressing (ECAP) system that can severely deform the rod shaped samples were designed and manufactured. The variations in the microstructure and mechanical properties of 2024 Al-alloy rods deformed by ECAP were investigated.

Finally, based on the experience gained, a Dissimilar Channel Angular Pressing (DCAP) system for severe plastic deformation of flat products was designed and manufactured; then, 6061 Al-alloy strips were deformed. By performing hardness and tension tests on the strips that were deformed by various passes, the capability of the DCAP set-up for production of ultra-fine grain sized high-strength aluminum flat samples were investigated.

Keywords: Severe Plastic Deformation, Equal Channel Angular Pressing (ECAP), Dissimilar Channel Angular Pressing (DCAP), Al-2024 and Al-6061 Alloys, Transmission Electron Microscopy

ÖZ

YAŞLANDIRILABİLİR ALÜMİNYUM ALAŞIMLARININ AŞIRI PLASTİK DEFORMASYONU

Tan, Evren

Doktora, Metalurji ve Malzeme Mühendisliği Bölümü

Tez Yöneticisi : Prof. Dr. Bilgehan Ögel

Ortak Tez Yöneticisi: Prof. Dr. Cemil Hakan Gür

Eylül 2012, 130 sayfa

Yüksek dayançlı alüminyum alaşımından mühendislik parçalarının üretimi, kapsamlı yatırım gerektiren büyük tesislerde termo-mekanik işlemlerle mümkün olmaktadır. Bu işlemlerin tane boyutunu ancak 10 mikrona kadar düşürebilmesi ve işlem parametrelerinin her alaşım için yeniden ayarlanma gerekliliği dezavantaj olarak değerlendirilmektedir. Bu nedenle, Al alaşımları için alternatif imalat tekniklerinin geliştirilmesi için son zamanlarda çok sayıda araştırma yapılmıştır. Çalışmalar, aşırı plastik deformasyon ile çok ince taneli iç yapı elde edilerek, Al-alaşımlarının mukavemetinde önemli artış sağlanabildiğini göstermiştir.

Bu çalışmanın konusu, alüminyum alaşımları için laboratuvar ölçekli aşırı plastik deformasyon sistemleri tasarlayıp imal etmek ve elde edilen numuneleri karakterize etmektir. Çalışmada gerçekleştirilenler aşağıda aşamalı olarak özetlenmiştir:

Önce, imal edilecek deformasyon düzeneklerinin tasarıma yardımcı olmak ve deformasyona etki eden faktörleri irdelemek için sonlu eleman analizi yöntemiyle modelleme çalışmaları yapılmıştır. İşlem parametrelerinin (kalıp geometrisi, sürtünme katsayısı) ve deforme edilen malzeme özelliklerinin (deformasyon pekleşmesi parametreleri/mekanizmaları ve deformasyon hızı hassasiyeti) işlem performansına etkileri incelenmiştir.

İkinci aşamada, çubuk şeklinde hacimli parçaları deforme eden Eş Kanallı Açısal Presleme (ECAP) sistemi tasarımı yapılarak imal edilmiştir. ECAP sistemi kullanılarak deforme edilen çeşitli alüminyum alaşımlarının mekanik özelliklerindeki ve mikroyapısındaki değişimler incelenmiştir.

Son aşamada, elde edilen tecrübeler ışığında, yassı mamulleri kesintisiz deforme edebilen Değişken Kanallı Açısal Presleme (DCAP) sistemi tasarımı yapılarak imal edilmiştir. Farklı sayıda pasodan geçirilen 6061 Al-alaşımı numunelere sertlik ve çekme deneyleri uygulanarak, DCAP paso sayısına bağlı olarak yüksek mukavemetli, ince taneli alüminyum levha üretilebilirliği incelenmiştir.

Anahtar Kelimeler: Aşırı Plastik Deformasyon, Eş Kanallı Açısal Presleme (ECAP), Değişken Kanallı Açısal Presleme (DCAP), Al-2024 ve Al-6061 alaşımları, Geçirim Elektron Mikroskopisi

*To TANs
&
THE ONES THAT SHARE A SECOND WITH ME*

ACKNOWLEDGEMENTS

I would like to express my sincere appreciation to Prof. Dr. Bilgehan Ögel for his supervision, patience, guidance throughout the study. I'm thankful to him for letting me to use his laboratory as a second home for over nine years.

I am sincerely grateful to Prof. Dr. C. Hakan Gür for his valuable guidance, patience, moral support and motivation. His leadership all through the years shared was very valuable in academic career point of view and in engineering perspective.

I wish to express my deepest thanks to Prof. Dr. Tayfur Öztürk for suggesting me this topic as a work area and let me use all the characterization devices available in the Department of Metallurgical and Materials Eng. with full rights.

I owe a debt to my parents, İbrahim and Sema Tan, and to my "little" sister Elvan Tan for their never-ending devotion, support and encouragements in my PhD journey and trust in me throughout the past 31 years. I must also send my sincere apologies for making them nervous in the final stages of this long journey.

I would like to express my pure love and respect to my love Güher Kotan, who is my friend, colleague, teacher, student, and my sweet hearted journey-mate. I am grateful to her and to any moment that have been shared together; which was inspiring and light emitting to the universe. We have grown together in the past few years and I feel very lucky to breath together with a soul like her.

I am grateful to my off-campus brothers and sisters: Ali Erdem Eken, Çağla Özgit Akgün, Deniz Keçik, Dr. Arda Çetin, Yankı Başaran Uzunçakmak, Göktürk Uzunçakmak, Fatih Gürçağ Şen, Alper Kınacı. Their motivation support from far-away places has encouraged me to finalize the thesis period.

Thanks to my dear friends Metehan Erdoğan, Emre Ergül, Dr. Volkan Kalem and Barış Akgün for sharing joy, laugh, sorrow, and worry at any time as well as at nights. Also thanks to Dr. Gülhan Çakmak, Irmak Sargın, Pelin Maradit Ergül, Berk Seçen, Başak Aysin, Ayşegül Afal, Şerif Kaya, Derya Kapusuz, Ebru Saraloğlu

Güler, Onur Bingöl, Tuba Demirtaş, A. Merve Genç, Serkan Yılmaz, Gül Çevik, Selen Gürbüz Güner, Tufan Güngören, Dr. Caner Şimşir, Dr. Tarık Aydoğmuş, and the other elders and young, I will not able to record all their names at the Department of Metallurgical and Materials Engineering, METU, for creating a warm working place.

I would like to thank Cengiz Tan, for his kind interest and fatherhood during my graduate education period. I would also thank to technical and administrative staff of Middle East Technical University, Department of Metallurgical and Materials Engineering.

This study covers one of the TUBITAK's national projects carried within the Dept of Metallurgical and Materials Eng. Some parts of the thesis are supported by the grand number 105M174. Simulation studies were carried out by Dr. Caner Şimşir and Dr. Pınar Karpuz. ECAP studies were established under the major responsibility of Ebru Saraloğlu. DCAP system construction and preliminary characterization had been completed with Göktürk Emre Uzunçakmak and first meaningful microstructural characterization was established with the collaboration of Alp Aykut Kibar. The other authors and MSc / PhD student contributors in Prof. Gür's research team are gratefully acknowledged. For me, this period of research would always been an unforgettable example of collaboration in an R&D study.

TABLE OF CONTENTS

ABSTRACT	iv
ÖZ	vi
ACKNOWLEDGEMENTS	ix
TABLE OF CONTENTS	xi
LIST OF TABLES	xiv
LIST OF FIGURES	xv
CHAPTERS	
1 INTRODUCTION	1
2 THEORY AND LITERATURE SURVEY	4
2.1. Aluminum Alloys.....	4
2.1.1. Alloys and Temper Designations	5
2.1.2. Strengthening in 2xxx & 6xxx	7
2.1.3. Precipitation Hardening Mechanisms	10
2.2. Thermo-mechanical Treatments.....	11
2.3. Severe Plastic Deformation.....	13
2.3.1. Strain Calculations in ECAP.....	21
2.3.2. Grain Refinement Mechanisms.....	25
2.3.3. Continuous Methods	27
2.3.4. DCAP System	29
3 EXPERIMENTAL PROCEDURE	33
3.1. Simulation Studies (Finite Element Analysis)	33
3.1.1. Simulation of Equal Channel Angular Pressing (ECAP).....	33
3.1.2. 3-Dimensional Analysis Method	36
3.1.3. Investigation of the Effect of Materials' Property	36
3.2. Equal Channel Angular Pressing (ECAP) System.....	38
3.2.1. System Design and Modernization	38
3.2.2. Material and Heat Treatment	40

3.2.3. Sample Characterization	41
3.2.3.1. Mechanical Characterization.....	41
3.2.3.2. X-Ray Diffraction Analysis	41
3.2.3.3. Microstructural Characterization	42
3.3. Dissimilar Channel Angular Pressing (DCAP) System	42
3.3.1. Continuous Deformation System Analysis	43
3.3.2. DCAP System Manufacturing and Revisions	44
3.3.3. Material and Heat Treatment	46
3.3.4. Sample Characterization	47
3.3.4.1. Mechanical Characterization.....	47
3.3.4.2. X-Ray Diffraction Analysis	47
3.3.4.3. Microstructural Characterization	48
3.3.4.4. Other Characterization Methods	49
4 RESULTS AND DISCUSSION	51
4.1. Finite Element Modeling of ECAP	51
4.1.1. Effect of Die Geometry	51
4.1.2. Effect of Friction	54
4.1.3. Comparison of 3D Analysis	57
4.1.4. Effect of Material Property and Corner Gap Formation Mechanism	59
4.1.5. Verification of FEM via experimental tests	62
4.2. Equal Channel Angular Pressing (ECAP) System.....	65
4.2.1. Improvement in Mechanical Properties	65
4.2.2. X-ray Diffraction Analysis of ECAPed Al-2024.....	67
4.2.3. Microstructural Investigations	69
4.2.3.1. Optical Microscopy and Scanning Electron Microscopy Investigations	69
4.2.3.2. Transmission Electron Microscope Observations.....	71
4.3. Dissimilar Channel Angular Pressing (DCAP) System	75
4.3.1. Effect of DCAP process on Mechanical Performance of Alloy	76
4.3.2. Results of X-ray Diffraction Analysis.....	81
4.3.3. Microstructural Investigations	87
4.3.3.1. Macro and Mezzo-Scale Investigations	87

4.3.3.2. Transmission Electron Microscopy Analysis	89
4.3.3.3. EBSD Analysis	102
4.3.4. Effect of DCAP on Defect Related Properties	110
4.3.4.1. Ultrasonic Sound Velocity	110
4.3.4.2. Electrical Conductivity	111
5 CONCLUSION	113
5.1. Finite Element Modelling	113
5.2. Equal Channel Angular Pressing (ECAP) System.....	114
5.3. Dissimilar Channel Angular Pressing (DCAP) of AA 6061 Sheet.....	114
6 FUTURE DIRECTIONS	116
REFERENCES.....	121
VITA	127

LIST OF TABLES

TABLES

Table 2.1 Crystal structure of phases formed during precipitation of 2xxx & 6xxx ...	8
Table 2.2 Coherency of phases formed during aging of 6000 series aluminum alloys	9
Table 2.3 Effect of ECAP processing parameters for a system with sharp corners...	24
Table 2.4 Dissimilar Channel Angular Pressing studies in literature	31
Table 3.1 Chemical composition of samples used in ECAP deformation and composition of standard AA-2024 alloy.....	40
Table 3.2 Chemical composition of samples used in DCAP deformation and composition of standard AA-6061 alloy.....	46
Table 4.1 EDS analysis for inclusions distributed in solutionized AA-2024 matrix	71
Table 4.2 Chemical composition of rod shaped phases	72
Table 4.3 Strain values imparted to specimen for each DCAP pass.....	76
Table 4.4 Variation of XRD peak intensity and broadening with DCAP processing	84
Table 4.5 Size-strain values for DCAPed AA-6061 sheet processed with different pass number and route calculated for <111>	87

LIST OF FIGURES

FIGURES

Figure 2.1 Principle aluminum alloys [3]	5
Figure 2.2 Aluminum temper designations chart [5]	7
Figure 2.3 Particle – dislocation interactions (a)Orowan looping, (b)particle cutting [10].....	10
Figure 2.4 Role of major hardening mechanisms during age hardening [11].....	11
Figure 2.5 Grain refining via thermomechanical treatment [13]	12
Figure 2.6 Principal illustration of the ECA pressing process	14
Figure 2.7 Fundamental processing routes in ECAP [25]. Also material rotation angles during re-feeding are given	16
Figure 2.8 TEM image of Al 6061 alloy after ECAP process a)1 pass, b)4 passes c)stress-strain curve after ECAP [40]	18
Figure 2.9 Change of hardness via ECAP deformation of AA-6061 [41].....	18
Figure 2.10 Comparison of engineering stress-engineering strain curves for the T6 treated commercial 6061 Al alloy and the ECAP processed 6061 aluminum alloy (4pass) with and without a low temperature aging treatment [41].....	19
Figure 2.11 The effect of ECAP process on mechanical properties of various aluminum alloys [34]	20
Figure 2.12 Variation of grain size with respect to annealing temperature [34].....	20
Figure 2.13 Schematical drawing of deformation in 2D	21
Figure 2.14 Schematical drawing of shear in ECAP	22
Figure 2.15 Velocity hodograph of ECAP deformation	23
Figure 2.16 The principle of shearing in the sample during ECAP	26
Figure 2.17 Schematic model of dislocation evolution at different stages during ECAP (a)initial cellular structure (subgrains) containing many dislocations; (b)cell experiencing partial annihilation of dislocations at the boundaries; (c) granular structure achieved with high angle boundaries. [46]	26
Figure 2.18 Schematic illustration of microstructural evolution during severe plastic deformation. (a)Homogeneous distribution of dislocations, (b)elongated cell formation, (c)dislocations blocked by subgrain boundaries, (d)break up of elongated subgrains and (e)reorientation of subgrain boundaries and formation of ultrafine grain size.	27
Figure 2.19 Adapted severe plastic deformation methods for continuous production (a) ECAP-Conform [49] (b) Conshearing [50] (c) DCAP [51]... ..	28
Figure 2.20 Schematic drawing of the deformation die system for repetitive deformation (a)General mechanism, (b) Die details.....	29
Figure 2.21 Microstructure condition of Al-1050 alloy after DCAP [53] (a)An optical micrograph showing the shear deformation patterns (b)Grain structure from region B (before DCAP) (c)Grain structure from region C	

(after DCAP) (d)TEM bright field image and a SAD pattern (formation of the cell structures after DCAP) (e)SEM micrograph showing the direction of the slip bands	30
Figure 3.1 Schematic view of ECAP system	34
Figure 3.2 Typical workpiece behavior during ECAP deformation	36
Figure 3.3 First system a) 30 ton vertical axis press, b) ECAP die (14x14mm square cross-section, 120°), c) a selected sample deformed AA-6066.....	38
Figure 3.4 a) Horizontal axis press, b,c,d) ECAP dies (14x14mm square cross-section, 120°; Ø =18mm circular cross-section, double 120°; Ø =18mm circular cross-section, 120°)	39
Figure 3.5 Schematic specimen order in the die	40
Figure 3.6 DCAP system design for continuous production	43
Figure 3.7 (a) Sample feeding in DCAP, (b) Sample exit with 5% reduction by inlet channel, (c) Sample exit with 20% reduction by inlet channel	44
Figure 3.8 DCAP system (a) first machine (b) final design.....	45
Figure 3.9 Manufacturing stages (a) channeled roller (b) patterned roller (c) semi-patterned roller	46
Figure 3.10 Ultrasonic sound velocity measurement setup	49
Figure 4.1 Plastic strain distribution for a frictionless simulation and corner gap formation. [65]	53
Figure 4.2 Effect of die geometry on the deformation homogeneity in the vertical section of workpiece (a) $\Phi = 90^\circ$, (b) $\Phi = 120^\circ$ [65].....	54
Figure 4.3 Equivalent strain distribution for different friction conditions: (a) $\mu=0$, (b) 0.050, (c) 0.100, (d) 0.150 [65]	56
Figure 4.4 The equivalent strain distribution at the vertical cross-section for 90° die with different friction levels [65]	57
Figure 4.5 Equivalent plastic strain distribution in the workpiece during ECAP process [65].....	58
Figure 4.6 Comparison of 2D and 3D analysis in terms of equivalent plastic strain distribution along central plane [65]	58
Figure 4.7 Equivalent plastic strain rate distribution during ECAP [65].....	60
Figure 4.8 Velocity distribution during ECAP process [65].....	61
Figure 4.9 Variation of corner gap angle (α) with strain hardening multiplier (K) and exponent (n) [65].....	62
Figure 4.10 Change in the meshing structure during single pass ECAP deformation of Al-alloy in a 90° die system (a) before deformation, (b) experimental results, (c) simulation result	63
Figure 4.11 Hardness distribution along vertical cross-section after ECAP: experimental and simulation results	64
Figure 4.12 Hardness of AA-2024 alloy in different conditions	65
Figure 4.13 Variation of 2024 Al-alloy hardness with aging time	67
Figure 4.14 Effect of processing steps on the characteristic xray peak for (111) plane of Al-2024 alloy	68
Figure 4.15 X-ray diffraction analysis for the (111) peaks of annealed and ECAPed samples.....	69
Figure 4.16 Optical micrograph of solutionized 2024 Al-alloy sample	70
Figure 4.17 SEM micrograph of solutionized 2024 Al-alloy sample	70
Figure 4.18 AA-2024 samples in the solutionized condition.....	72

Figure 4.19 ECAPed AA-2024 samples (a) BF image, (b) DF image.....	73
Figure 4.20 Dislocation arrangements in ECAPed Al-2024 alloy.....	73
Figure 4.21 Post-ECAP annealed AA-2024 samples.....	74
Figure 4.22 TEM BF of AA-2024 (a) aged at 190°C, (b) one pass ECAPed and aged at 190°C.....	75
Figure 4.23 FEM analysis of strain variation on strip surface during DCAP processing	77
Figure 4.24 Variation of sample hardness with DCAP passes number and accumulative strain (0 pass corresponds to annealed condition).....	78
Figure 4.25 Improvement in the strength of AA-6061 sheets via DCAP processing	79
Figure 4.26 Strengthening behavior of AA-6061 sheets via DCAP processing (a) along LD, (b) along TD	80
Figure 4.27 XRD patterns of AA-6061 sheet DCAPed along LD after annealing....	83
Figure 4.28 XRD patterns of AA-6061 sheet DCAPed along TD after annealing....	83
Figure 4.29 Williamson-Hall plots for DCAPed Al-6061 sheet processed with different pass number (a) DCAPed along LD (b) DCAPed along TD	86
Figure 4.30 Macro-scale observation of the 250µm thick AA 6061 sample in (a)annealed condition, (b) 5 pass DCAPed condition.....	88
Figure 4.31 Optical micrographs of AA-6061 sheet in (a)annealed condition, (b) 5 pass DCAPed condition	88
Figure 4.32 Secondary electron image of annealed AA-6061	89
Figure 4.33 Bright field TEM images of annealed AA-6061 sheet	90
Figure 4.34 Intermetallic particles observed in (a) annealed AA 6061 sheet, (b) 5 pass DCAPed sheet.....	91
Figure 4.35 EDS analysis of the intermetallic phase under TEM.....	92
Figure 4.36 TEM micrograph of annealed AA-6061 sheet containing β precipitates	93
Figure 4.37 TEM micrograph of 5 pass DCAPed AA-6061 sheet containing β precipitates (a)bright field image, (b) selected area diffraction pattern (SA=100µm), (c-d) dark field images from the selected spots of 1 & 2 respectively	93
Figure 4.38 TEM images of AA-6061 sheets after 2-pass LD-DCAP (a) as-deformed, (b) annealed at 200°C, (c) annealed at 350°C [].....	95
Figure 4.39 TEM micrographs of AA-6061 sheets annealed at 350°C after (a) single pass LD-DCAP, (b) 2-pass LD-DCAP, (c) 5-pass LD-DCAP [77]....	95
Figure 4.40 Boundary evolution during DCAP of AA-6061 sheets (a) single pass LD-DCAP, (b) 2-pass LD-DCAP, (c) 5-pass LD-DCAP [77]	96
Figure 4.41 TEM micrograph of 5 pass TD-DCAPed AA-6061 sheet (a) Bright field image, (b) SADP, (c) Dark field image	97
Figure 4.42 Boundaries of 5-pass TD-DCAPed AA-6061 aluminum alloy	98
Figure 4.43 Dislocation arrangements in five pass TD-DCAPed AA-6061 sheet (a) ordered structure, (b) zigzag type arrangement when tilt γ was increased 2°, (c) PWD type boundary observation when tilt γ was increased 4°	99
Figure 4.44 Dislocation alignment in the form of zigzag, composing PDW type boundaries within AA-6061 sheet (a) single pass TD-DCAPed, (b) five pass TD-DCAPed	100

Figure 4.45 Effect of DCAP on microstructure and SADP (a-b) Annealed 6061, (c-d) 5 DCAPed AA-6061 (selected area region was also shown “aperture size:20 μm ”).....	101
Figure 4.46 Image Quality Maps for annealed AA-6061 sheet	103
Figure 4.47 Inverse Pole Figure maps for annealed AA-6061 sheet (a) 200x200 μm area with step size 0.65 μm , (b) 45x45 μm area with step size 0.2 μm	104
Figure 4.48 Image Quality Maps for 5 pass DCAPed AA-6061 sheet	105
Figure 4.49 Inverse Pole Figure maps for 5 pass DCAPed AA-6061 sheet (a) 200x200 μm area with step size 0.65 μm , (b) 45x45 μm area with step size 0.2 μm	107
Figure 4.50 Grain boundary maps (0.65 μm scan step) (a) Annealed AA-6061 sheet, (b) 5 pass DCAPed AA-6061 sheet.....	108
Figure 4.51 Grain boundary map of 5 pass DCAPed AA-6061 sheet (0.2 μm scan step).....	109
Figure 4.52 Grain orientations (a-b) pole figure and inverse pole figure of annealed AA-6061 sheet, (c-d) pole figure and inverse pole figure of 5 pass DCAPed AA-6061 sheet.....	110
Figure 4.53 Effect of DCAP on four point electrical resistivity of AA-6061 sheets.....	112
Figure 6.1 High resolution electron image of 5 pass DCAPed AA-6061 sheet.....	118
Figure 6.2 HREM investigation of annealed AA-6061 sheet (a) HREM image of annealed single grain, (b) FFT of grain, (c) filtered FFT, (d) Inverse FFT image (single crystal orientation was observed).....	118
Figure 6.3 HREM investigation of 5 pass DCAPed AA-6061 sheet (a) HREM image of DCAPed single grain, (b) FFT of grain, (c) filtered FFT, (d) Inverse FFT image of c (cubic crystal probably (141)), (e) second filtered FFT, (f) Inverse FFT image of e (tetragonal crystal).....	119

CHAPTER 1

INTRODUCTION

Aluminum and its alloys are very popular among the industrial and scientific applications. Especially when deformed, high ductility, excellent corrosion resistance, ease of machining and its light weight make them attractive for such applications in automotive and aeronautics.

The production procedure of aluminum and its alloys in integrated facilities (i.e. Seydişehir) or thin casting facilities (i.e. ASSAN) usually starts with casting. In integrated facilities; the procedure continues with hot and cold deformation and in thin casting facilities only cold deformation is applied. If required; heat treatment might be the final step.

The production of high strength aluminum alloys (6xxx, 2xxx, 7xxx) is possible in integrated facilities only; due to high degree of hot deformation requirements. It is obligatory to establish the hot deformation step in a controlled program. These thermo-mechanical treatments are very important in terms of final grain size obtained and determination of post aging procedures for required mechanical performance.

In this respect, Turkey is incapable of producing high strength aluminum alloy in sheet form. Although Seydişehir is the most available plant for its integrated structure; due to its lack of capacity, 2xxx, 6xxx, 7xxx type sheets cannot be produced. Severe plastic deformation (SPD) appears to be an alternative way to the conventional technology discussed above. This new technology has the potential of high strength aluminum sheet production in thin casting and small scale companies.

SPD methods are of great interest in industrial forming applications, as they give rise to significant refinement in microstructures and improvements in mechanical and physical properties. In the “Equal Channel Angular Pressing (ECAP)”, which is the most common method for production of ultrafine grained bulk samples, very high plastic strains are introduced into the bulk material without any change in cross section.

ECAP has a story back to 1980s. Commercialization of ECAP based ultrafine grain sized materials was the consequence of the enormous study activity in the last 10-15 years. From aluminum to titanium, magnesium to steels, wide range of metals and alloys were sacrificial materials of ECAP trials. The handicap of ECAP system is its inconvenience for continuous deformation of aluminum alloy sheets which are widely used as structural components. This necessitates industrially applicable continuous severe plastic deformation methods.

Dissimilar channel angular pressing (DCAP) is one of the promising techniques used for sheet or strip deformation. In this process, the workpiece is fed into the die by using a feeding roll. The forming die has been composed of two intersecting channels, whose thicknesses are different from each other in a way that the thickness of the inlet channel is slightly smaller than that of the outlet channel. Such a die configuration enables the multi-pass operation to take place in a continuous manner.

The aim of this study is to establish a background for the development of a new technology for the production of high strength aluminum alloy semi-products (sheets) in small scale companies with a cost effective, simpler method resulting higher mechanical performance. Various setups were designed and produced for severe plastic deformation of bulk rod shaped Al 2024 and Al6061 sheets. On the onset of designing; finite element simulations were performed and used for the critical decisions of the die systems. Finally, materials produced were characterized in terms of mechanical performance development and microstructure evolution.

The following chapter, theory and literature review, were written to introduce severe plastic deformation with its types and mechanisms to remind key points about the topic. Preceding chapters, starting with experimental procedure were recorded to

bound the method and its outcomes. The results chapter was divided into three subsections as finite element analysis, bulk SPD deformation (ECAP) of 2024Al rods and continuous SPD deformation (DCAP) of 6061Al sheets. Hardness and tensile test data obtained for different deformation and artificial aging routes were visually presented via graphs and also microstructural development was examined via high resolution electron microscopy. The challenging results and improvement were discussed with use of the physical metallurgy tools in terms of strengthening mechanisms. Finally, in the last chapter, namely Future Directions, the questions about stability of the high mechanical performance and fine grain structure were directed to the following researcher as a grain boundary engineer.

CHAPTER 2

THEORY AND LITERATURE SURVEY

The development of civilization is closely linked with that of metals. Among the common metals, aluminum now cedes first place only to steel. If measured by volume rather than weight, it now exceeds in quantity all other non-ferrous metals combined, including copper and its alloys, lead, tin and zinc. Because of its unique properties, from the beginning aluminum has competed with and replaced much older, established materials, such as wood, copper and steel. Aluminum has won this position even though its industrial production began only in the late 19th century; therefore, it is a latecomer among common metals [1].

2.1. Aluminum Alloys

Today more than half of the semi-finished production is delivered in alloys, most of the remainder in commercial purity aluminum with only a small quantity of super-purity aluminum being produced [1].

When the alloying element additions to the aluminum are concerned; none of them is found to be completely miscible with aluminum in the solid state. Of all elements, zinc has the greatest solid solubility with 66.4 at%. In addition to zinc, silver, magnesium and lithium are the three elements that have solid solubilities greater than 10 at%. Following this four; gallium, germanium, copper and silicon formed the group that has maximum solubilities of less than 10 but greater than 1 at%. All other elements are less soluble [2].

Copper, magnesium, manganese, silicon and zinc are the alloying additions commonly present in commercial aluminum alloys to provide increased strength – particularly when coupled with strain hardening by cold working or with heat treatment, or both. Figure 2.1 shows the various combinations of these elements added to form the principle aluminum alloys [3].

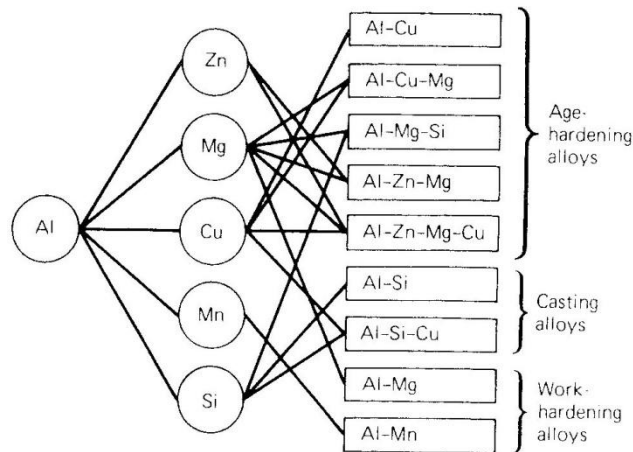


Figure 2.1 Principle aluminum alloys [3]

When the content of an alloying element exceeds the solubility limit, the alloying element produces second-phase microstructural constituents that may consist of either the pure alloying ingredient or an intermetallic compound phase. In the first group are silicon, tin and beryllium. Manganese and chromium are included in the other group.

2.1.1. Alloys and Temper Designations

The production of semifabricated products utilizes three different types of aluminum, namely super purity, commercial purity and alloys. Alloys are used for producing castings or fabricating wrought products. The alloys used for casting contain a greater amount of alloying additions than those used for wrought products. The

addition of alloying elements has the effect of strengthening the wrought alloys and improving the castability of the casting alloys [1].

Hence, it is convenient to divide aluminum alloys into two major categories: casting compositions and wrought compositions. A further differentiation for each category is based on the primary mechanism of the property development. Cast and wrought alloy nomenclatures have been developed by Aluminum Association which is the most widely recognized one [3].

Wrought alloy compositions with a wide variety of strengths and other properties related to the alloying element content. The properties of wrought alloys can be described by adopting two basic classes: non-heat treatable alloys and heat treatable alloys. Non-heat treatable alloys include all the various grades of pure aluminum and all those other alloys in which the strength is developed largely by strain hardening from the basic annealed temper. They are in the 1xxx, 3xxx, 4xxx and 5xxx series. Heat treatable alloys are those containing appreciable amounts of the elements that are soluble in solid aluminum. They are soluble in aluminum in considerable amounts at elevated temperatures, but to a much smaller degree at room temperature. This characteristic renders these alloys susceptible to heat treatment. They are designated in the 2xxx, 6xxx and 7xxx series [2].

Since wrought alloy products are offered for sale in a variety of conditions that determine strength and other characteristics; a uniform system of temper designations is a necessity. The three basic temper designations are “O” for “annealed”, “T” for “heat treated (i.e. for age hardening alloys)” and “H” for “strain hardened (i.e. for non age hardening alloys)” Temper designations tabulated in handbooks [1,4,5] are schematically summarized in Figure 2.2.

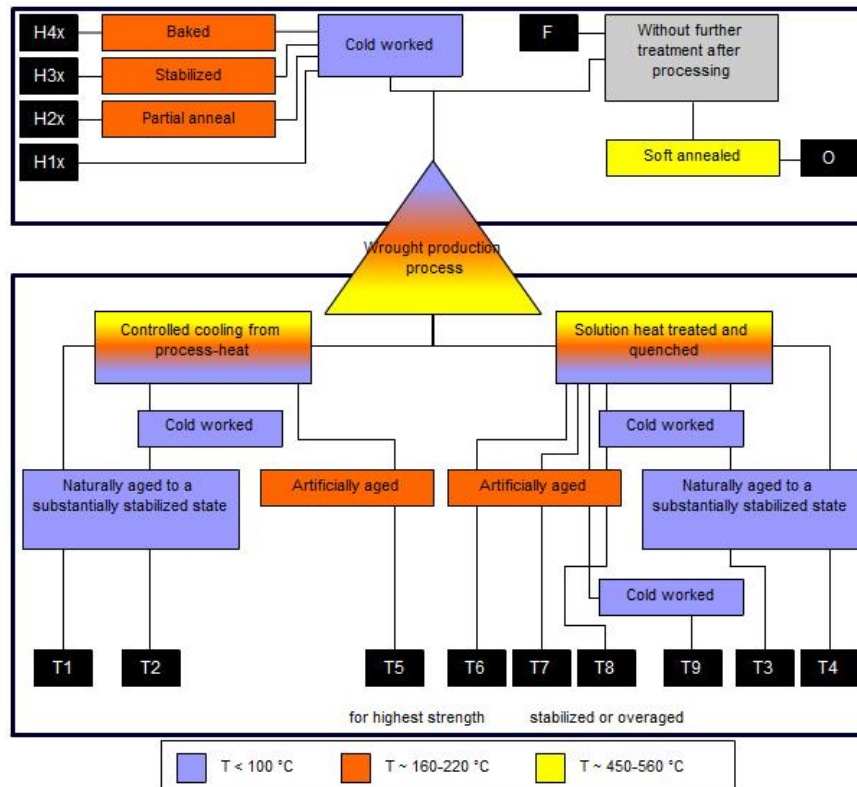


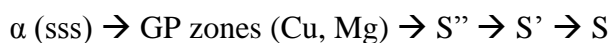
Figure 2.2 Aluminum temper designations chart [5]

2.1.2. Strengthening in 2xxx & 6xxx

2xxx series aluminum alloys, containing copper as the major alloying element, are age hardened by formation of stable and metastable modifications of θ (CuAl_2) phase. Each phase has different structure, shape and coherency with matrix that changes the properties of the alloy. The sequence starts with α (sss), the super saturated solid solution formed after quenching. The following part of the sequence can be roughly divided into following steps:



In the case of AA2024 where Mg is the second alloying addition, S (Al_2CuMg) phase and its metastable variations would form the aging sequence as:



6xxx series aluminum alloys, containing magnesium and silicon as the major elements, are strengthened by precipitation of metastable precursors of the equilibrium β (Mg_2Si) phase. It is generally agreed that; the precipitation process in Al-Mg-Si alloys can be roughly divided into:



For the case of AA6061, Cu-containing precipitates such as θ and Q have also been observed in the precipitation sequence of 6xxx aluminum alloys. The sequence for this case has been suggested by Chacrabarti et. al. [6]:



where Q ($Al_4Cu_2Mg_8Si_7$), β (Mg_2Si) and θ (Al_2Cu)

The crystal structure of these numerous phases were tabulated in Table 2.1[7].

Table 2.1 Crystal structure of phases formed during precipitation of 2xxx & 6xxx

Alloy	Phase	Crystal Structure
2xxx	θ''	Monoclinic
	θ'	Tetragonal a=b=0.404nm c=0.580nm
	θ (Al_2Cu)	Body centered tetragonal a=b=0.607nm c=0.487nm
	S (Al_2CuMg)	Orthorhombic a=0.400nm b=0.925nm c=0.714nm
6xxx	β''	Monoclinic
	β'	Hexagonal a=0.705 nm c=0.405 nm
	β (Mg_2Si)	CaF ₂ structure a=0.639nm
	Q quaternary phase	Hexagonal a=1.04nm c=0.405nm

During aging, formation of stable and metastable phases affects the material properties. The change from totally coherent to semi-coherent and incoherent precipitates (Table 2.2) is important in terms of strengthening [8].

Table 2.2 Coherency of phases formed during aging of 6000 series aluminum alloys

Phases	Coherency	Remarks
GP Zones	Coherent	Spherical
β''	Coherent	Needles with spherical cross-section along $\langle 100 \rangle_{Al}$; totally coherent in Al-matrix
β'	Semi-coherent	Rods with ellipsoidal cross-section along $\langle 100 \rangle_{Al}$; mostly coherent, but end of rods are incoherent to Al-matrix
β	Incoherent	Platelets on $\{100\}$ of Al; totally incoherent to Al-matrix

Solid solution hardening is the main resistance against dislocation motion for the super saturated solid solution obtained after solutionizing. As GP zones form, the hardness increases more since extra stress is required to force dislocations through the coherent zones. Tensile strength continues to increase with the formation of coherent β'' precipitates due to dislocation motion in the highly strained matrix. The force needed for precipitate shearing increases as aging continues and β'' needles become thicker, transforming into β' rods. In the final stages of aging, β platelets forms by thickening and transformation of β' . At that time, coarse precipitates, lower particle density and large inter-particle distance is attained where less force will be required for dislocation movement [9]. Any deformation applied in this production sequence affects the dislocation-precipitation interactions.

2.1.3. Precipitation Hardening Mechanisms

The strength increase of an age-hardenable alloy is due to the interaction of the dispersed precipitate phase with dislocation. The interaction of glissile dislocations with the dispersed second phase will increase the critical resolved shear stress by a number of mechanisms. Three groups can be formed depending on how the dislocation manages to penetrate the dispersed particle: Dislocation can loop the particle; cut through the particle or cross slip around particle [10].

Particle looping (also referred as Orowan looping) is the mechanism in which the dislocation firstly bows out, and then is separated from the looped region leaving one loop around particle (Figure 2.3 a). A loop is formed around each precipitate every time a dislocation passes the precipitates. This mechanism becomes effective for small spacing between precipitates having small diameters.

Particle cutting mechanism on the other hand, is applicable for small sized particles in which dislocations are not stopped at the particle-dislocation contact and glide right through the particle (Figure 2.3 b).

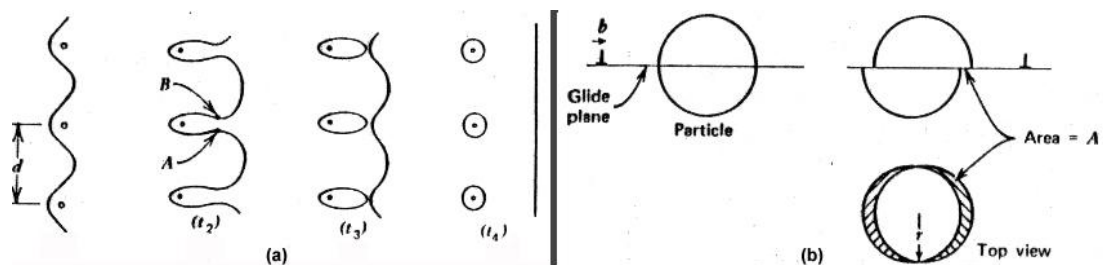


Figure 2.3 Particle – dislocation interactions (a)Orowan looping, (b)particle cutting [10]

During aging process, initially particle cutting mechanism operates due to small precipitate sizes. As aging continues, particle radii increase looping becomes easier [11]. The role of hardening mechanisms during aging is schematically shown in Figure 2.4.

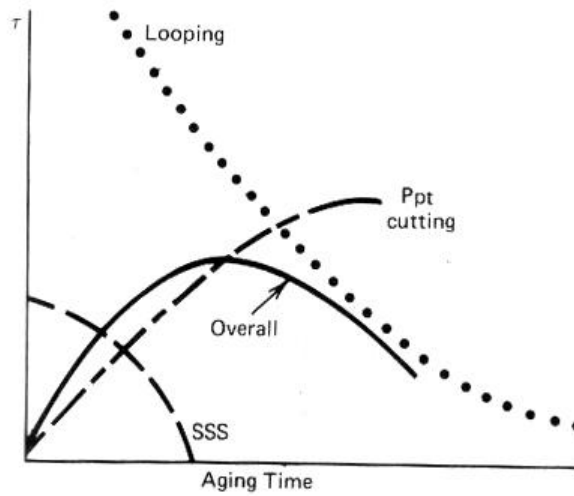


Figure 2.4 Role of major hardening mechanisms during age hardening [11]

2.2. Thermo-mechanical Treatments

Although the leading mechanism for age hardenable aluminum alloys is precipitation hardening; the desired mechanical and microstructural properties could be attained by recovery and recrystallization mechanisms that operated due to synergetic effects of deformation and heat treatment applied. Hence controlling the static mechanisms during annealing and the dynamic ones during deformation becomes so important that the topic of thermo-mechanic behavior was the subject of many researchers [12]. Thermomechanical treatment can be simply divided into two procedures: classical route and the nowadays patented route.

The classical route consists of the homogenization step of the cast semi-product and the hot processing afterwards. In this route the final shape was given to the metal. During deformation most of the alloying additions exists in the matrix as solutionized and the Fe based particles formed during casting were broken and aligned with the deformation axis. These distributed ingredients would eventually inhibit the static recrystallization and the products with elongated pancake type grains could be attained. The solutionizing-quenching-aging cycle to reach the

desired microstructure had a positive effect on mechanical strengthening preserving the main skeleton formed during the hot deformation [13].

Nowadays, thermomechanical route is the combination of deformation and heat treatment series which were designed to reach fine grain structure. The typical processing scheme applied to the cast or powder metallurgy product of age hardenable aluminum alloys was presented in Figure 2.5.

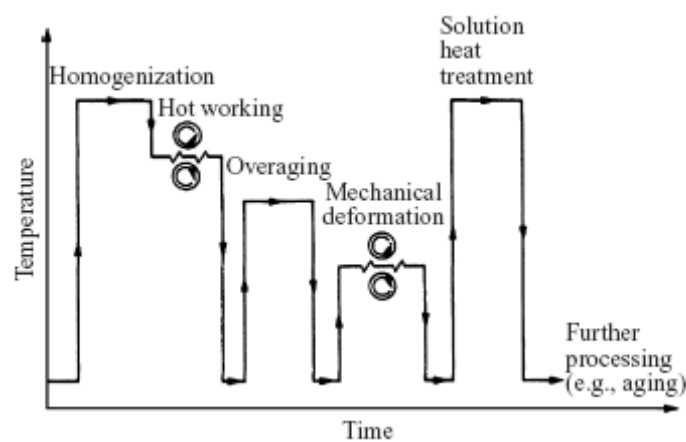


Figure 2.5 Grain refining via thermomechanical treatment [13]

During overaging step, precipitates approximately $75\mu\text{m}$ in size was formed; deformation zones between these coarse precipitates was the evidence of warm-deformation carried on afterwards. The highly stressed regions tend to form nucleation sites during recrystallization hence this mechanism was called as the particle-stimulated nucleation. Once recrystallization continues, the grain growth was retarded by the particles present and hence fine grained aluminum alloys could be attained. It was found that the recrystallized grain size could be reduced by increasing the deformation amount and the particle density. By this way the microstructure of the aluminum alloy could be controlled. This route was patented by Waldman [14] and Paton-Hamilton [15] in 1970s.

Paton-Hamilton [15] has been summarized the thermomechanical processing of AA6061 as follows:

- Solutionizing 520 – 535°C
- Quenching
- Overaging at 340°C for 8 hours
- At least %40 hot deformation (at 340°C or less)
- Recrystallization at 485°C
- Standard precipitation hardening afterwards

The patent has shown that minimum grain size attained by the classical route ($\approx 100\mu\text{m}$) was reduced to $\approx 10\mu\text{m}$ with these cycles of deformation and heating.

2.3. Severe Plastic Deformation

In the high strength aluminum alloys, the desired strength is mainly obtained by precipitation hardening. But optimum properties were achieved by taking into consideration of other mechanisms like grain size control via thermo-mechanical treatments. Thermo-mechanical processing involves step by step thickness reduction of slabs via hot deformation processing which necessitates complicated establishments and large amounts of investment to produce Al alloys. In addition, as Frukova et. al. [16] clarified there have been two more disadvantages of thermomechanical processing. One has been the limited capability of decreasing grain sizes to 10 microns. And the other one has been the requirement of rearrangement of thermomechanical processing details for each alloy set. Especially, the first one impedes obtaining Al alloys with better properties; since it has been known from Hall-Patch relation that, properties can be improved with obtaining nanometer grain sizes.

Ultra-fine grained (UFG) materials, having grain sizes in the submicrometer range, have been the focus of extensive research in the field of materials science. It has been established that UFG materials have excellent mechanical properties and interesting

physical properties by comparison with coarse-grained materials as well as fine-grained materials having grain sizes of a few micrometers [17]. Recently the interest in UFG materials has increased because of the possibility of producing bulk UFG materials by severe plastic deformation (SPD) methods which may solve the difficulties of fabricating many structural applications of UFG materials. The Equal Channel Angular Pressing (ECAP) method is one of the promising SPD methods to produce UFG materials and is most attractive because the cross sections of materials experience no change during the ECAP process and according to Yamashita et. al. ECA pressing has been the only method since the ability to produce relatively large samples [18].

The ECAP method, first introduced by Segal and co-workers, is now extensively used to refine grain structures in bulk materials. The principle of ECAP processing is illustrated schematically in Figure 2.6. It is apparent that the sample is pressed through the die and exits without any change in the cross-sectional dimensions.

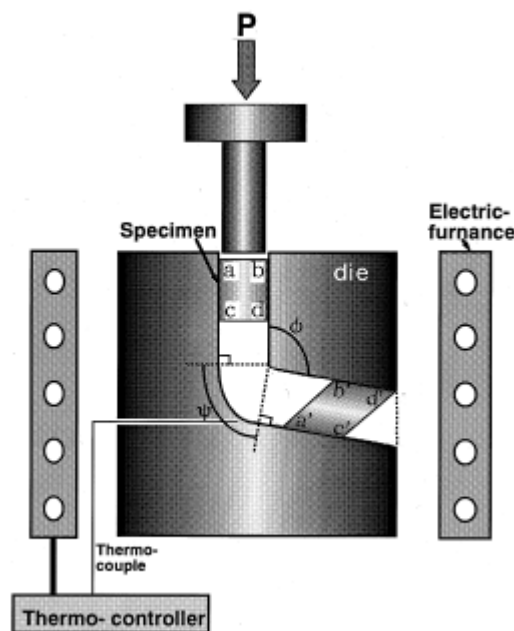


Figure 2.6 Principal illustration of the ECA pressing process [19].

In ECAP system, two channels of the same cross section intersect at a certain angle to form the die. The billet, either of round or square cross section, is pushed from the top by means of a flat faced ram. A heating system may be available for hot production purposes. Since there is no change in the cross section of the specimen, it is possible to repeat the pressing for a number of passes to obtain very high shear strain levels. Thus, ultra fine homogeneous grain structure could be obtained. As a result a very strong refinement of the microstructure down to the sub-micrometer or even nanometer scale may be achieved [20].

In addition to the capability of achieving desired microstructures and properties, the ECAP method shows a potential for scaling up the technique for industrial applications which makes it especially attractive in practice. Horita and Langdon applied ECAP onto samples of several aluminum alloys with diameters from 5 to 40 mm and found that the samples attained an ultrafine-grained microstructure and advanced mechanical properties independent of the initial sample sizes [21].

Although it seems that the ECAP is an easy method for obtaining ultrafine-grained materials; lots of parameters must be controlled to reach the desired properties. Factors influencing the material characterization processed by ECAP can be classified as die geometry (die angles, number of pressing and routes), material properties (number of slip system [22], stacking fault energy [23]) and experimental conditions (temperature, speed, friction, back pressure).

It is understood that die channel parameters are very effective during severe plastic deformation. These parameters are; Φ which corresponds to the angle between the two intersecting channels and Ψ which defines the angle at the outer arc of curvature of the two intersecting channels. According to the experiments carried by Nakashima et. al. [24], optimum conditions to achieve ultra fine grain with high angle grain boundaries was obtained when Φ is close or equal to 90° . At these conditions a large plastic strain (approximately true strain of 1) is imposed on the material in each passage through the die. The details were explained in the following section.

The properties of the material strongly depend on channel feeding types in a multi-pass system. The most frequently used four fundamental processing routes in

literature are given below by Nakashima et. al [25]. The rotations of the sample between consecutive pressings are 0° for route A, 90° in the positive or negative direction alternately for route B_A, 90° in the same direction for route B_C and 180° for route C.

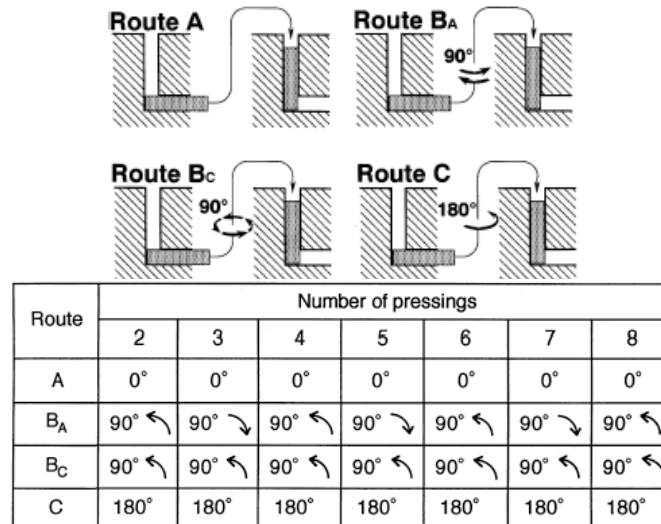


Figure 2.7 Fundamental processing routes in ECAP [25]. Also material rotation angles during re-feeding are given [26]

Lee et. al. suggests B_C route as the optimum to achieve homogeneous grain refinement [27]. Furthermore, they relate this result to the ease of formation more grains with high angle grain boundaries.

Extensive research has been carried out either experimentally or by using Finite Element Method to evaluate various factors that may influence ECAP. Both die and feeding parameters are the working subjects which are mainly focused on. These works include finite element method and aim to determine optimum die parameters [28, 29, 30].

In the last decade; ECAP process has been applied to mainly aluminum and aluminum alloys then copper, magnesium, nickel, titanium and steel. Especially the work has been carried on age hardenable aluminum alloys and it is discussed in terms of replaceability of ECAP with the classical thermo-mechanical treatment.

ECAP process has been studied for 2xxx series Al alloys by Lee et. al. [27], Mao et. al. [31], Kim et. al. [32], Zheng et. al. [33] and Horita et. al. [34]. According to the experiment of Lee et. al., quenched Al-2024 alloy has been exposed to 8 passes through the ECAP die at 25°C which leads to grain sizes of 0.3 µm [27]. This study has also showed the material's thermal stability that after annealing at 400 - 450 °C, grain sizes have not been exceed 1 µm.

Similar studies have been carried out for 7xxx alloy by Zheng et. al. [33], Horita et. al. [34]. Zao et. al. [35] and Xu et. al. [36-37]. Zheng et. al., have deformed Al-7050 alloy which has initially 20 µm grain size and after four passes grain size has been decreased to 0.7 µm [33]. They have also combined aging and ECAP processes in different combinations. The strength obtained for the ECAPed and then aged alloy has been higher than that of the conventional T6- treated alloy.

ECAP process has been studied for 6xxx series Al alloys by Horita et. al. [34], Chang et. al. [38], Chang and Shan [39], Chung et. al. [40] and Kim et. al. [41]. Chang and Shan have deformed Al-6065 alloy which has 100 µm grain size initially and after single pass they have obtained a grain structure with 0.3-0.4 µm grain size [39].

In a similar study, Chung et. al. have investigated the effects of pass number on grain size and mechanical properties [40]. They found that strength have been improved significantly in one pass and the improvement trend has decreased with the following passes (Figure 2.8).

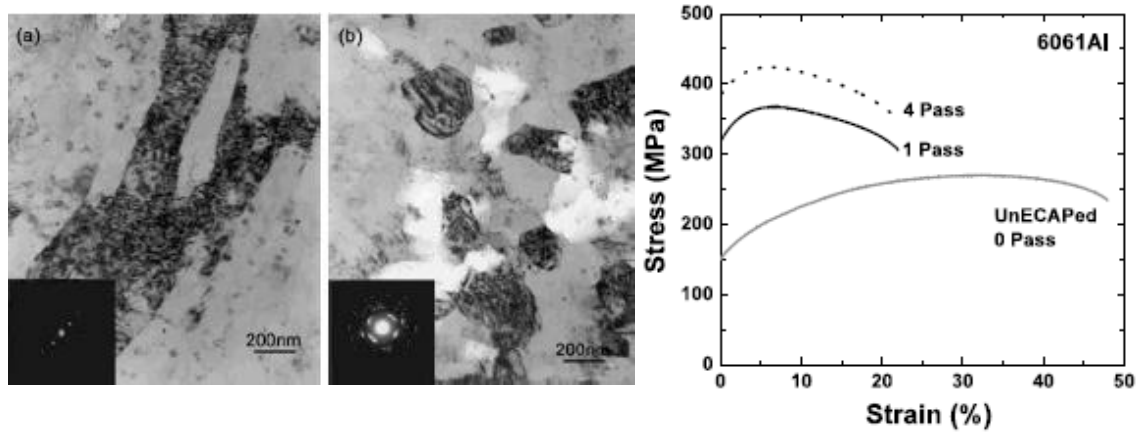


Figure 2.8 TEM image of Al 6061 alloy after ECAP process a)1 pass, b)4 passes c)stress-strain curve after ECAP [40]

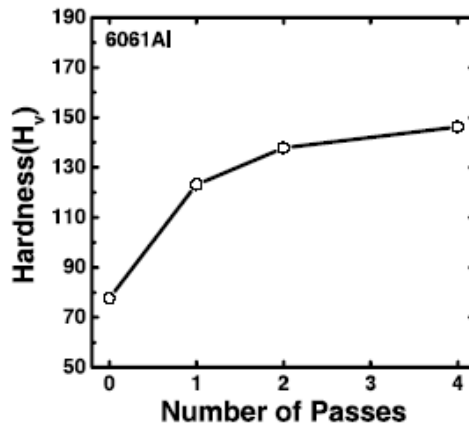


Figure 2.9 Change of hardness via ECAP deformation of AA-6061 [41]

According to the study of Kim et. al., similar trend in material hardness has been determined [41]. The hardness of an AA6061 alloy has been increased from 80 VSD to 120 VSD in one pass; but in the following passes (150 VSD at fourth pass) it has not been increased as much as in single pass. (Figure 2.9)

Studies show that in some cases multi-pass ECAP process may cause cracking on materials. Chung et. al. suggested applying ECAP process at higher temperatures (~100 – 125 °C) instead of room temperature to overcome cracking problem [40]. A study carried by Chang et. al. on ECAP process of 6xxx series aluminum alloys at

temperatures 100 °C and 300 °C have shown that although number of passes could be increased with increasing temperature; the material's strength decreases with increasing temperature in ECAP process [38].

The research by Kim et. al. point out the improvement of the strength observed in the ECA pressing is better than that of the conventional peak-aged 6061 alloy [41]. The resultant graphs were shown in Figure 2.10. It has been concluded that strength has been increased by % 40 as compared to conventional peak-aged alloy.

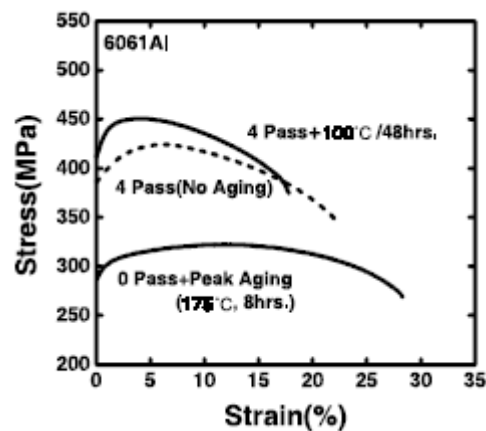


Figure 2.10 Comparison of engineering stress-engineering strain curves for the T6 treated commercial 6061 Al alloy and the ECAP processed 6061 aluminum alloy (4pass) with and without a low temperature aging treatment [41]

ECAP process is desired for 6xxx series Al alloys and other high strengthened Al alloys (2xxx and 7xxx) due to the ability to obtain micron and sub-micron grain sizes, high strength and hardness, and advantages over standard peak-aging treatment. This remarkable improvement provided by ECAP in Al alloys have been summarized by Horita et. al. in Figure 2.11 [34].

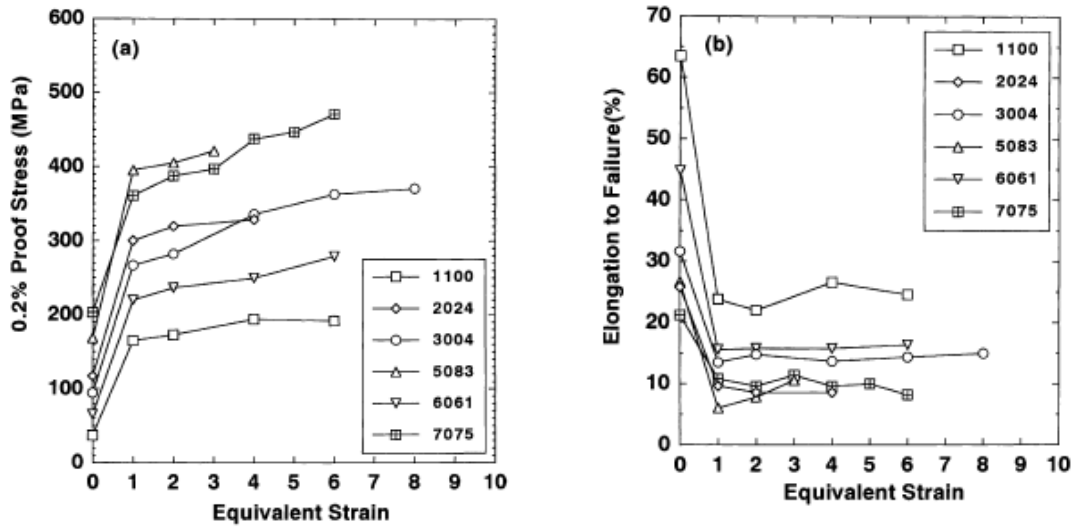


Figure 2.11 The effect of ECAP process on mechanical properties of various aluminum alloys [34]

Another attraction of ECAP has been thermal stability of the material during subsequent annealing process after deformation. In most of the alloys, the grain size has remained unchanged up to a temperature of 200 °C. As seen from Figure 2.12 that; this temperature is higher (up to 300 °C) for 2xxx and 7xxx series aluminum alloys.

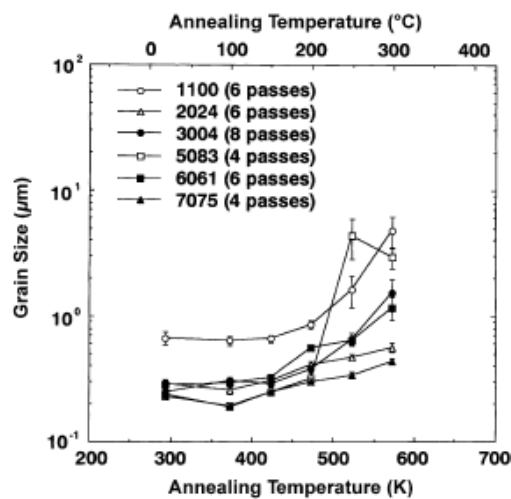


Figure 2.12 Variation of grain size with respect to annealing temperature [34]

2.3.1. Strain Calculations in ECAP

As stated previously; the effect of ECAP and the amount of strain induced is directly related to the die angles. It was suggested by Segal et. al [42] that the magnitude of shear strain imposed on material at a single pass is just a function of Φ . With a system having a die containing square cross-sectioned channel, the maximum effective strain for the frictionless condition can be calculated by using the slip line field theory and velocity hodograph. The shear strain in 2D (Figure 2.13) can be calculated by using the formula (2.1). In the case of ECAP (Figure 2.14), deviation in the element can be calculated by investigating velocity hodograph. The hodograph for this case is presented in Figure 2.15 where α is the half of intersection angle, V is the velocity of the punch and the ΔV is the shear velocity along the shear axis. Shear strain in the element flowing through the channel intersection could be calculated by equation (2.2). With the use of basic geometry in the hodograph, equation (2.3) was obtained. Hence the magnitude of shear strain could be calculated from the equation (2.4) which was the combination of the two equations.

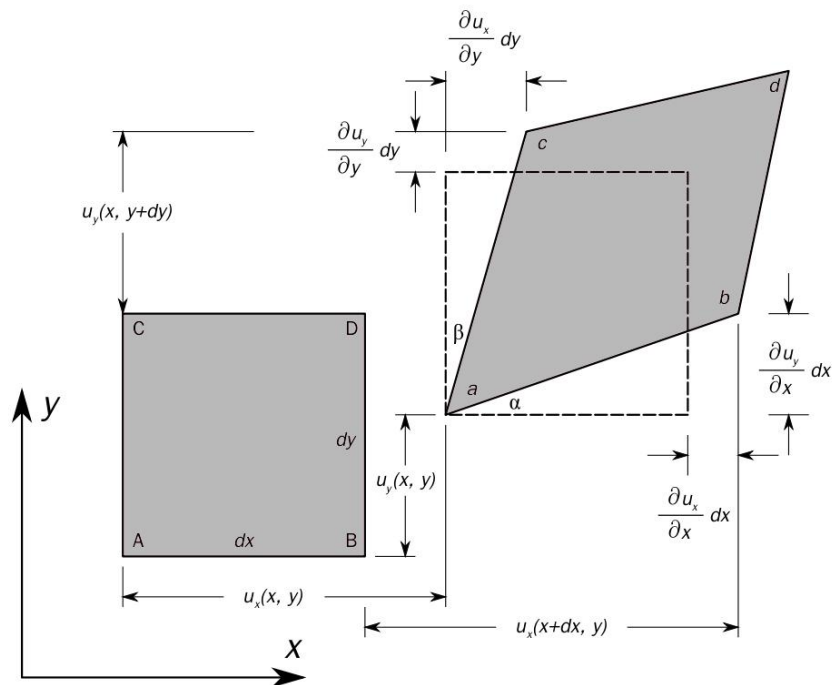


Figure 2.13 Schematic drawing of deformation in 2D [43]

$$\gamma_{xy} = \frac{\partial u_y}{\partial x} + \frac{\partial u_x}{\partial y} \Rightarrow \gamma_{xy} = \frac{\Delta x}{y} \quad 2.1$$

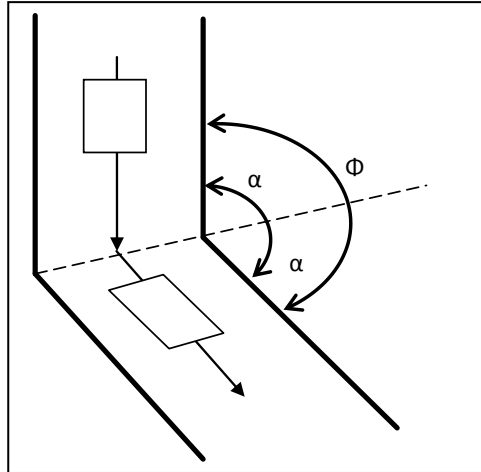


Figure 2.14 Schematic drawing of shear in ECAP

$$\gamma_{xy} = \frac{\Delta V}{V \sin \alpha} \quad 2.2$$

$$\Delta V = 2V \cos \alpha \quad 2.3$$

$$\gamma_{xy} = 2 \cot \alpha = 2 \cot \frac{\phi}{2} \quad 2.4$$

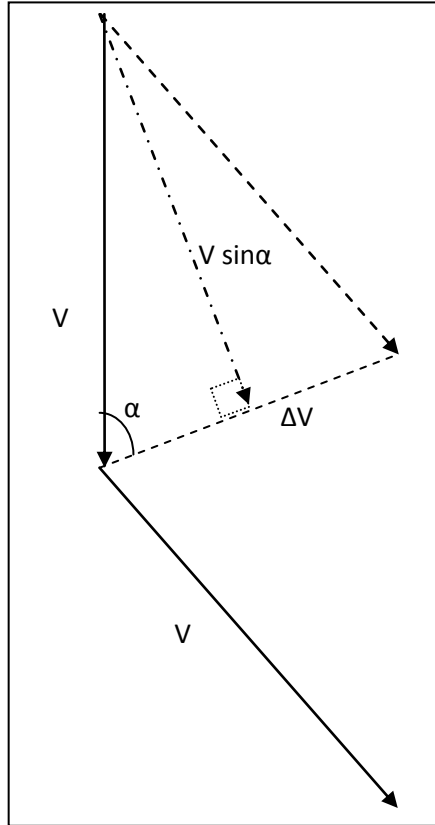


Figure 2.15 Velocity hodograph of ECAP deformation

The effective strain in a basic working operation is given by equation (2.5) when Von Mises yielding is considered. The basis of ECAP deformation is the conservation of pure shear mode, leading to a simplification in the effective strain definition as stated in the equation (2.6). Hence the equivalent strain can be derived as equation (2.7) with the N being the number of passes.

$$\bar{\varepsilon} = \frac{\sqrt{2}}{3} \left(\varepsilon_x^2 - \varepsilon_y^2 + \varepsilon_y^2 - \varepsilon_z^2 + \varepsilon_z^2 - \varepsilon_x^2 + \frac{3}{2} (\gamma_{xy}^2 + \gamma_{yz}^2 + \gamma_{zx}^2) \right)^{1/2} \quad 2.5$$

$$\varepsilon_x = \varepsilon_y = \varepsilon_z = \gamma_{yz} = \gamma_{zx} = 0 \Rightarrow \bar{\varepsilon} = \frac{1}{\sqrt{3}} \gamma_{xy} \quad 2.6$$

$$\bar{\varepsilon} = \frac{2}{\sqrt{3}} N \cot\left(\frac{\phi}{2}\right) \quad 2.7$$

Later on the effect of Ψ – outer channel angle was also calculated and the equation (2.8) was suggested by Iwahashi et.al. for the calculation of equivalent strain in ECAP type severe plastic deformations [44].

$$\bar{\varepsilon} = \frac{1}{\sqrt{3}} N \left[2 \cot \left(\frac{\Phi}{2} + \frac{\Psi}{2} \right) + \Psi \operatorname{cosec} \left(\frac{\Phi}{2} + \frac{\Psi}{2} \right) \right] \quad 2.8$$

All these calculations clarifies that the amount of strain induced in ECAP is directly related to the die angles and the number of passes. Assuming an ECAP die with sharp corners ($\Psi=0$); the strain that could be imparted to the material was tabulated (Table 2.3) for the angles 90°, 120°, 150° and for the passes from one to five.

Table 2.3 Effect of ECAP processing parameters for a system with sharp corners

N	1		2	3	4	5
	ε	%AR	ε	ε	ε	ε
90	1.155	68.5	2.309	3.464	4.619	5.774
120	0.667	48.7	1.333	2.000	2.667	3.333
150	0.309	26.6	0.619	0.928	1.238	1.547

The benefit of ECAP is the ability to obtain this high level of strain in a single pass. Equivalent strain could also be expressed as the reduction in area to underline the magnitude of strain attained in a single pass and compare it with conventional metal working operations.

Strain can also be expressed as equation (2.9) where A_0 and A_f area the initial and final cross-sectional area in the conventional metal working operations. In the meanwhile percent area reduction during the extrusion process can be calculated with equation (2.10). For the ECAP system implementation of equivalent Von Mises strain results the formulations stated in equation (2.11) and (2.12).

$$\varepsilon = \ln \frac{A_0}{A_f} \quad V=\text{constant} \quad 2.9$$

$$\%AR = 100 \left(1 - \frac{A_f}{A_0} \right) \quad 2.10$$

$$\frac{A_0}{A_f} = \exp \left(\frac{2}{\sqrt{3}} N \cot \left(\frac{\phi}{2} \right) \right) \quad 2.11$$

$$\%AR = 100 \left[1 - \exp^{-1} \left(\frac{2}{\sqrt{3}} N \cot \left(\frac{\phi}{2} \right) \right) \right] \quad 2.12$$

As shown in Table 2.3; deformation obtained during a single pass ECAP with a 90° die is equivalent to 70% reduction in conventional metal working processes. It is a known fact that attaining so high strains with a single pass rolling is impossible; since the maximum workability for cold rolling is 20% reduction in area. Another known advantage of ECAP process is the preservation of shape during deformation. Since there is no shape change, all the work during internal shearing is used for dislocation motion and creation leading to a high dislocation density. This fact is used to generate an ultra-fine grained microstructure.

2.3.2. Grain Refinement Mechanisms

The clue behind the improvement of mechanical properties with ECAP process is the formation of ultrafine grained microstructure. But up to now, there are still no well accepted theories or models to describe the grain refinement mechanism in ECAP. It is generally believed that the grain refinement is associated with large accumulative shear strains and the interaction of shearing planes in the process. On passage through the die, the sample undergoes straining by simple shear as illustrated in Figure 2.16. Simple shear is considered a “near ideal” deformation method for structure and texture formation in metal working. It enables the sample to be subjected to a large amount of strain without the damage that occurs in conventional metal working such as rolling.

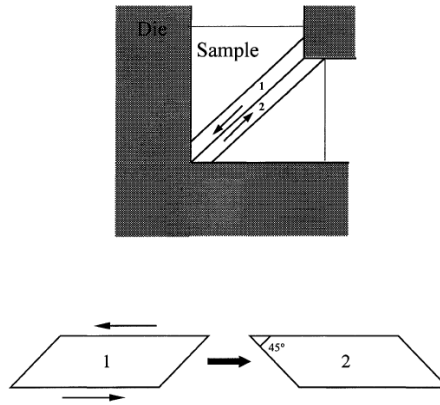


Figure 2.16 The principle of shearing in the sample during ECAP

Also the microstructures developed by cold rolling are usually cellular substructures having boundaries with low angle misorientations. But, ECAP technique is capable of fabricating structures of a granular type containing mainly high angle grain boundaries [45]. Valiev et al, later proposed a model for the formation of grain boundaries during ECAP [46] as shown in Figure 2.17. The model can explain the granular structure observed in ultrafine-grained materials by ECAP and the evolution of high angle boundaries during repetitive ECA pressings.

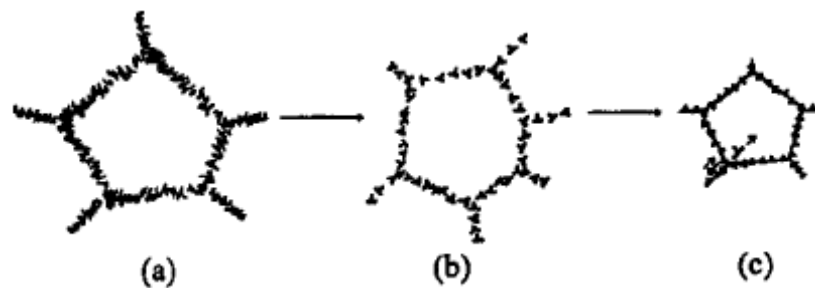


Figure 2.17 Schematic model of dislocation evolution at different stages during ECAP (a)initial cellular structure (subgrains) containing many dislocations; (b)cell experiencing partial annihilation of dislocations at the boundaries; (c) granular structure achieved with high angle boundaries. [46]

Later on different modeling studies related to the grain refinement mechanisms were proposed. Based on Meyer et al.'s model [47], Mishra et al. proposed a sequence of events leading to the formation of the ultrafine grain size in Figure 2.18 [48]. Study shows that a homogeneous dislocation distribution is replaced by energetically favorable subgrains. These subgrain walls present a barrier for dislocation propagation and the misorientation between adjacent grains increases gradually with plastic strain. The elongated subgrains are preferred over equiaxed ones and calculated the optimum aspect ratio. The thickness of these oblate spheroids ultimately determines the grain size; upon subdivision, the equiaxed structure is formed.

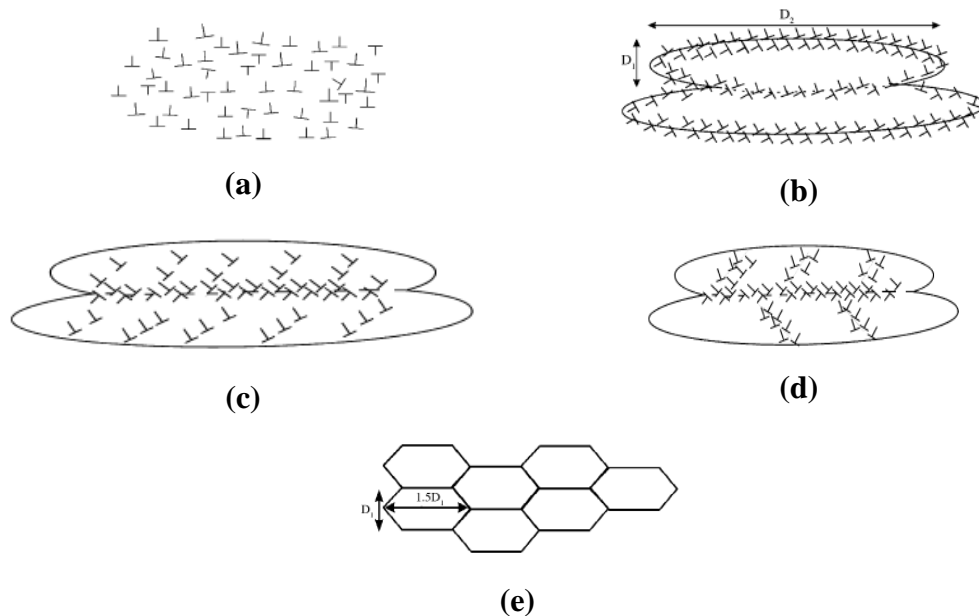


Figure 2.18 Schematic illustration of microstructural evolution during severe plastic deformation. (a) Homogeneous distribution of dislocations, (b) elongated cell formation, (c) dislocations blocked by subgrain boundaries, (d) break up of elongated subgrains and (e) reorientation of subgrain boundaries and formation of ultrafine grain size.

2.3.3. Continuous Methods

The bases that are given above are according to laboratory conditions. The work-piece length is limited in these examples due to the die and feeding system (ram of a

hydraulic press). The constrained travel distance of the press ram makes ECAP a discontinuous process, with low production efficiency for industrial purposes. Producing long, large UFG materials for real structural applications adaptation to a continuous processing is required. Some of them are ECAP-Conform [49], conshearing process [50] and dissimilar angular pressing [51] in which feeding is established via rolls instead of pressure application by the hydraulic press ram.

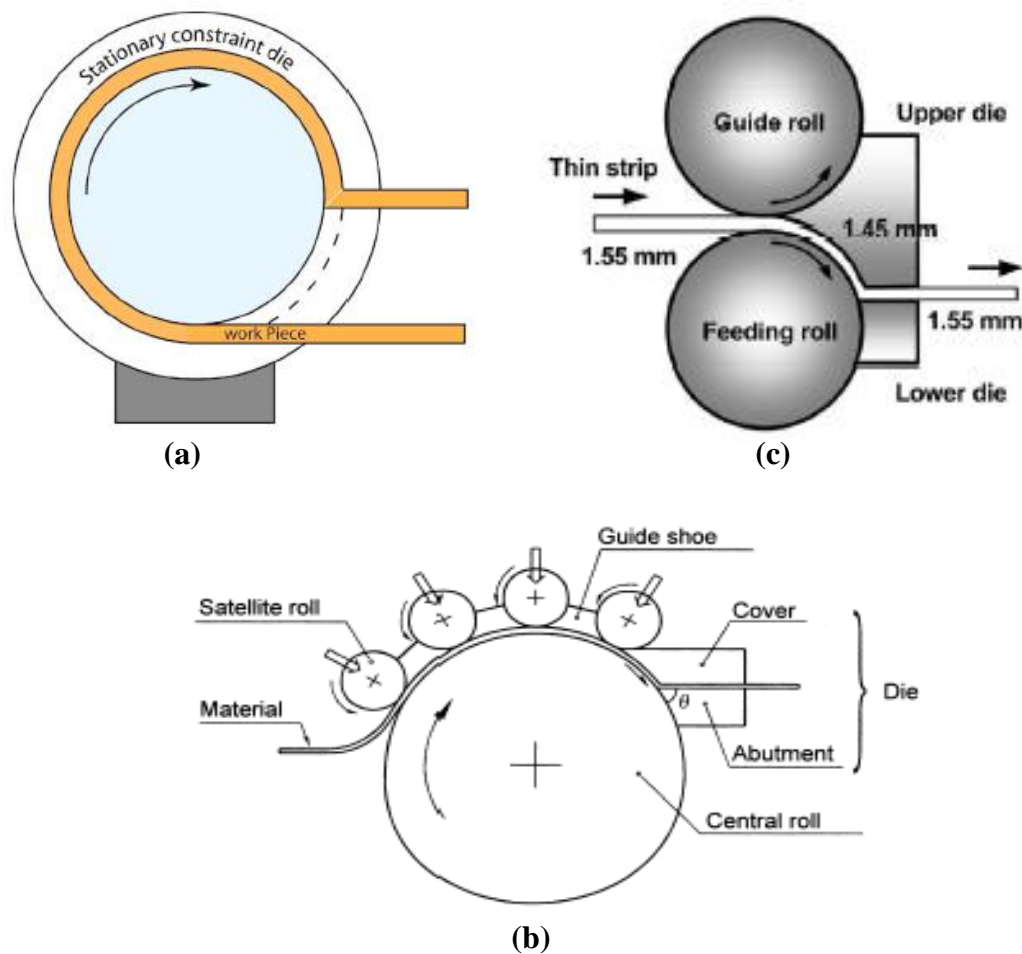


Figure 2.19 Adapted severe plastic deformation methods for continuous production
 (a) ECAP-Conform [49] (b) Conshearing [50] (c) DCAP [51]

ECAP-conform set up seems like rolling, a rotating shaft in the center contains a groove and the work-piece is fed into this groove as it is shown in the diagram. The

work-piece is carried by frictional force and it is turned round at an angle of 270° . Finally it leaves the stationary constraint die by an exit channel which is parallel to the first one. However, this method (Figure 2.19a) requires a different set up for each material thickness / cross-section and applicable for wires and thin strip only. There are alternative methods given in Figure 2.19b&c, which do not require set up changes and only requires simple adjustments [50-51].

2.3.4. DCAP System

After 2002; there is an increase in the number of the research on Dissimilar angular pressing (DCAP). According to Lee et.al. DCAP is the most appropriate system for production of sheet materials [52]. It is composed of rolling system (Figure 2.20) which feeds the sheet to a rigid die containing an ECAP channel of $100\text{-}140^\circ$. The only difference is that the upper portion of the channel is narrower than the exit channel. This difference is established to make the feeding of the sheet possible.

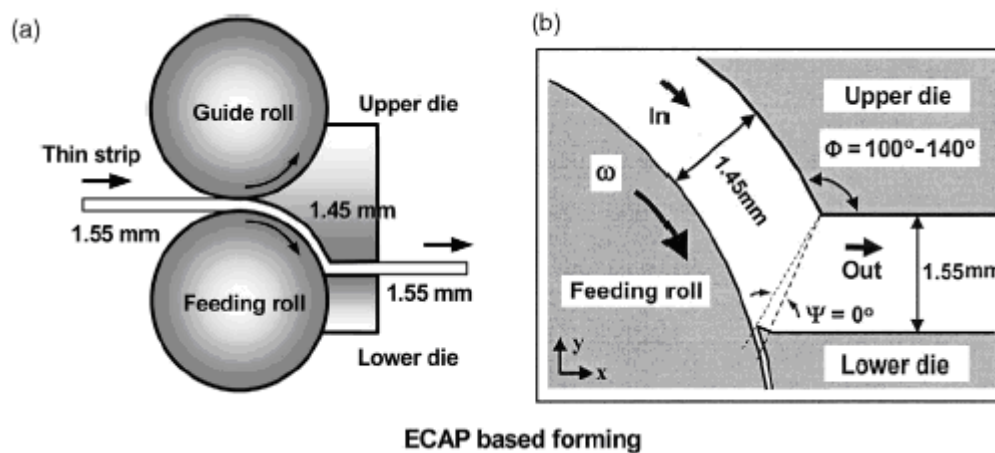


Figure 2.20 Schematic drawing of the deformation die system for repetitive deformation (a)General mechanism, (b) Die details

Like ECAP process; mechanical properties are improved via grain refinement. Change in microstructure by single pass DCAP deformation of Al-1050 alloy was

summarized by Lee et. al. [53]. In Figure 2.21, the microstructure of the alloy before and after DCAP is compared.

In the case of age hardenable aluminum alloys; the effect of precipitates makes the things more complicated in terms of strengthening mechanisms. A study done by Nam et. al on Al-7050 Aluminum plates showed that the microstructural change during DCAP deformation was greatly affected by the presence of large platelike $MgZn_2$ and tiny spherical Al_3Zr precipitates [54].

Some other DCAP studies on Aluminum sheets are summarized in Table 2.4.

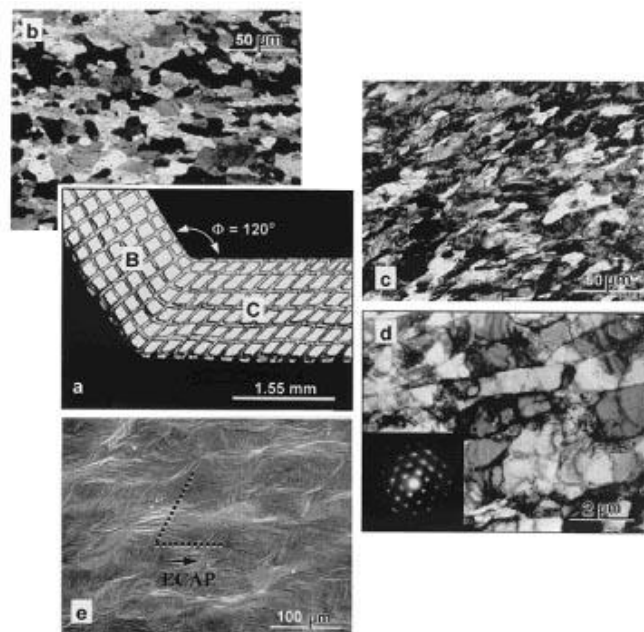


Figure 2.21 Microstructure condition of Al-1050 alloy after DCAP [53]
 (a) An optical micrograph showing the shear deformation patterns
 (b) Grain structure from region B (before DCAP)
 (c) Grain structure from region C (after DCAP)
 (d) TEM bright field image and a SAD pattern (formation of the cell structures after DCAP)
 (e) SEM micrograph showing the direction of the slip bands

Table 2.4 Dissimilar Channel Angular Pressing studies in literature

Reference	Material	Method	Number of pass	Temp	Investigation
Han et. al. [55]	Al-1050 (5mm)	Rolling (1.55mm)+ Anneal + DCAP	1	RT	<input type="checkbox"/> Texture (Pole Figures)
Han et. al. [56]			1	RT	
Han et. al. [57]			1-32	RT	
Han et. al. [58]			1	RT	
Han et. al. [59]			1	RT	
Han et. al. [60]			1-32	RT	<input type="checkbox"/> TEM Micrographs <input type="checkbox"/> Pole Figure
Lee et. al. [53]	Al-1050 (5mm)	Rolling (1.55mm) + Anneal + DCAP	1	RT	<input type="checkbox"/> XRD Investigation <input type="checkbox"/> Texture (Pole Figure)
Lee et. al. [51]	Al-1050 (5mm)	Rolling (1.55mm) + Anneal + DCAP	1-50	RT	<input type="checkbox"/> TEM investigations <input type="checkbox"/> Hardness <input type="checkbox"/> Strain Calculations
Lee et. al. [52]	Al-1050	Strip cast (1.55mm) + DCAP	1	RT	<input type="checkbox"/> Finite Element Analysis <input type="checkbox"/> TEM investigations <input type="checkbox"/> Hardness <input type="checkbox"/> Texture (Orientation Distribution Functions)
Lee et. al. [61]	Al-1050 (5mm)	Rolling (1.55mm) + Anneal + DCAP	1-100	RT	<input type="checkbox"/> Hardness <input type="checkbox"/> TEM investigations <input type="checkbox"/> Boundary Mismatch Calculations <input type="checkbox"/> EBSD
Nam et. al. [54]	Al-7050	Hot Roll (1mm) + Anneal + DCAP	1-6	RT	<input type="checkbox"/> TEM Investigations <input type="checkbox"/> Microhardness
Jining et. al. [62]	Al-6061 (5mm)	Warm Roll (1.55 mm) + DCAP	1-5	RT	<input type="checkbox"/> TEM <input type="checkbox"/> Texture (Orientation Distribution Functions)
Suh et. al. [63]	FEM Analysis	-	-	-	<input type="checkbox"/> Compare ECAP & DCAP texture

Most of the studies in literature cover the deformability of pure aluminum sheets; there are few studies on complex systems like age-hardenable sheets. Most of the work has been established to investigate the texture. Although there are lots of studies on ECAP version; which covers numerous factors like age hardening and high temperature deformation effects; all the studies of DCAP has been established at room temperature. Hence, in this study it is planned to shorten the TMP of aluminum alloy sheets and to suggest an alternative way for high strength, high quality aluminum alloy sheets.

CHAPTER 3

EXPERIMENTAL PROCEDURE

In the first part; simulation studies were carried out to get design hints for the machine construction and to investigate the parameters effecting the deformation. Afterwards; an Equal Channel Angular Pressing (ECAP) die system for deformation of rods, and then, a Dissimilar Channel Angular Pressing (DCAP) system for sheet metal deformation was constructed. Al2024 rods and Al6061 sheets were deformed upto several passes, and the deformed metals were investigated by mechanical, microstructural and several other characterization tools.

This chapter includes the analysis method for modeling, the design and construction keypoints of the ECAP and DCAP systems. The details and method for the deformed sample characterization was also explained in this chapter.

3.1. Simulation Studies (*Finite Element Analysis*)

The main aim of the study was to construct a continuous severe plastic deformation system for sheet materials. However; before system design ECAP method was studied to construct a basement for continuous version (DCAP). Effect of material properties and process variables on ECAP performance was also studied.

3.1.1. Simulation of Equal Channel Angular Pressing (ECAP)

ECAP process is being applied with the system shown in Figure 3.1. In the system there are two channels with same die cavity intersected at a die arc angle of Ψ and a

die channel angle of Φ . The workpiece that is fed with a punch to the inlet channel passes through the deformation zone and goes out from the outlet channel.

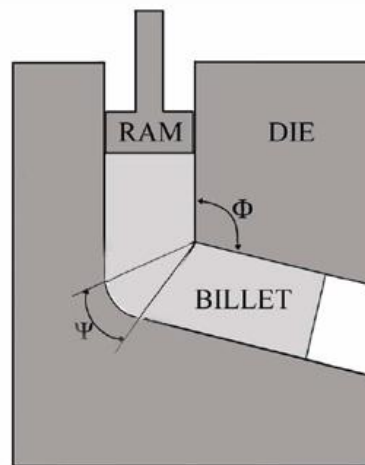


Figure 3.1 Schematic view of ECAP system

Effective strain calculations for a system having a die containing square cross-sectioned channel was presented in the preceding section. The maximum effective strain for the frictionless condition can be calculated from the equation (2.8). These equations were obtained with the assumption of not-ideally strain hardening materials; so they could not solve the problem of die cavity formation and its effect on material deformation. Beneath the effect of parameters like friction and deformation speed could not be guessed with analytical methods. So finite element modeling was carried out.

Deformation homogeneity is an important parameter for severe plastic deformation processes. Because, the homogeneity of strain distribution is required for uniform grain size and shape (uniform mechanical properties). Any effect that destroys the homogeneity would also deteriorate the final properties obtained. Inhomogeneous deformation might also lead to distortion and high residual stresses in the material. Distortion and residual stresses would cause several problems in the following production schemes. Especially for the sheet and plates; this risk is much more

pronounced. For these reasons, it is required to obtain homogeneous vertical and horizontal strain distribution. Die and system design seems to be a key point.

Except from materials properties; process parameters like die geometry and friction coefficient has an effect on deformation homogeneity during ECAP processing. Hence, simulations were carried out to find the optimum ones. Simulations were carried out Msc. Marc software. To simplify the problem and decrease the processing time, plane strain condition was assumed and a plane passing through the center of the die and billet was simulated. Also it was assumed that the process was completed at constant temperature. In literature some observations of temperature increase during ECAP deformation processes were present [64]. But, it seems acceptable to assume an isothermal process for low ram speeds such as 1 mm/sec employed and a well lubricated die with cooling system. And also it is not projected to have adiabatic slip field formation due to local heating; because of high thermal conductivity of aluminum.

The effect of deformation speed on material properties and failure models like crack formation, tearing, fracture were ignored. For simulation of the process, a hypothetical material was defined to resemble a high strength aluminum alloy. It was assumed that:

- the material shows elasto-plastic deformation behavior,
- elastic to plastic transformation was specified by von Mises yield surface,
- plastic yielding vector was specified by relational yielding law,
- material hardening takes place via piecewise continuous isotropic hardening

Typical values of Young's modulus of 69 GPa, Poissons' ratio of 0.3 was chosen and equation (3.1) was used to relate stress-strain in the plastic zone. $\bar{\sigma}$ is effective yield strength and $\bar{\epsilon}$ is effective plastic strain respectively.

$$\bar{\sigma} = 150 + 250\bar{\epsilon}^{-0.3} \quad 3.1$$

3.1.2. 3-Dimensional Analysis Method

In order to verify the 2-dimensional “plane-strain” assumption; some of the simulations were repeated and compared with the same parameters and 3-dimensional models. For 3-dimensional simulations; a die system with 90° intersecting channels was used. A work piece having a size of 50mm x 10mm x 10mm was modeled with a 5000 element mesh. It was assumed that the press and die would not change dimensions during deformation. Due to bulging and high amount of deformation, global remeshing choice was activated. Also excitation methods like finer meshing were applied to increase the precision in the deformation zone. 3-dimensional simulations took 16-20 times more time as compared to 2-dimensional cases.

3.1.3. Investigation of the Effect of Materials' Property

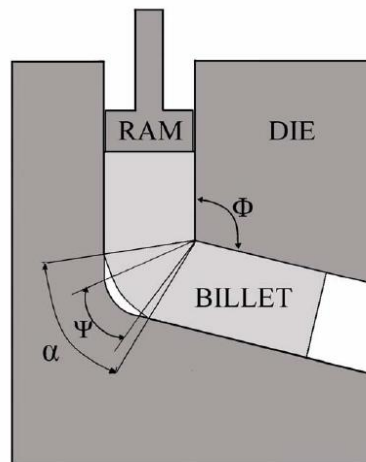


Figure 3.2 Typical workpiece behavior during ECAP deformation

In literature, there are numerous papers investigating the effect of die geometry on ECAP performance and strain homogeneity. However, the effects of material's plastic deformation characteristics were not systematically examined.

During die design it was observed that there would be substantial deviation in the equivalent total strain guessed. According to Iwamatho's formula (equation (2.8)) equivalent strain depends on channel's inner and outer angles of the die only. However; as seen from Figure 3.2 corner gap formation was a predictable observation for strain hardening materials which affects the equivalent strain guessed. It was found that equivalent strain guessed approaches to real values, if material corner gap angle (α) is used instead of geometrical die arc angle (ψ) in the equation (2.8). Hence, the die arc angle should be the material corner gap angle; and the die design should be done accordingly. Otherwise the death metal zone causes an inhomogeneous strain distribution.

According to the problem stated above; simulations were carried out to observe the effect of material properties to the ECAP performance. The system was constructed as a die with 90° channel inner angle. The problem was reduced to a 2D case assuming plane strain condition. Parameters like deformation speed and temperature change were ignored. A rectangular workpiece with 50mm x 10mm was meshed into 2000 finite elements. As in the previous case, die and the punch were assumed to be rigid bodies. Elasto-plastic material model was assumed and 69GPa, 0.33 and 2.7 g/cm³ was used as elastic modulus, Poisson's ratio and density, respectively. Ludwick law (equation (3.2)) was preferred as the law determining the material's behavior in the plastic zone.

$$\sigma = \sigma_0 + K\varepsilon^n \quad 3.2$$

In the equation; σ_0 is the yield strength; K and n are the strain hardening multiplier and exponent respectively. During analysis the K and n values were varied and corner gap angle (α) was measured from the Figure 3.2.

3.2. Equal Channel Angular Pressing (ECAP) System

Equal Channel Angular Pressing (ECAP) is the basement method of continuous version (DCAP). Hence, the first severe plastic deformation studies were started with ECAP method. An ECAP system was constructed and modernized to deform 2024Al samples. The aim was to investigate severely deformed Al alloy with single pass ECAP deformation and carry the experience to the continuous severe plastic deformation of Al sheets being deformed many passes. Samples after single pass ECAP deformation was characterized mechanically and microstructurally. In this section the procedure followed was summarized; where the details of system construction and results were presented in the TUBİTAK project 105M174[65].

3.2.1. System Design and Modernization

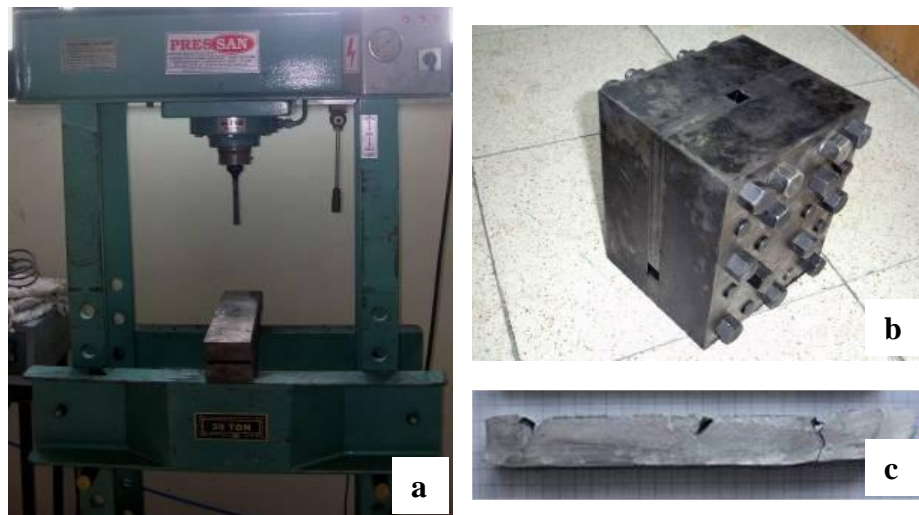


Figure 3.3 First system a) 30 ton vertical axis press, b) ECAP die (14x14mm square cross-section, 120°), c) a selected sample deformed AA-6066

During system construction two types of presses (horizontal and vertical axis) and numerous die sets were tried. The first system was composed of a 30 ton hydraulic vertical press and a tool steel die, in which channels were intersected at an angle of 90°. In this system; formation of cracking in the front and last regions was inevitable

(Figure 3.3). Also it was observed that rigidity of the system was very important; hence the idea was transferred to a more rigid horizontal axis press. With this system several dies (14x14mm square cross-section, 120°; Ø =18mm circular cross-section, double 120°; Ø =18mm circular cross-section, 120°) were tested (Figure 3.4).

The final setup was H13 hotwork tool steel die with Ø =18mm circular cross-sectional channels intersected at an angle of 120°. The surfaces of the channels were electropolished and plasma nitrided to remove surface irregularities. Also MoS₂ including gress and pellets pressed from Mo powder lubricant were used for further friction removal. Tungsten carbide punches were used to feed the material to the system.

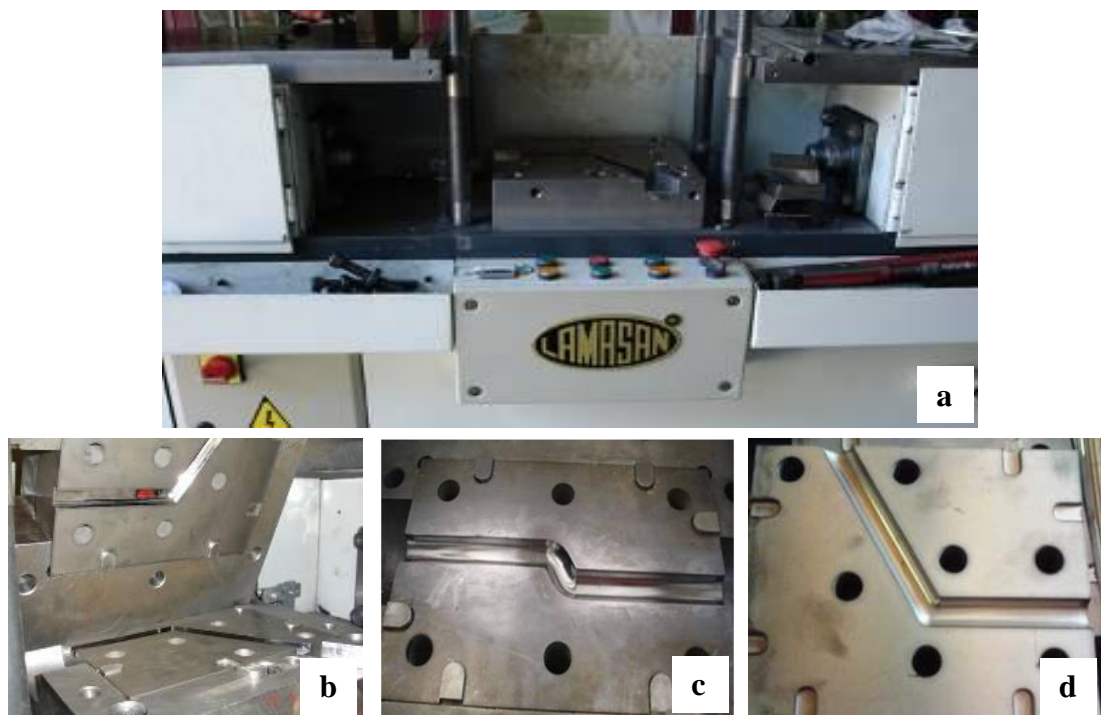


Figure 3.4 a) Horizontal axis press, b,c,d) ECAP dies (14x14mm square cross-section, 120°; Ø =18mm circular cross-section, double 120°; Ø =18mm circular cross-section, 120°)

As discussed in the finite element simulations part; corner gap formation should be prevented to remove unhomogeneous strain distribution and material cracking during

processing. In the trial and error stages; using Cu blocks was found to be the ideal way to apply back pressure and remove cracking and corner gap formation. The most effective way of processing within the maximum limits of the press system was schematically shown in Figure 3.5.

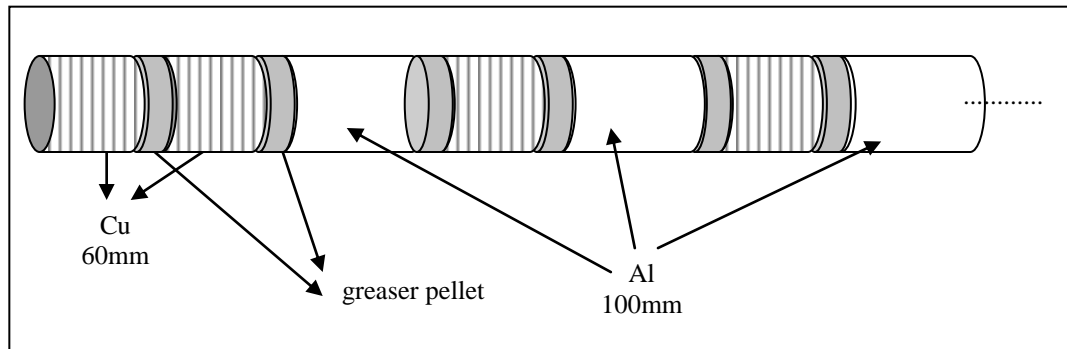


Figure 3.5 Schematic specimen order in the die

3.2.2. Material and Heat Treatment

Along the systematic deformation practice; AA-2024 alloy whose chemical composition given in Table 3.1 was used. Samples with the dimensions of $\varnothing = 18\text{mm}$, length=100mm were machined and heat treated before ECAP.

Table 3.1 Chemical composition of samples used in ECAP deformation and composition of standard AA-2024 alloy

	Al	Cu	Mn	Mg	Si	Fe	Zn	Ti	Cr
	92.6	4.9	0.595	1.24	0.106	0.217	0.156	0.0292	0.0166
standard	90.7–94.7	3.8–4.9	0.3–0.9	1.2–1.8	<0.5	<0.5	<0.250	< 0.150	<0.100

Samples cut to their dimensions were solutionized in a muffle furnace at 495°C for 1hr and directly quenched to icy-water at 0°C on the onset of ECAP deformation. Samples were kept in a deep freezer (@ -18°C) to get rid of natural aging. For aging

practices; a sensitive oil bath with silicon oil was used; 0.25 – 12hr time interval at 80 – 190°C temperature were the operating parameters of the oil bath. For some set of samples an annealing treatment for duration of 1hr in a furnace at 400°C was applied to ECAPed samples to investigate thermal stability of the deformed samples.

3.2.3. Sample Characterization

3.2.3.1. Mechanical Characterization

According to the literature; it was a known fact that; after severe plastic deformation; there was a remarkable enhancement in mechanical properties of the samples. Due to limited size of the samples produced; tension tests could not be applied. However, change in hardness values were checked after each step. For that purpose Brinell hardness values were collected with 2.5mm steel indenter under 31.25 or 62.5kP load.

3.2.3.2. X-Ray Diffraction Analysis

X-ray diffraction profiles were obtained with Rigaku DMAX2200 device using Cu K α ($\lambda=1.54183\text{\AA}$) radiation. Diffraction data was collected for the (111) plane ($2\theta = 37.5^\circ - 40^\circ$) and the results were compared according to peak broadening and peak shift.

It was observed that; the peaks broaden after ECAP deformation. Hence Full Width at Half Maximum (FWHM) values was measured for the annealed (reference) case as B_R and for the ECAPed (deformed) case as B_E . Scherer formula (3.3) was used to calculate cell size.

$$t = \frac{0.9\lambda}{B \cos\theta} \quad 3.3$$

where t is the cell size in \AA , θ is the angle of the peak used and B is the structural broadening measured in radian. B can be calculated from the measured FWHM values with the use of $B^2 = B_E^2 - B_R^2$ formula.

3.2.3.3. Microstructural Characterization

Optical microscopy (OM), scanning electron microscopy (SEM) and transmission electron microscopy (TEM) techniques were used to differentiate the microstructures developed during deformation and post ECAP aging. Before OM and SEM investigations, samples were prepared with standard metalgraphic methods and etched with Keller's reagent (2.5ml HNO₃ + 1.5ml HCl + 1.0ml HF + 95ml water). Nikon Optiphot-100 optical microscope and Jeol JSM6400 SEM was used for investigations. For detailed examinations and correlation of the cell size measured by XRD; TEM samples were prepared. Samples were thinned to 60µm than electropolished in 25% nitric acid + 75% methanol solution at -30°C till to perforation. JEOL 2100 (LaB6) microscope located at TUBİTAK Gebze was used to investigate the samples. Bright field, darkfield and selected area diffraction methods were applied to characterize the samples.

3.3. Dissimilar Channel Angular Pressing (DCAP) System

Experiences obtained in the Equal Channel Angular Pressing (ECAP) studies were used to design severe plastic deformation machine for thin samples in the form of strip and sheet. System design, construction and trials were summarized in this part. Initially the appropriate method was decided and DCAP system was manufactured. Numerous DCAP die and roller surface designs were carried on to increase the deformation amount (number of successive pass) without losing surface quality. 6061Al alloy sheets having 2 mm thickness were successfully deformed up to 5 passes. Final stage of the product was characterized by using mechanical, microstructural and spectroscopical methods. In this section the procedure followed was summarized. The details of system construction and characterization methodology with preliminary results could be found in the TUBİTAK final report [65] and in the two MSc Thesis [66-67].

3.3.1. Continuous Deformation System Analysis

In literature, based on the ECAP principle, researchers have suggested, a number of different severe plastic deformation processes for thin samples. The similarity in these processes was the way that it should be applied to feed such a thin sample to severe plastic deformation (ECAP) die. The high length over thickness ratio makes the sheet unstable under compression via hydraulic press. Bending and necking might be selected deformation mode under compression and tension respectively. Processes like ECAP-Conform [49], conshearing process [50] and dissimilar angular pressing [51]; in which feeding is established via rolls instead of pressure application by the hydraulic press ram; are the main processes suggested for continuous deformation of sheet materials. The purpose of this study was to produce a simpler severe plastic deformation machine for Al alloy sheets. Hence, in the decision step, conshearing process was eliminated due to its complexity (lots of rollers and requirement of complicated motor design). ECAP-Conform have been used to deform wire / strip products. Finite element simulations with Marc software showed that ECAP-Conform process was practically difficult to construct such a system for sheet materials thicker than 1mm. Finally DCAP system, whose technical drawing shown in Figure 3.6, was constructed according to the FEM simulation criteria.

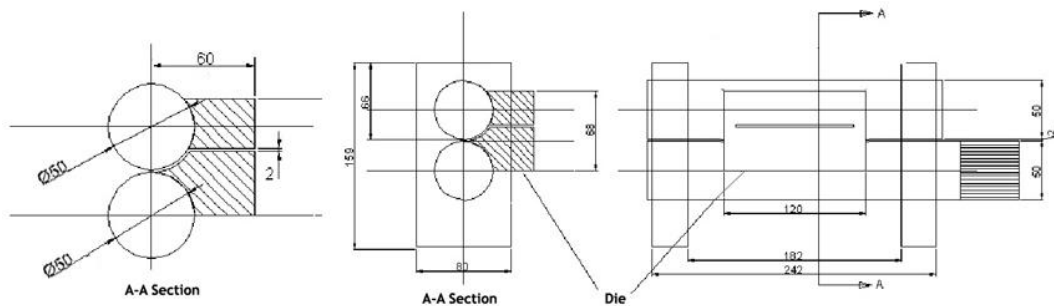


Figure 3.6 DCAP system design for continuous production

In DCAP process, determination of initial deformation amount was critical to satisfy no-crosssectional change criteria and satisfaction of ideal amount of frictional forces

during feeding. This problem that could be faced with during deformation was previously solved in the design stages with the help of FEM tools. The analysis showed that the entrance deformation applied by the rolls must not be greater than 8% to make the specimen fill the DCAP outlet channel. This is the necessity of no cross sectional change during the operation. Some results representing the successful and wrong deformation amount are given in Figure 3.7.

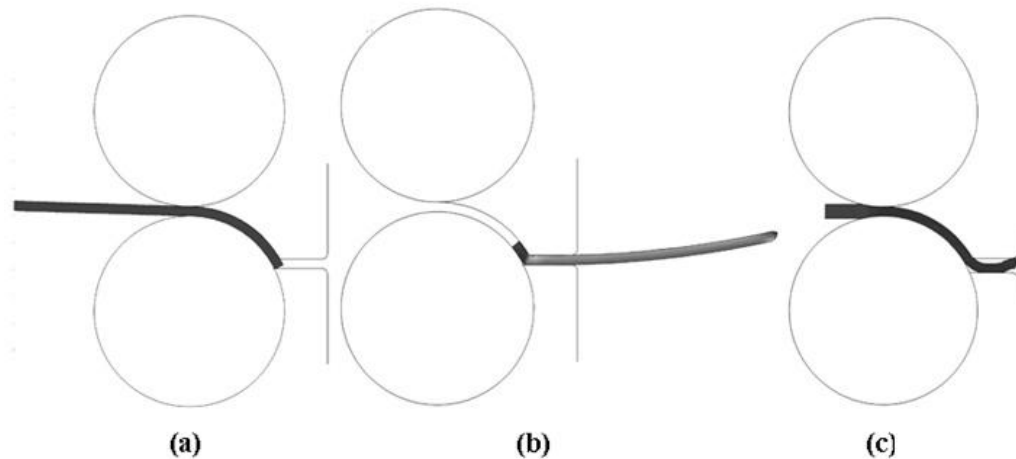


Figure 3.7 (a) Sample feeding in DCAP, (b) Sample exit with 5% reduction by inlet channel, (c) Sample exit with 20% reduction by inlet channel

3.3.2. DCAP System Manufacturing and Revisions

According to the highlights of FEM simulations; the device shown in Figure 3.8a was constructed. The system is composed of a driving motor having a constant velocity of 20cm/min, a roller set used to feed the material to system and the exit die set where the severe plastic deformation takes place. The system was capable of severe plastic deformation of 2mm thick sheet samples.

The main problem was the very small number of maximum pass attainable and the poor surface quality in the deformed sample. Hence a series of die and roller revisions has been made to increase the pass number and feedability; to improve the surface quality and applicability of mechanical testing (get rid of notch effect).The

modifications were summarized in Figure 3.9. In the final stage the system could deform samples up to 5 passes.

In the finalized version of the machine (Figure 3.8b), the feeding and guide rollers have a diameter of 50mm and a length of 120mm which have patterned and smooth surfaces. Patterned surfaces were used as easy feeding of the material and the material which belongs to that surface has been discarded. On the other hand, smooth regions were appropriate for notch free tension test specimens and microstructural investigations. Die set were made up of H13 tool steel and had an entrance die cavity of 1.9 mm intersecting to the exit cavity of 2.0 mm. with an intersection angle of 120°.



Figure 3.8 DCAP system (a) first machine (b) final design

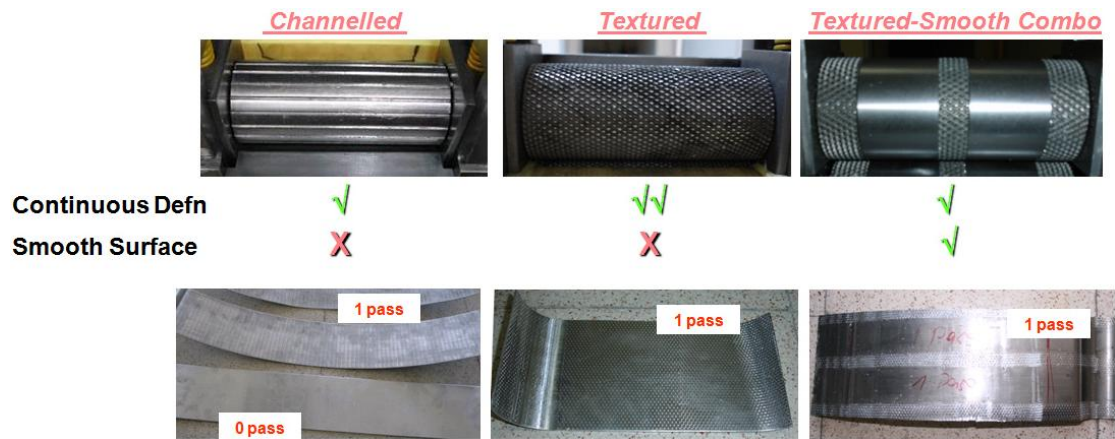


Figure 3.9 Manufacturing stages (a) channeled roller (b) patterned roller (c) semi-patterned roller

3.3.3. Material and Heat Treatment

For the systematic deformation practice; AA-6061 alloy sheets whose chemical composition given in Table 3.2 was used. Samples with the dimensions of 110x250x2mm were machined and heat treated before DCAP.

Table 3.2 Chemical composition of samples used in DCAP deformation and composition of standard AA-6061 alloy

	Al	Mg	Si	Cu	Fe	Mn	Cr	Zn	Ti
	97.9	0.736	0.583	0.187	0.318	0.043	0.145	0.022	0.028
std	95.8–98.6	0.8–1.2	0.4–0.8	0.15–0.4	<0.7	<0.15	0.04–0.35	<0.25	<0.15

One edge of the sample was further thinned to make the entrance of the sheet to the system easier. Samples were annealed in a muffle furnace at 450°C for 16hr on the onset of DCAP deformation.

DCAP deformation was performed in two different ways as longitudinal direction (LD) and transverse direction (TD). In the LD case, samples were machined in a way that the rolling direction of the sheet and the DCAP would be parallel. On the other

hand for the TD case sheets had been DCAPed, perpendicular to the sheet rolling direction. By this way the effect of material history before severe plastic deformation had been investigated.

3.3.4. Sample Characterization

3.3.4.1. Mechanical Characterization

After each deformation step; Brinell hardness values were collected from the samples with 2.5mm steel indenter. For each set of samples minimum five indentations were made and their averages were compared.

For tensile testing sub-size specimen according to ASTM B557M-02a standard [68] was cut from the deformed sheet. The specimens were tested with the use of a Schimatzu machine which has a max capacity of 10kN. Samples were drawn with a cross-head speed of 0.5mm/min and their load-elongation behaviors after each pass were investigated. For each set 2 samples from the same region were used.

3.3.4.2. X-Ray Diffraction Analysis

X-ray diffraction profiles were obtained with Rigaku DMAX2200 device using Cu $K\alpha$ ($\lambda=1.54183\text{\AA}$) radiation. Diffraction data was collected with FT step scan mode between $20^\circ - 90^\circ$ 2theta angles having 0.2° step size and 3 sec step duration. Results for the deformed and undeformed cases were compared according to peak intensities and positions.

It was observed that; the peaks broaden after DCAP deformation. For Full Width at Half Maximum (FWHM) values, curve fitting methods like Lorentz and Gaussian were used. For some peak positions, deconvolution methods were applied to separate the width related to the K_β shoulder. Approximate cell sizes were tried to be calculated by using Scherer formula (3.3). Williamson-Hall analysis [69] was also applied to distinguish the structural line broadening (β) due to size (D_{WH}) and strain (ϵ_{WH}) separately. For that purpose Williamson-Hall plot (β^* vs d^*) was drawn and size – strain values were extracted from the ordinate intercept and slope respectively (equation (3.4)).

$$\beta^* = \frac{1}{D_{WH}} + 2\varepsilon_{WH}d^* \quad 3.4$$

where $\beta^* = \beta \cos\theta/\lambda$ and $d^* = 2\sin\theta/\lambda$ being 2θ the peak position and λ the x-ray wavelength. For all analysis broadening of annealed sample was subtracted from the whole FWHM as instrumental broadening.

3.3.4.3. Microstructural Characterization

The change in microstructure during deformation was examined by microscopy techniques from macroscale down to nanoscale through optical microscopy (OM) to scanning electron microscopy (SEM) and transmission electron microscopy (TEM).

Samples were prepared from the two regions; namely the lateral surface and the cross-section. For precise sampling, Buchler precision cutter was used if required. Before OM and SEM investigations, samples were prepared with standard metalgraphic methods and etched with Keller's reagent (2.5ml HNO₃ + 1.5ml HCl + 1.0ml HF + 95ml water). Nikon Optiphot-100 optical microscope and FEI Nova NanoSem430 was used for macroscale and mezoscale investigations.

For detailed examinations and correlation of the cell size measured by XRD; TEM samples were prepared. Samples with thickness of 250 μ m were obtained by precision cutter and thinned down to 200 μ m before disc punching. The discs were further thinned to 60 μ m and dimple grinded from two sides where the center thickness remains approximately 10 μ m. Finally they were electropolished in 25% nitric acid + 75% methanol solution at -30°C till to perforation. JEOL 2100F field emission microscope located at the department was used to investigate the samples. Bright field, darkfield and selected area diffraction methods were applied to characterize the samples.

For severe plastic deformation, grain boundary types and grain orientations are important features to be checked. Electron back scattered diffraction (EBSD) technique was used observe the grain structure differences between deformed and annealed samples. Also this method was used to measure the grain sizes where the observation area was much more larger than those of TEM investigations. The SEM

samples were further polished with electropolishing. Struers LectroPol-5 system was used. A 25% nitric acid + 75% methanol solution with a flow rate of 20 hit to the sample from the 0.5 cm² orifice while 20V was applied for 15 seconds. Highly polished surfaces were investigated with EDAX-EBSD camera under SEM.

3.3.4.4. Other Characterization Methods

There are also simpler check methods to determine whether the deformation was successful or not before proceeding to detailed characterization methods. The effects of defects caused by severe plastic deformation were measured in terms of electrical conductivity and ultrasonic sound velocity variations.

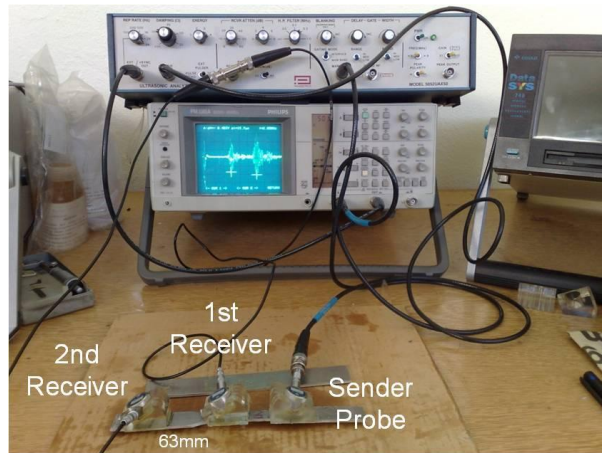


Figure 3.10 Ultrasonic sound velocity measurement setup

Sound velocity measurements were done by establishing wave transmission through one sender and two receiving probes separated at a distance of 63mm. For measurements 4 MHz, Ø=10mm longitudinal wave probes were used (Figure 3.10). The velocity change was calculated by using equation (3.5) with the use of annealed sample's travel time as the reference.

$$\Delta v = \frac{\Delta x}{\Delta t} = \frac{63}{\Delta t} \quad 3.5$$

For electrical conductivity measurements; thin wires having dimensions of 70x2x2 mm were prepared with precision cutter. Currents ranging from 0.001 to 0.01A were applied to the samples by using a nano-voltmeter in the 4 probe measurement mode. Electrical conductivity was calculated by using the equation (3.6)

$$S = 1/\rho = 1 \times 1000 / Rwt \quad 3.6$$

where S is the conductivity in Ωm^{-1} , ρ is the resistivity in Ωm , l, w, t are the length, width and thickness of the wire in mm respectively and R is the resistance in Ω , calculated from $R = V/I$ where I is the applied current and V is the voltage reading in the device.

CHAPTER 4

RESULTS AND DISCUSSION

As stated in the previous chapter, FEM studies and bulk deformation via ECAP had been studied before investigations of continuous severe plastic deformation of sheet materials. This chapter was sub divided into three sections namely: FEM, ECAP and DCAP. Some of these results were also published in the final report of research project submitted to TUBİTAK [65]. In the following sub-sections; you could find more data on ECAP microstructural characterization and DCAP characterization studies from macroscale to nanoscale in order to enlighten a way through understanding severe plastic deformation of aluminum 6061 alloy sheet.

4.1. Finite Element Modeling of ECAP

In the modeling studies; the effect of ECAP process parameters (die geometry and friction coefficient) and material properties (deformation strain hardening parameters and deformation strain rate sensitivity) on ECAP performance was questioned. The results presented here are the summary of the ones in TUBİTAK final report [65]. Also much more data and evaluation is present in a PhD thesis [70].

4.1.1. Effect of Die Geometry

The effect of die geometry on strain homogeneity throughout the sample was examined by various simulations in which Φ and ψ angles were changed. For Φ 90° and 120°; for ψ 0°, 22°, 30° and 60° were used.

A scene during simulation was captured and shown in Figure 4.1. In first sight deformation was observed to be homogeneous in horizontal section. But throughout the sample thickness (vertical section), heterogeneity was observed due to plastic strains changes. Also there was corner gap formation very similar to the death metal zone formation in extrusion process. For strain hardening materials, initially deformed regions strain hardens fast and flow slowly in the following stages. For that reason there exists difference in velocities of upper and lower regions of the work-piece. This phenomenon was the primary reason of corner gap formation and deformation homogeneity loss.

As stated above there was a change in the strain values in the vertical section. These strains were measured from top through bottom region and plotted as in Figure 4.2. Strain values made a plateau in the middle region and decreased towards side regions. Near top region, the decrease turned to be a slight increase whereas this was not observed in the bottom side. Hence maximum strains were observed in the middle regions and minimum values were seen near bottom side of the work-piece.

Another important finding was that the maximum effective strain imposed to the material was changed with die channel angle (Φ). Strain values measured in the central regions were found to be in the vicinity of theoretical values calculated by using equation 2.8. Maximum equivalent plastic strains for $\Phi = 90^\circ$ and 120° dies were calculated as 1.1 and 0.6 respectively. According to Figure 4.2 as Φ increased; maximum plastic deformation that could be reached was reduced as predicted. However, die arc angle (ψ) was only effective for the 90° die case. For wider angles; there was no significant effect of ψ on the maximum plastic strain.

The strain values obtained during simulation were lower than the theoretical calculations. The main reason was the presence of corner gap formation. In the theoretical formation, it was assumed that the sample was non-strain hardening and no corner gap was formed. However, in reality this was not the case due to different strain hardening in different regions of the sample at same time. For non-strain hardening materials, there were no velocity variations throughout the sample so no corner gap formation was possible.

When deformation homogeneity was concerned; Φ angle was much more effective than the angle ψ . Moreover for wider Φ angles; the effect of ψ angle to the profiles was very low that could be ignored. It was difficult to evaluate deformation homogeneity quantitatively. So this term was related to the width of the central homogenous region and the ratio of maximum to minimum strain. Accordingly deformation homogeneity was increased for the wider angled systems. But for this case maximum strain imposed in single pass was diminished and the process should be repeated more than twice to obtain grain size refinement. For similar homogeneity, 90° die with wider die arc angles like $\psi = 60^\circ$ might also be used with a little discount in the maximum strain. Hence die parameters were effective to optimize the maximum strain imposed in single pass with the deformation homogeneity.

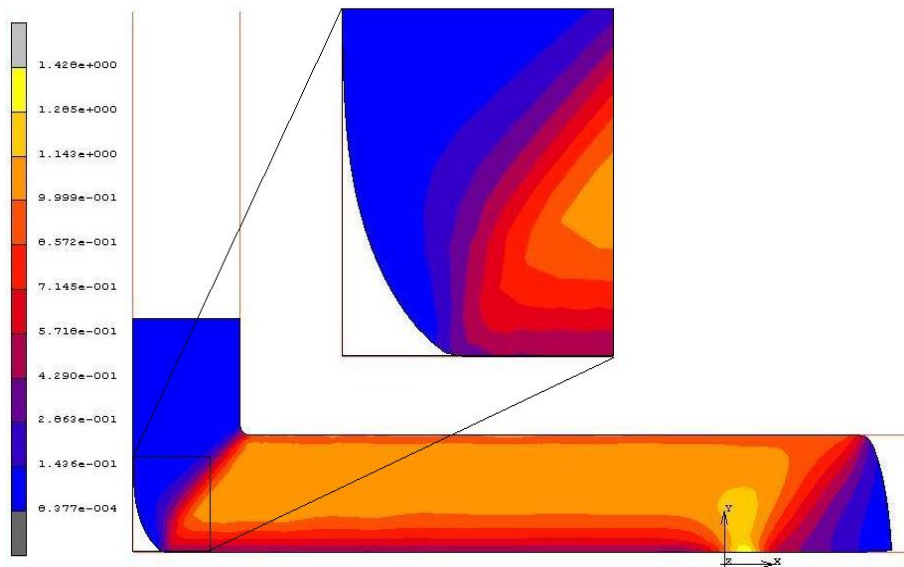


Figure 4.1 Plastic strain distribution for a frictionless simulation and corner gap formation. [65]

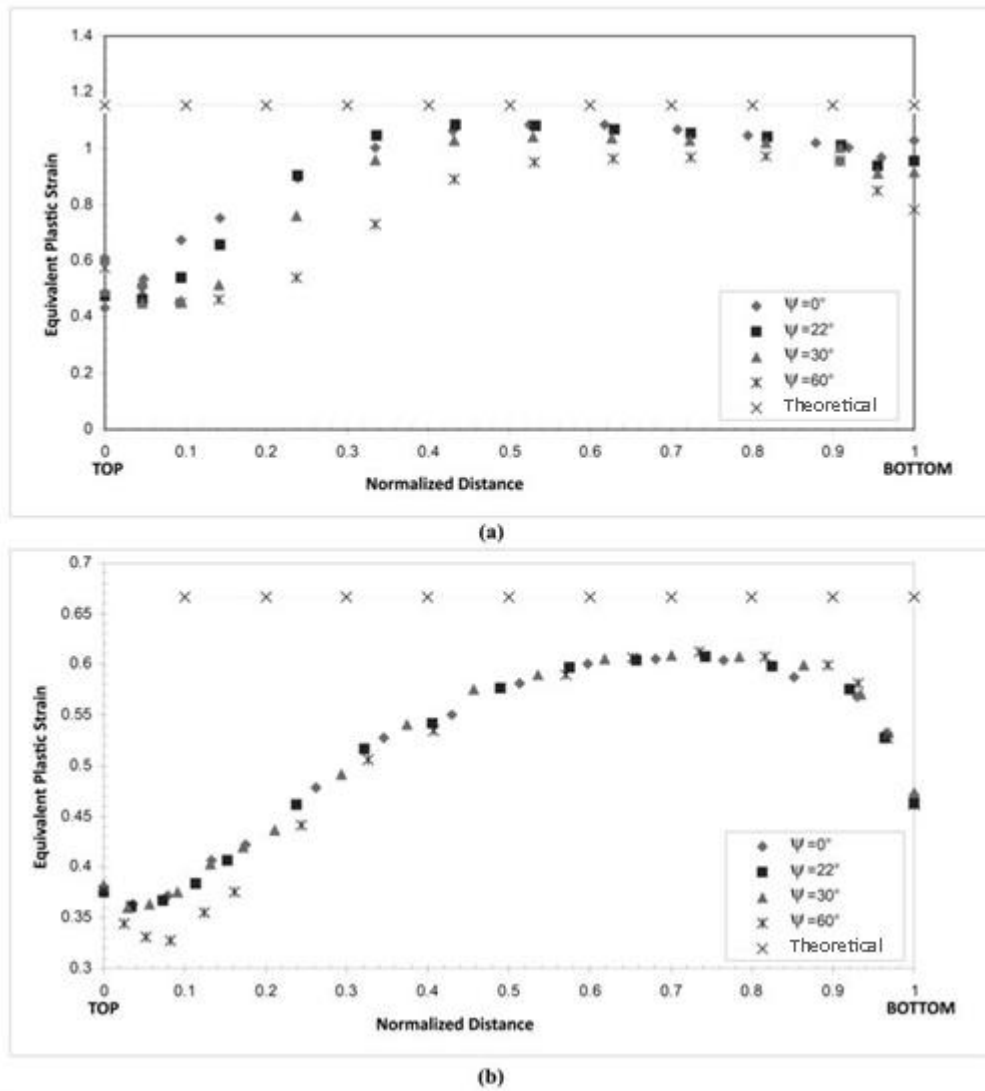


Figure 4.2 Effect of die geometry on the deformation homogeneity in the vertical section of workpiece (a) $\Phi = 90^\circ$, (b) $\Phi = 120^\circ$ [65]

4.1.2. Effect of Friction

In order to investigate the effect of friction on the deformation homogeneity, simulations were repeated for the die with $\Phi=90^\circ$. The surface friction coefficients were changed from 0 to 0.15 and simulation results were presented in Figure 4.3 and Figure 4.4.

According to Figure 4.3, as friction coefficient increased, corner gap formation was hindered and moreover above $\mu=0.1$ corner gaps were totally diminished. The corner

gap formed in the initial stages was closed after a period of time due to reverse flow of material caused by the extreme frictional forces on the bottom surfaces. Although the gap was eliminated, the deformation homogeneity was lost.

In Figure 4.4, the effect of friction on the deformation homogeneity throughout the vertical cross section was presented. For the cases where $\mu > 0.1$, the bottom surface had extremely deformed local regions due to presence of frictional shear forces. It could be stated that; some amount of friction had a positive effect on deformation homogeneity. The flow velocity difference between upper and lower portion of the sample was decreased and the effect of strain hardening was decreased. But after a point, the flow of matter in the lower parts was reversed, resulting with corner gap disappearance. According to the graph, the frictional constant μ should be in between 0.075 and 0.1 for ideal deformation homogeneity.

Another possibility to increase the deformation homogeneity was to apply slightly higher friction in the bottom surfaces as compared to upper portions. But for practical approach, it was difficult to construct such a die system with different surface roughness or greasing conditions. So the simulations for these conditions were not applied.

To summarize, these results could be drawn from the modeling studies:

The die channel angle (Φ) should be 90° or 120° . For dies with 90° angle, larger die cavity angles (ψ) should be preferred. By that way, both high plastic strains and suitable deformation homogeneity could be achieved.

Lubrication should be as better most as possible. Although homogeneous deformation was observed for friction coefficients of $\mu = 0.075-0.1$, it was practically difficult to attain such precise levels. Hence achievable lubrication was a must; because low frictional forces were found to be less harmful as compared to higher frictions.

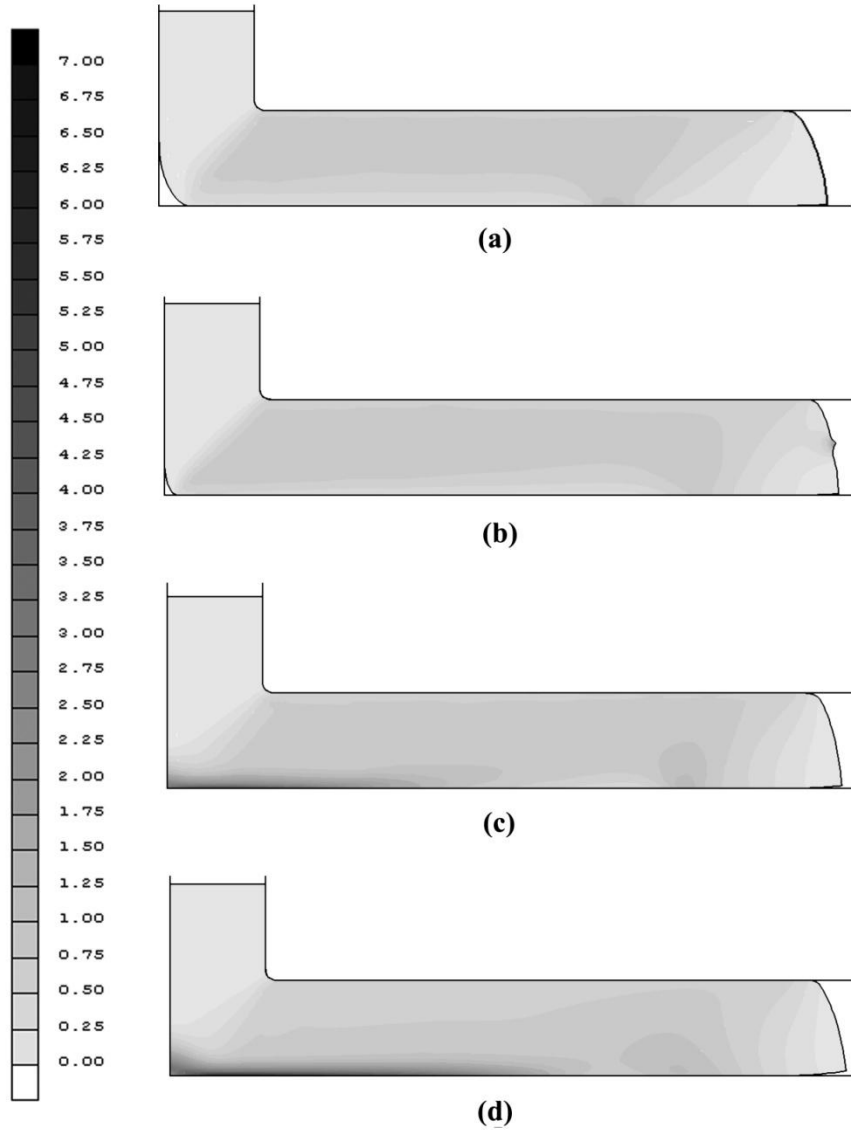


Figure 4.3 Equivalent strain distribution for different friction conditions: (a) $\mu=0$, (b) 0.050, (c) 0.100, (d) 0.150 [65]

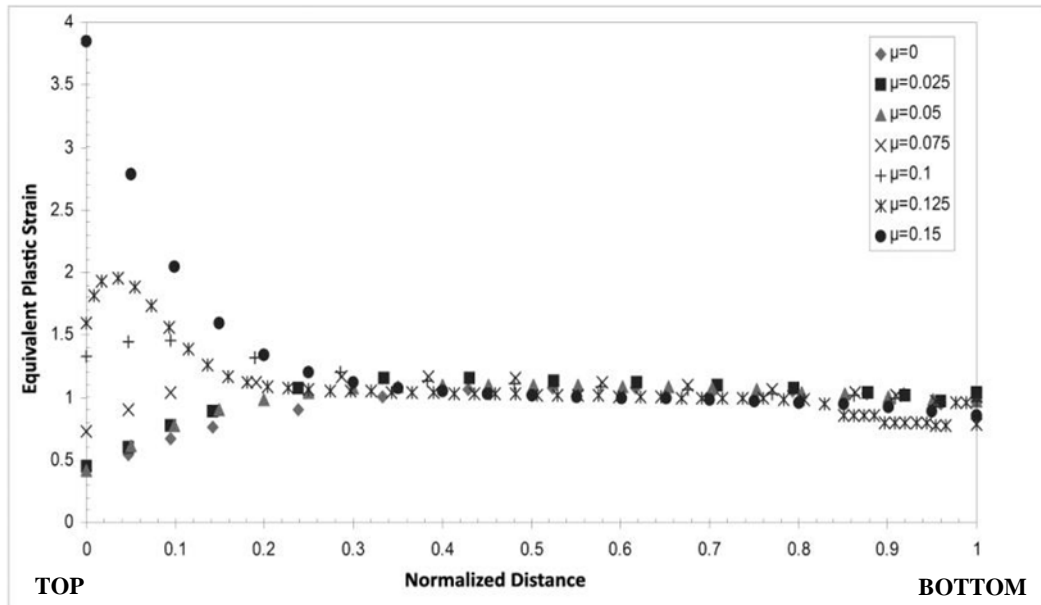


Figure 4.4 The equivalent strain distribution at the vertical cross-section for 90° die with different friction levels [65]

4.1.3. Comparison of 3D Analysis

The 3D simulation results on equivalent plastic strain distribution along the deformed body were presented in Figure 4.5. Principally 2D assumption could be checked by investigating the distribution along the depth axis. It was clearly seen from figure that the strain distribution on x-y and y-z planes were quite homogeneous.

At the same time the distribution on a plane section cut along the half depth of the workpiece was compared with 2D analysis. The comparison was presented in Figure 4.6 and similar results were obtained. 3D analysis took much more time as compared to 2D ones; so it was reasonable to assume plane strain condition and carry the simulations in 2D.

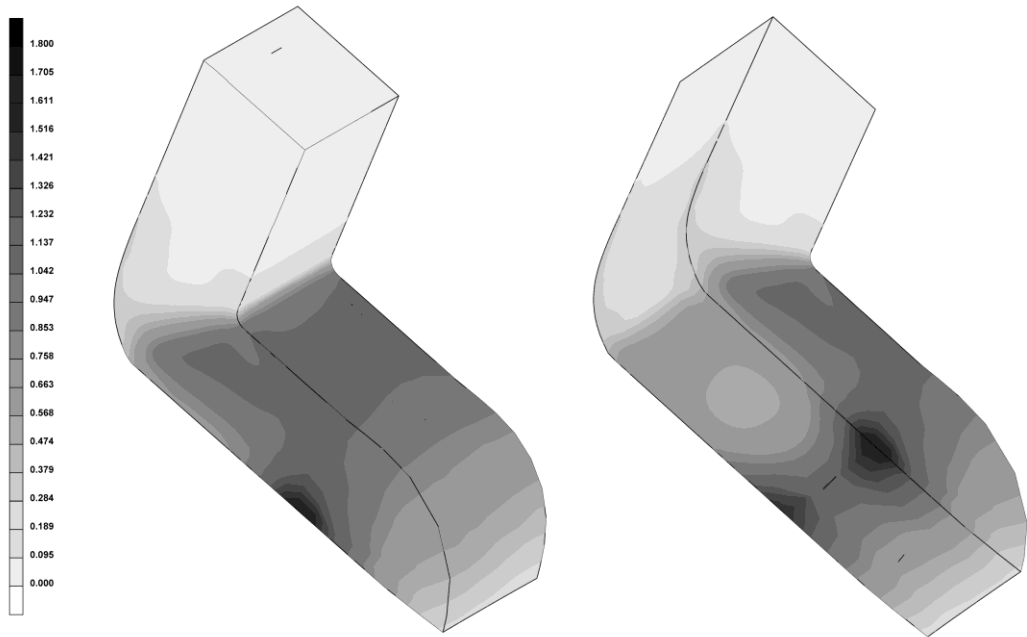


Figure 4.5 Equivalent plastic strain distribution in the workpiece during ECAP process [65]

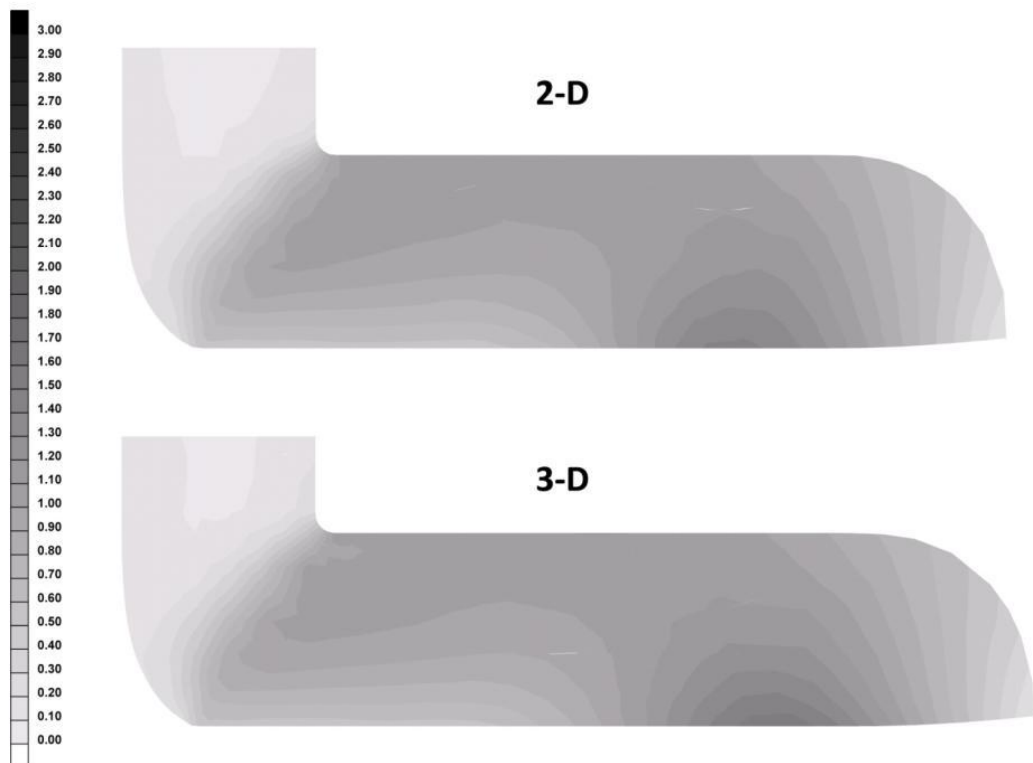


Figure 4.6 Comparison of 2D and 3D analysis in terms of equivalent plastic strain distribution along central plane [65]

4.1.4. Effect of Material Property and Corner Gap Formation Mechanism

During ECAP process in ideal case, the deformation takes place via slip in the plane that connects the inner and outer dies. But it was seen that in reality the case is much more complex. Due to flow path difference and material strain hardening characteristics, corner gap was formed. And hence the deformation zone was transformed to a volumetric one rather than a planer zone. Equivalent strain rate or equivalent stress contours might be used to define deformation zone during ECAP. According to Figure 4.7; the deformation zone was not planer; it was rather an elliptical zone. Another important finding was the difference in strain rates in the zone.

The reason for corner gap formation was determined as the velocity differences in the upper and lower portions of the deformation zone. The variation of velocity throughout the deformation zone was presented in Figure 4.8. According to the figure, the lower portion which was in contact with the die surface was flowing faster than the upper portion contact surface. Consequently corner gap formation was inevitable. This velocity difference was caused by path distance difference, friction and material strain hardening properties.

Whether the sample was strain hardening type or not, during deformation, the path flowed for the upper portion was shorter than the lower regions. But this situation did not cause a huge velocity difference whether the sample was not too thick. In literature, there was no pronounced corner gap formation for AA-6061 type slight strain hardening materials.

Friction was also effective in corner gap formation due to its strengthening the path difference effect. But the consequence might be ignored; if it was assumed that small frictional forces were affected on both upper and lower portions in similar amounts. From this point of view; a smaller increase in the upper surface's friction would be used as a corner gap elimination tool.

Consequently; the strain hardening properties of the material remained as the most important reason for flow velocity difference and corner gap formation during

ECAP. In the initial stages of ECAP; the material portions those were entering to the deformation zone had different straining histories. For example, the regions shown with A were subjected to more strains as compared to the regions B. Local hardening took place in A regions, whereas B regions remained softer. According to yielding and normality laws, length of the plastic strain velocity vector is directly proportional to the derivative of yield functional with respect to relevant stress state. Hence; the more hardened A regions would flow more slowly. This plastic strain rate difference would affect the material flow velocity leading to corner gap formation.

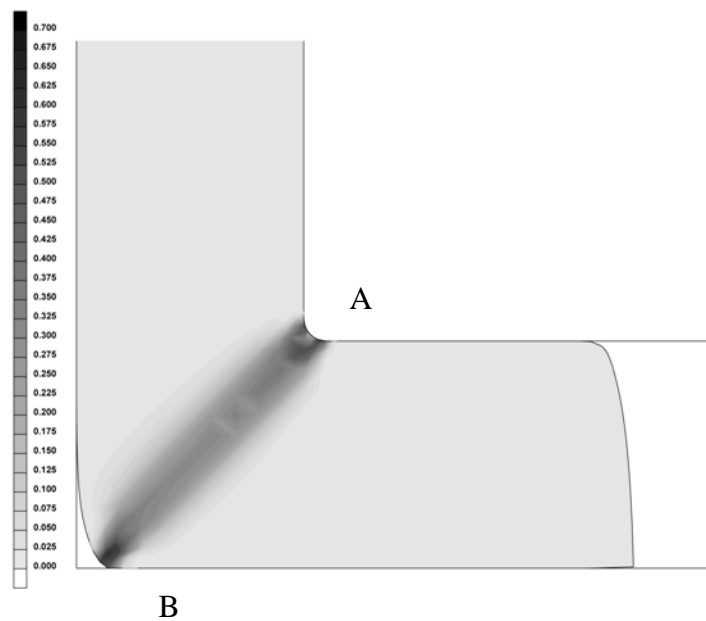


Figure 4.7 Equivalent plastic strain rate distribution during ECAP [65]

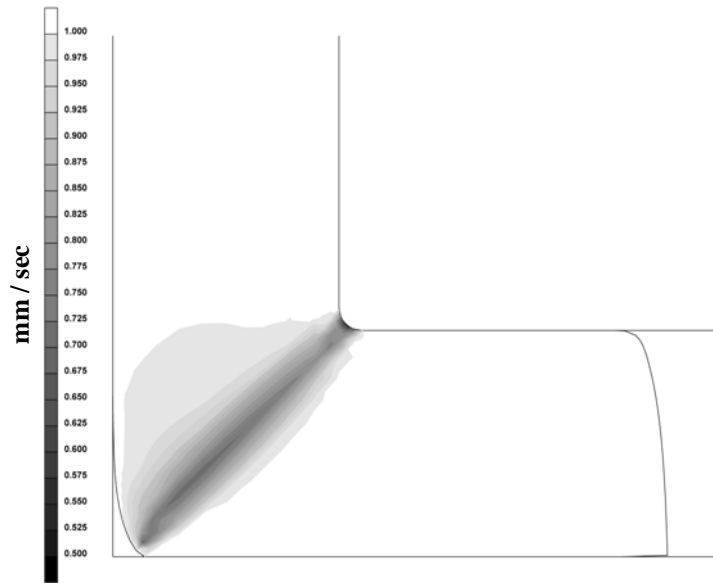


Figure 4.8 Velocity distribution during ECAP process [65]

Any reason that intensifies the local flow stress would help the formation of corner gap. The reason for that might be localized strain hardening due to different plastic history or strain rate sensitivity. Generally strain rate sensitivity was low for the strain ranges observed in room temperature ECAP processing of aluminum alloys. In this study; 1 mm/sec deformation speed was chosen and its effect on corner gap formation was neglected.

The corner gap angle was measured for different strain hardening coefficients of Ludwik law (equation (3.2)). The variation of corner gap angle (α) with strain hardening multiplier (K) and exponent (n) were plotted in Figure 4.9 as 3D graph. A second degree surface was obtained from the regression analysis. According to the graph, the corner gap (α) was related to K linearly and to n in parabolic manner. Corner gap and subsequently the deformation heterogeneity was increased with the increase of n values. Higher values of n states the cases where the yielding stress difference for upper and lower portions are increased; resulting a slower flow in the upper portions of the cross section. Hence the corner gap angle was increased.

Similar effect was true for the K parameter. But the effect of K was much less pronounced as compared to the n parameter; its effect was higher for high values of n.

Consequently, it was found that the designer should take care the material's properties beside geometrical considerations when designing an ECAP system for strain hardening materials.

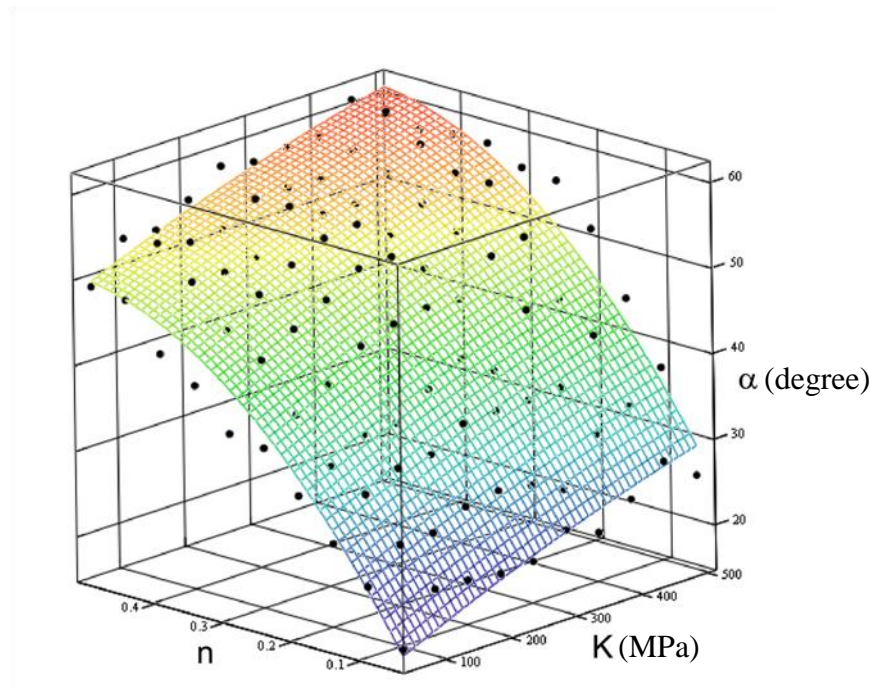


Figure 4.9 Variation of corner gap angle (α) with strain hardening multiplier (K) and exponent (n) [65]

4.1.5. Verification of FEM via experimental tests

It was known that the main mechanism in the ECAP deformation was shearing. Before ECAP deformation, the lateral surface was meshed and the change in the structure was examined. Also the results were compared with the meshing structure of simulations. In Figure 4.10, the shape change in the square meshes was presented. It was observed that all the meshes turned to be a parallelogram with a main shearing

angle of 57° - 58° . There was a slight shearing in the lower regions with 15° - 20° . In Figure 4.10c, a scene during ECAP deformation simulation was also presented. In the simulations the main shearing angle and the lower region's shearing angle were measured to be 60° and 14° , respectively. The simulation results were similar to the ones observed in real experimental case. In another study carried by Han et al., the shearing angles were measured to be 56.8° , 50.5° , 43.7° and 36.9° for the severe plastic deformation systems having 100° , 110° , 120° and 130° intersection angles [56]. Hence both experimental and simulation results for the 90° case were in good agreement with literature.

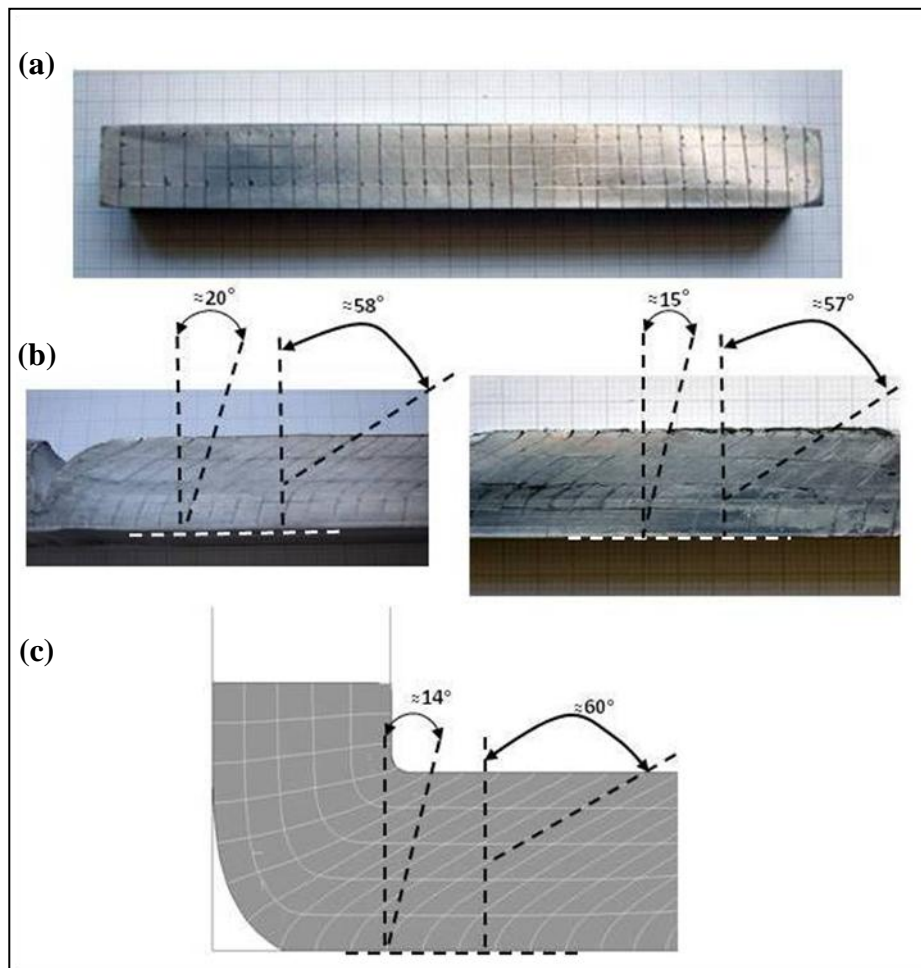


Figure 4.10 Change in the meshing structure during single pass ECAP deformation of Al-alloy in a 90° die system (a) before deformation, (b) experimental results, (c) simulation result

Mechanical performance after ECAP (ie hardness) is directly related to the strain induced during deformation. The variation of strain along the cross section was presented in the FEM analysis shown in Figure 4.2. Predicted hardness values during FEM were checked with experimental observations. The change in hardness along the vertical cross-section was scanned via Knoop microhardness. The variation was presented in Figure 4.11. Maximum hardness was obtained in the central regions. A decreasing trend was observed towards upper or bottom surfaces. Near upper side this decreasing trend was saturated and there was a slight increase in hardness; whereas the regions near to the bottom surface remained with its lowest hardness. In the same figure, predicted hardness profiles simulated for small friction cases (found to be more appropriate) were also drawn. The simulation results were parallel to the experimental findings.

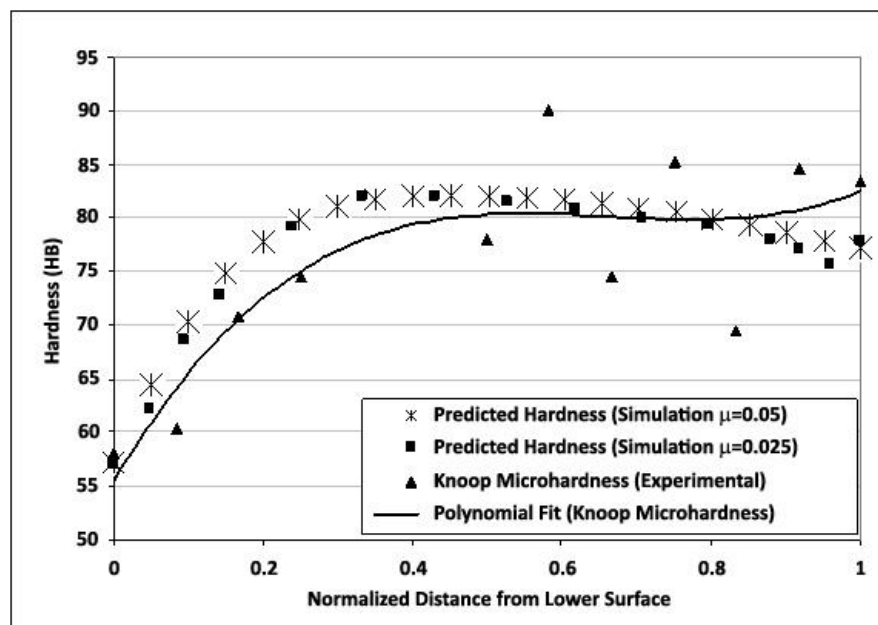


Figure 4.11 Hardness distribution along vertical cross-section after ECAP: experimental and simulation results

4.2. Equal Channel Angular Pressing (ECAP) System

This section involves the data obtained from experimental studies of ECAP processing of 2024 Al alloy. The modernization steps leading to one successful ECAP pass without any failure was explained in the experimental procedure chapter. By using the gained information, 2024 Al-alloy having $\text{Ø}=18\text{mm}$ diameter in the quenched state was successfully deformed. In this section the effect of ECAP on mechanical properties and microstructure were presented. Furthermore the effect of post ECAP aging and annealing was discussed. The details of characterization methodology had also been presented in an MSc Thesis [71] prepared within the research group.

4.2.1. Improvement in Mechanical Properties

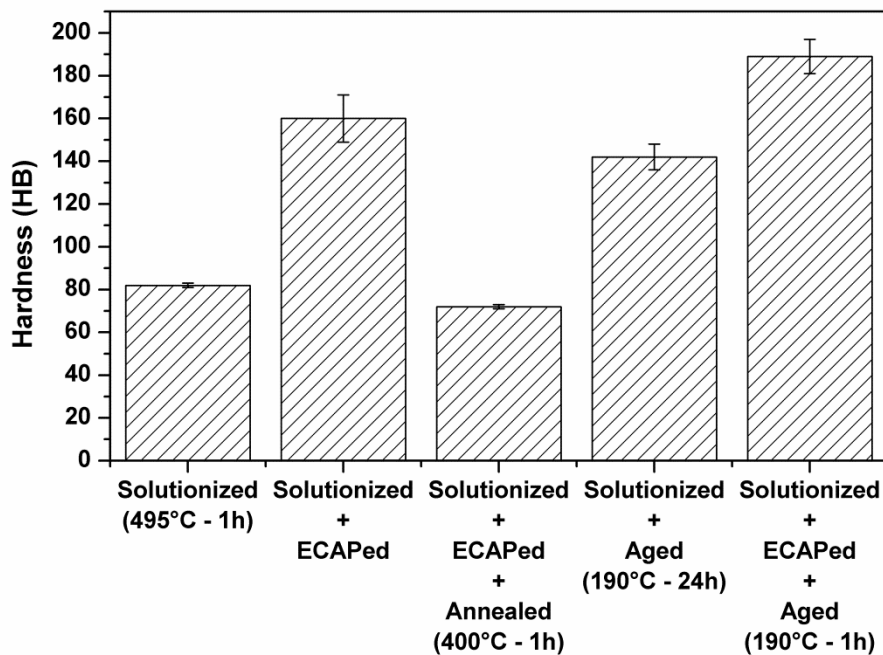


Figure 4.12 Hardness of AA-2024 alloy in different conditions

The hardness values of Al-2024 in different conditions were measured and plotted in Figure 4.12. There was a remarkable increase in the hardness of solutionized sample after one pass of ECAP. The hardness was increased to 160 HB from 82HB. Due to aluminum's high stacking fault energy nature (ie.200-260mJ/m²), full dislocations could easily glide or cross slip into tangles; leading to high dislocation density and increased hardness.

The hardness value was decreased to 72HB after post-ECAP annealing at 400°C for 1h. It was known that hardness was related to dislocation amount and distribution. Softening by annealing was predicted for metals like aluminum which has high stacking fault energy. During annealing; the dislocations would easily rearrange by recovery mechanism leading to a hardness loss.

The advantage of 2xxx type aluminum alloys was the possibility of hardness increase by aging. Maximum hardness (141HB) was obtained by aging at 190°C for 24h after solutionizing. The effect of ECAP on aging regime was checked for different temperature aging processes. Samples deformed in ECAP was aged at 80°C, 100°C and 190°C and aging profiles were presented in Figure 4.13.

Post-ECAP aging yield higher hardness as compared to the standard aging procedure. It was observed that; although the hardness that could be obtained was decreased with decrease in aging temperature; it was still above the hardness of alloy that was just aged after solutionizing. When the aging at 190°C was compared; the hardness for the ECAPed case was higher and moreover the maximum hardness was reached in shorter aging times. A maximum hardness of 141HB was obtained by standard aging procedure at a temperature of 190°C for 24h. Same values could be obtained after 1h aging by just adding a single ECAP pass between solutionizing and aging. This showed that ECAP had increased the aging kinetics. It was thought that the increased dislocation density during ECAP would yield an increase in nucleation sites for precipitation. Hence the increase in kinetics was due to the activation of heterogeneous nucleation during aging. By this way the time to reach maximum hardness was reduced. This was one of the most important advantages of ECAP processing of 2024 type aluminum alloys.

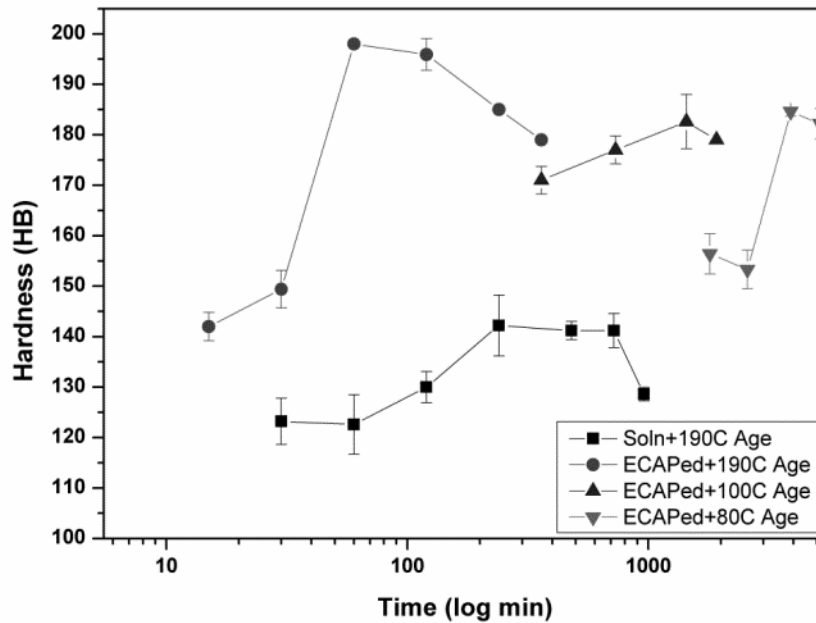


Figure 4.13 Variation of 2024 Al-alloy hardness with aging time

4.2.2. X-ray Diffraction Analysis of ECAPed Al-2024

Microstructure change and strain state caused by deformation and heat treatment steps could be controlled by x-ray peak breath analysis. The most intense peak of aluminum was obtained at $2\theta=38.3^\circ$ which corresponds to the characteristic x-ray diffraction of the (111) plane. In Figure 4.14, changes in the (111) characteristic x-ray peak with respect to different production steps were shown.

It was seen that peak broadening and/or shifting was the consequence of each steps applied. A small increase in the FWHM after solutionizing the annealed Al-2024 alloy was attributed to the residual stress accumulation. After ECAP deformation; the peak intensity was reduced and peak was broadened more. In the post-ECAP aged case the peak was shifted to the right together with the intensity drop. This was most probably due to the slight lattice parameter change as a result of aging.

Cell size after ECAP deformation was calculated as approximately 50nm by using Scherer formula (equation (3.3)) where the annealed case was used to be as reference. The X-ray data were fit by Lorentzian function and FWHM were determined as B_R and B_E for annealed and ECAPed case respectively (Figure 4.15).

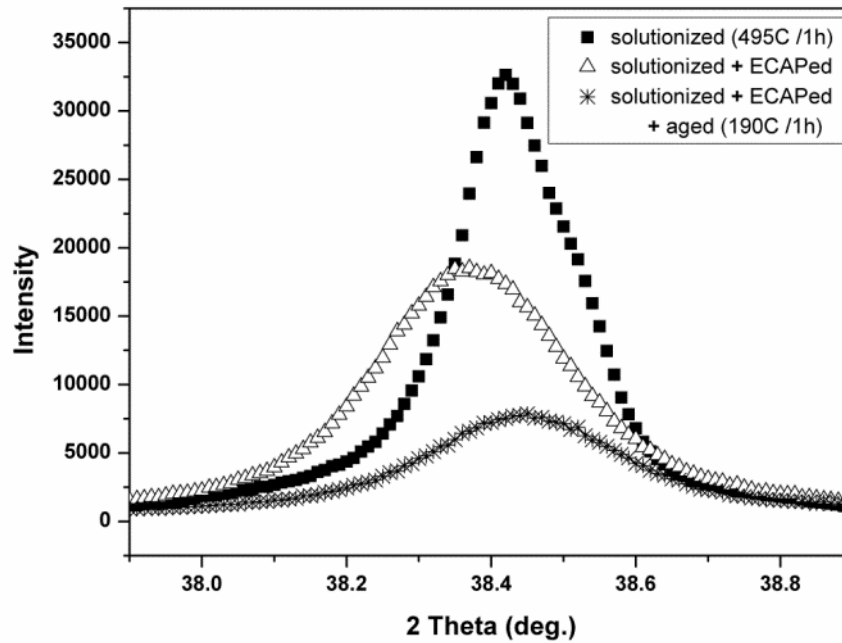


Figure 4.14 Effect of processing steps on the characteristic xray peak for (111) plane of Al-2024 alloy [72]

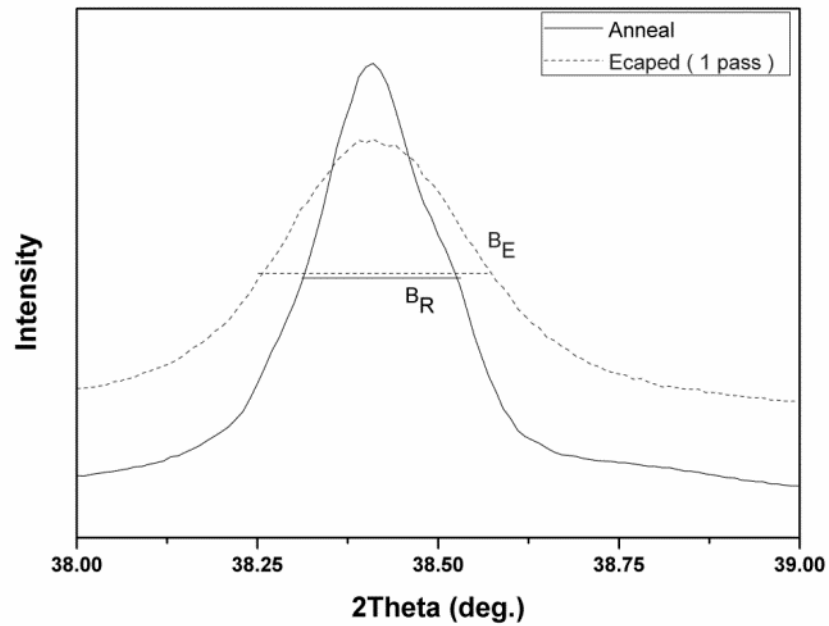


Figure 4.15 X-ray diffraction analysis for the (111) peaks of annealed and ECAPed samples

4.2.3. Microstructural Investigations

Initial condition of the Al-2024 sample was checked via optical microscopy and scanning electron microscopy techniques. The effects of ECAP and post ECAP heat treatments (aging and annealing) on the grain structure were investigated under transmission electron microscopy. The cell structure calculated with the use of X-ray analysis was correlated with the micrographs.

4.2.3.1. Optical Microscopy and Scanning Electron Microscopy Investigations

The optical micrograph of Al-2024 alloy in the solutionized temper was presented in Figure 4.16. According to the investigations the mean initial grain size was measured to be 35 μm . It was also observed that some type of inclusions were well distributed all along the sample. SEM analysis (Figure 4.17) showed that the inclusions were in the size of 1 μm and rich in Fe, Cu and Mn according to the chemical compositions

determined by EDS measurements. EDS results for the matrix and the inclusions were tabulated in Table 4.1.

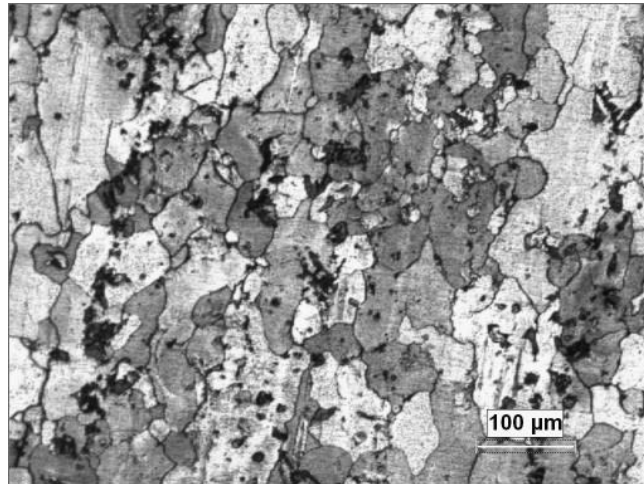


Figure 4.16 Optical micrograph of solutionized 2024 Al-alloy sample

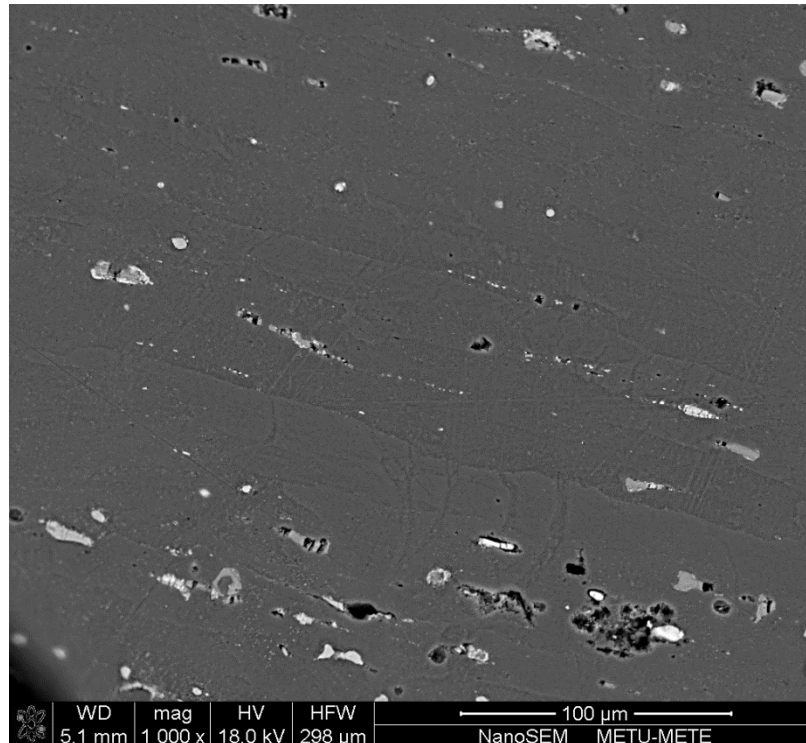


Figure 4.17 SEM micrograph of solutionized 2024 Al-alloy sample

Table 4.1 EDS analysis for inclusions distributed in solutionized AA-2024 matrix

Matrix		Inclusion	
Element	wt %	Element	wt %
Al	93.82	Al	56.86
Cu	4.25	Cu	27.91
Mg	1.93	Fe	8.54
		Mn	5.15
		Si	1.54

4.2.3.2. Transmission Electron Microscope Observations

Development in microstructure was investigated under TEM for four conditions as solutionized, ECAPed, post-ECAP annealed and post-ECAP aged. Various methods like dark field imaging (DF), selected area diffraction (SAED) and EDS were used to characterize the sample sets in terms of grain size and morphology, inclusion and precipitation level and dislocation structure.

- Solutionized Al-2024

The initial condition of the alloy was shown in Figure 4.18. It was observed that rod shaped phases were present throughout the sample. The EDS analysis was tabulated in Table 4.2. These Mn, Cu rich phases were very stable that the solutionizing did not change its morphology so it was thought that these rods were formed in the early stages of aluminum alloy's production stages like casting. Likewise there were similar observations in literature that $Al_{20}Cu_2Mn_3$ type T-phase dispersoids were extrinsically added during casting stages to control the grain size and recrystallization [73].

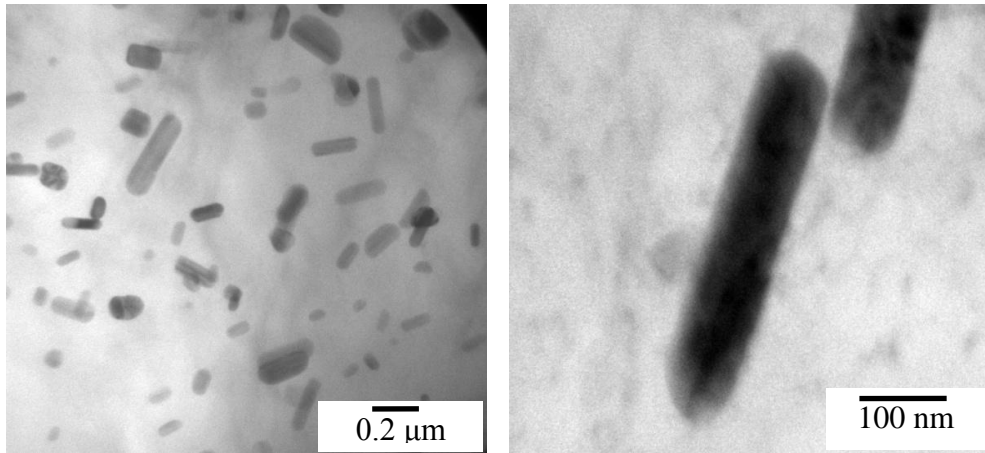


Figure 4.18 AA-2024 samples in the solutionized condition

Table 4.2 Chemical composition of rod shaped phases

Element	wt %	at %
Al	86.81	93.15
Cu	4.70	2.48
Mg	0.69	0.82
Mn	7.79	3.55

- ECAPed Al-2024

The microstructure obtained after single ECAP pass could be observed from the TEM micrographs in Figure 4.19. Also the selected area diffraction pattern was presented. It was seen that the spots were arranged along rings which was the indication of small grain sizes oriented along different planes. White tiny features in the sizes of 50nm shown in the dark field image (Figure 4.19b) were the consequence of grain refinement during ECAP deformation. This finding was also well consistent with the X-ray analysis as discussed above.

During the investigations, it was observed that obtaining a sharp grain boundary image was impossible in this highly strained condition. Even more dislocations were tend to arrange together as forests along bands and some of them were tangled

around T-phase dispersoids as seen from Figure 4.20. Hence besides grain refinement, dislocation-dislocation and dislocation-particle interactions were responsible for the mechanical performance improvement in ECAPed Al -2024 alloy.

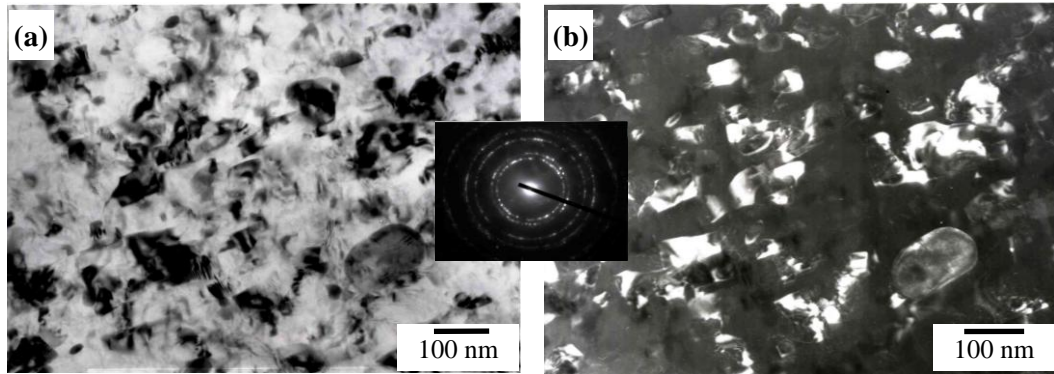


Figure 4.19 ECAPed AA-2024 samples (a) BF image, (b) DF image

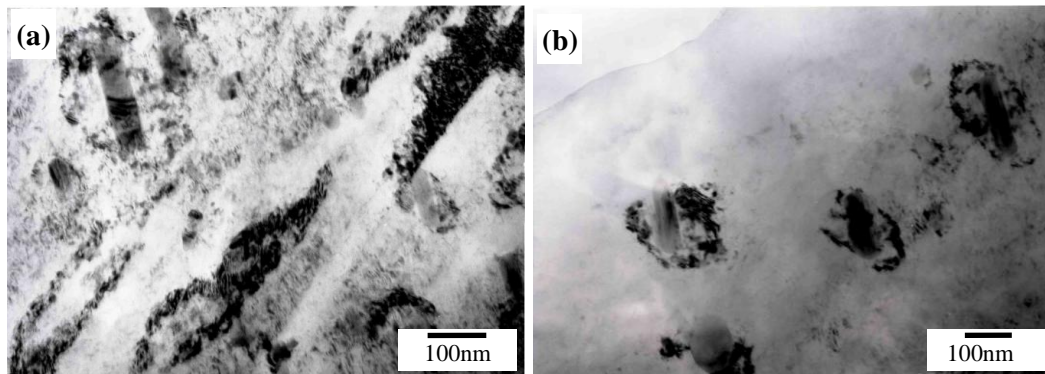


Figure 4.20 Dislocation arrangements in ECAPed Al-2024 alloy

- Post ECAP Annealed Samples

After ECAP deformation, grain boundary observation became difficult due to the high strain field regions formed by the increased dislocation density. A post ECAP annealing process was applied to activate recovery and recrystallization mechanisms and to achieve grain boundary images. It has been proposed in the literature that

ECAPed samples had thermal stability to preserve the grain size attained. In Figure 4.21, some TEM micrographs for post ECAP annealed samples were attached. It has been observed that although grain boundary contrast was obtained, there was a slight increase in the cell size by annealing the samples at 400°C for 1 hour. The cell sizes were in the range of 200 – 500 nm whereas it was approximately 50 nm before annealing. Hence there was a contradiction with literature in terms of thermal stability of ECAPed samples. Detailed investigations showed that the researcher's thermal stability argument was for the samples deformed more than 4 pass. This interesting finding showed that although grain refinement took place in the first ECAP pass; the requirements for thermal stability (HAGB formation and impinging during thermal treatment) could not be attained. In the meantime; it was also observed that there were still some dislocations remained in the cell structure which was the indication of incomplete recrystallization process.

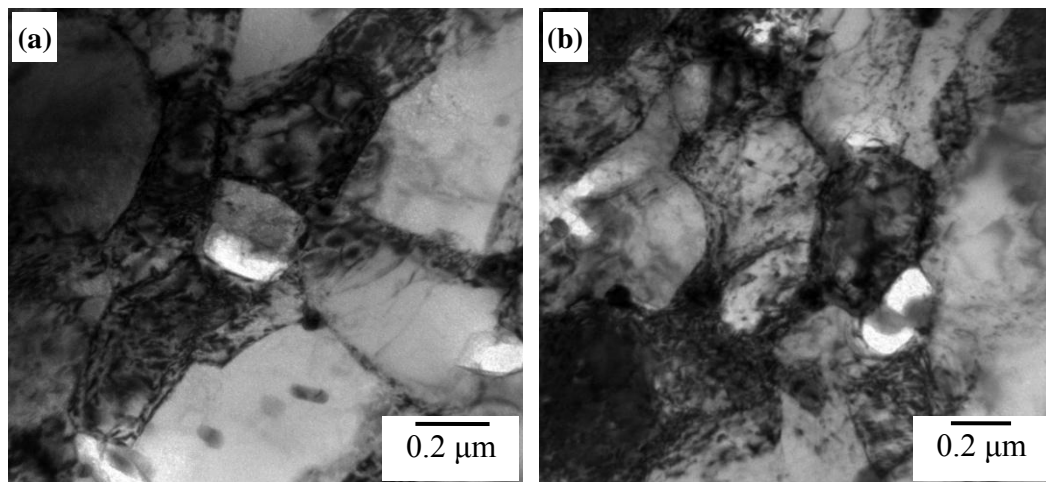


Figure 4.21 Post-ECAP annealed AA-2024 samples

- Effect of Post ECAP aging on Al-2024 Alloy Samples

Effect of aging on the mechanical performance was presented in Figure 4.13. In the ECAPed samples; higher hardness could be achieved in shorter time periods. Micrograph for Al-2024 alloy that was subjected to aging treatment was presented in

Figure 4.22a. Sharp rod shaped θ' precipitates could be clearly observed in the matrix. It has been proved that the precipitates were Al_2CuMg (θ') from the EDS analysis. The TEM image for the ECAPed and aged case was also shown in Figure 4.22. When two figures were compared; the precipitates in the post-ECAP aged samples were much smaller than the ones of standard aged samples. It should be noted that the photograph in Figure 4.22b was taken at higher magnifications. High dislocation density obtained during ECAP had a positive effect on increasing the nucleation sites for precipitates; leading to well distributed tiny precipitate formation. This is one of the most important improvements of ECAP processing.

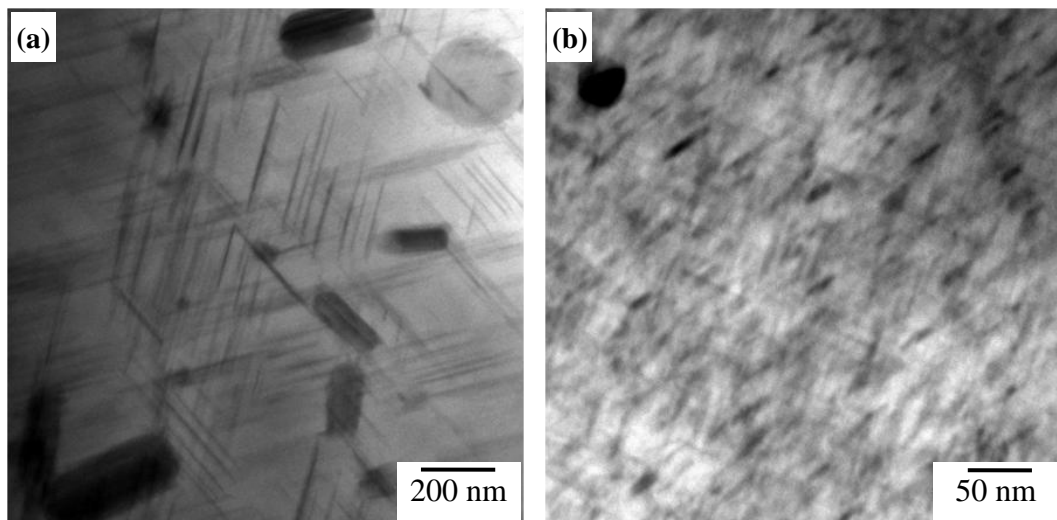


Figure 4.22 TEM BF of AA-2024 (a) aged at 190°C, (b) one pass ECAPed and aged at 190°C

4.3. Dissimilar Channel Angular Pressing (DCAP) System

This section involves the experimental data obtained during DCAP processing of 6061 Al alloy sheets. The modernization steps leading to five successful DCAP pass without any failure were explained in the experimental procedure chapter. 6061 Al-alloy sheets having the dimensions of 110x250x2mm in the annealed state were successfully deformed by using the gained information. In this section the effect of DCAP on mechanical properties and microstructure is presented. The effect of

previous history of the material is shown by deforming along longitudinal direction (LD) or transverse direction (TD). Furthermore the influence of DCAP on sheet's final texture and electrical conductivity properties are discussed.

4.3.1. Effect of DCAP process on Mechanical Performance of Alloy

The deformation behavior of DCAP could be predominantly characterized as shear deformation which leads to the equivalent true strain. In metal forming, it is usual to analyze the variations in the mechanical properties with correlation of effective strain. The effective strain attainable from DCAP can be expressed in terms of the passage number (N), the thickness ratio (K), and the oblique angle (Φ) by the equation (4.1) derived by Lee et al. [51]. Table 4.3 summarizes the strain values attained for each pass through a 120° die for K= 0.950 (1.9/2.0).

$$\varepsilon = \frac{2N}{\sqrt{3}} K^2 \cot \frac{\phi}{2} \quad 4.1$$

Table 4.3 Strain values imparted to specimen for each DCAP pass

N	1	2	3	4	5
ε	0.602	1.203	1.805	2.407	3.008

DCAP system's unique property was the higher strain values attainable by means of shear deformation in a single pass. A sample snapshot from FEM analysis was presented in Figure 4.23, where there was a variation of strain along the sample surface from 0.3 to 0.6 for one passage. This high strain values might only be reached by rolling with extreme percent reduction ($\approx 40.5\%$).

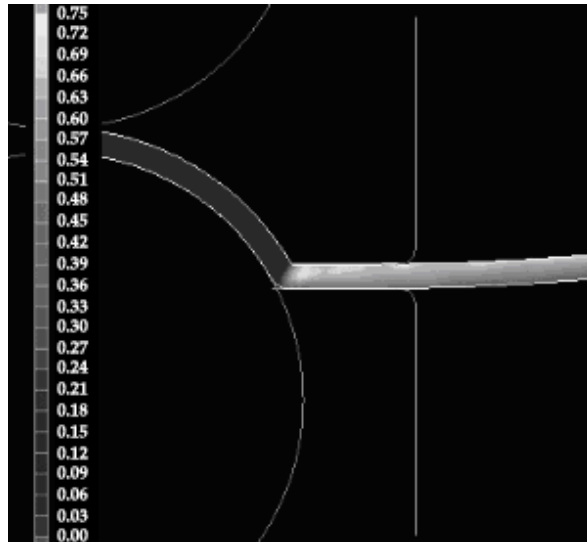


Figure 4.23 FEM analysis of strain variation on strip surface during DCAP processing [74]

It was thought that, since there was no cross-sectional change, all the energy was consumed for dislocation creation, and hence better mechanical properties could be obtained. The improvement in the hardness was presented in Figure 4.24. The variation of hardness through sheet thickness was ignored since the tiny variations in the microhardness were in the limits of experimental testing error.

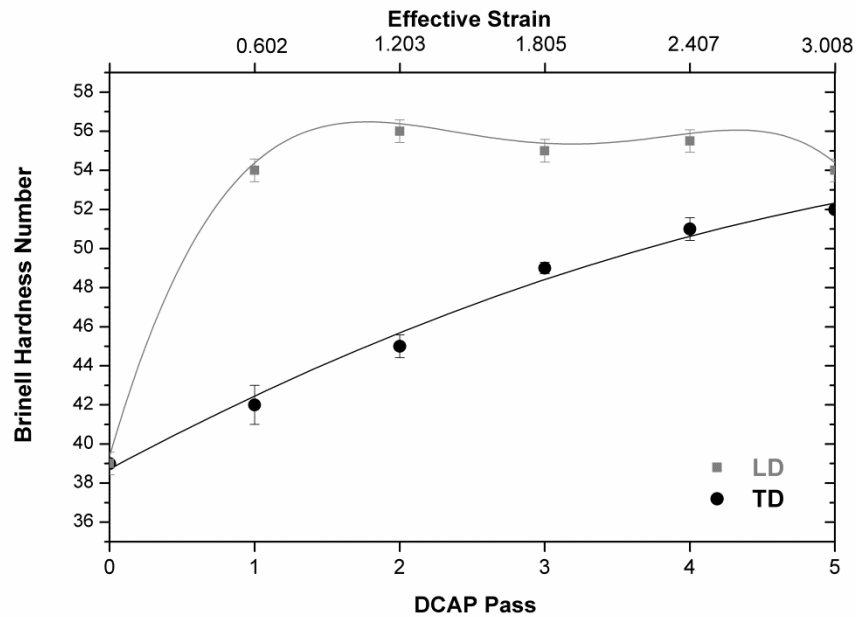


Figure 4.24 Variation of sample hardness with DCAP passes number and accumulative strain (0 pass corresponds to annealed condition)

It was observed that the hardness was increased with increasing DCAP pass. There was a continuous improvement in the TD case; whereas the pronounced improvement for the LD case was achieved in the first pass ($\approx 40\%$) and the hardness increase was saturated in the following passes. These results showed the importance of material's previous deformation history for DCAP processing. Hardness is known as the resistance of material to the localized plastic deformation. For the LD case, maximum hardness was attained after second pass which corresponds to accumulated strain level of 1.2, meaning that the localized plastic deformability was saturated. This critical level was also reported by Lee et al in his research [51]. However the accumulated strain level for 6061 Al sheets could be increased with DCAP using TD route. By that means further shaping of the sheet material was thought to be under less forming stresses.

DCAPed samples performance under tension conditions was presented in Figure 4.25; a pronounced improvement in yield strength could be observed in these graphs. After single DCAP pass, the yield strength of the material increased from 45 to 130

MPa for the TD case and from 114 to 173 MPa for LD case. The improvements were 188% and 52% for the TD and LD cases respectively. This increase might possibly due to grain size refinement as stated by Hall-Petch relation.

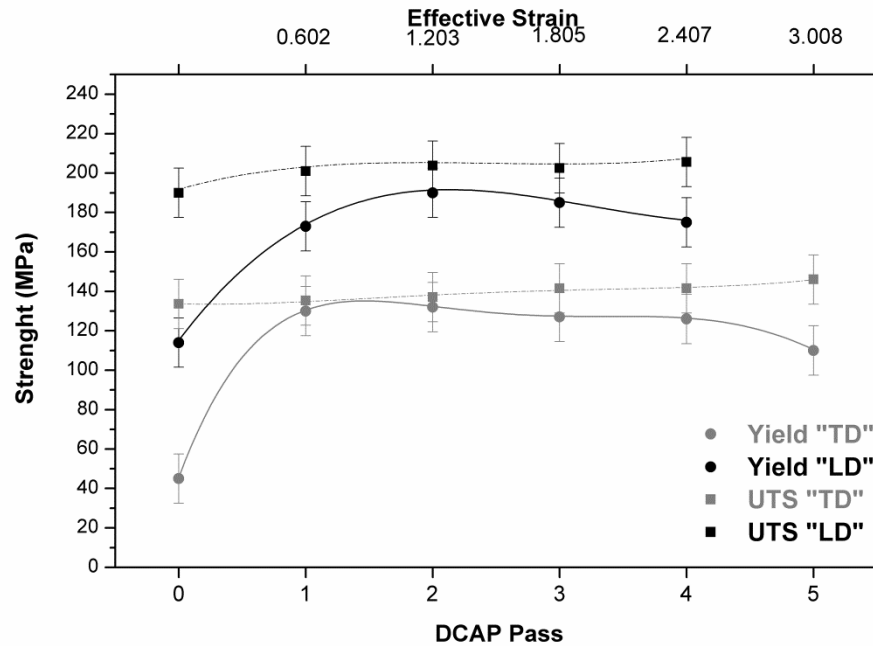


Figure 4.25 Improvement in the strength of AA-6061 sheets via DCAP processing

Materials' stress-strain behavior was presented in Figure 4.26. It was observed that the strength was increased as the DCAP pass number increased without so much ductility loss. In the LD case, ductilities were found to be in the range of 0.25 for annealed samples and 0.195 for one DCAP passed samples. For the TD case; these values were 0.36 and 0.195 respectively. Although the ductility loss for the TD case was more than the LD case; the ductilities of the samples after 3rd and fifth passes were much higher than the ones for the LD case. There was still higher ductility (0.13) for the 5-pass DCAPed samples along TD. The excessive loss in ductility (ie. 0.095 in 3rd pass) for the LD case was related to the saturation in the accumulated strain level of 1.2 as discussed above. Moreover,

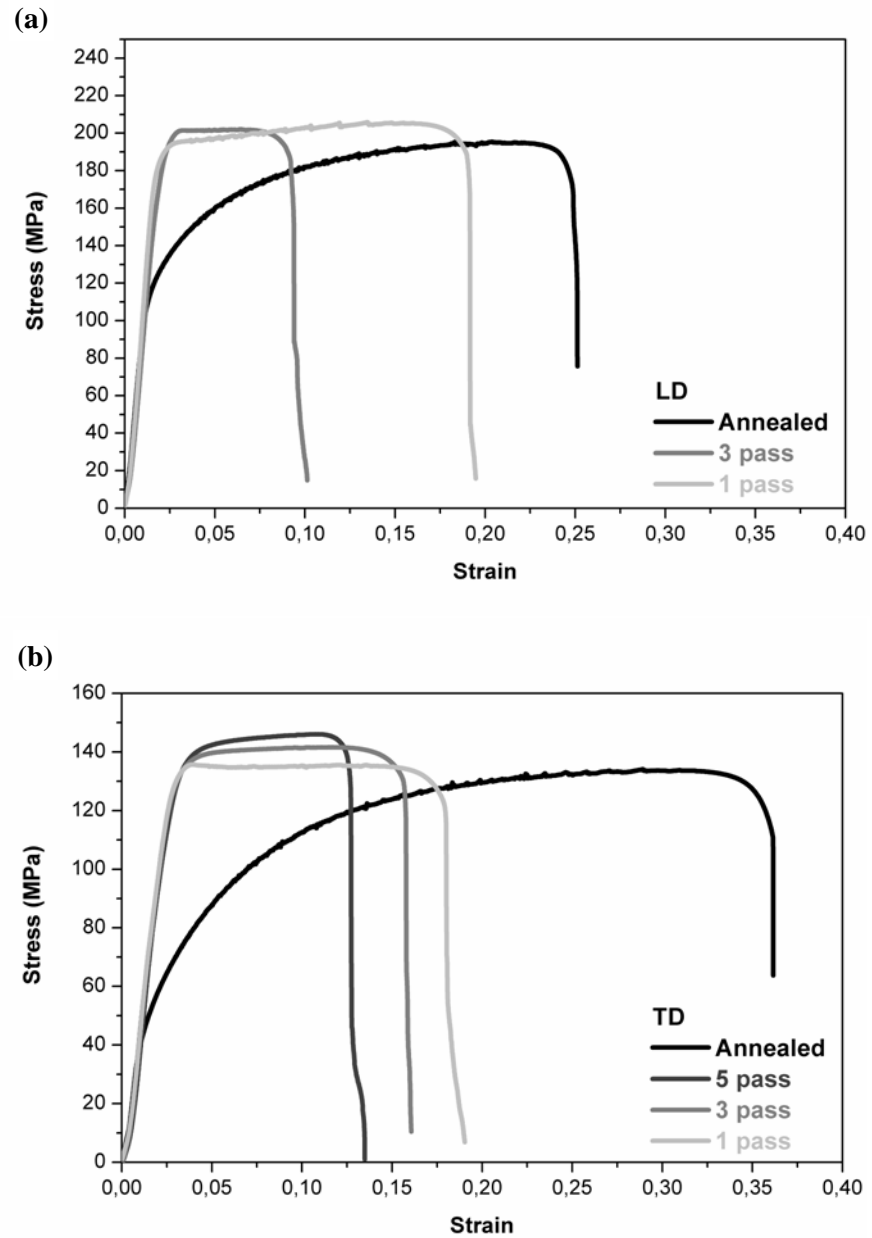


Figure 4.26 Strengthening behavior of AA-6061 sheets via DCAP processing (a) along LD, (b) along TD

An interesting finding was the observation of perfectly plastic behavior in the material after 1 and 3 passes. However, this behavior was changed towards strain hardening in the following DCAP passes as the dislocation density and the probability of dislocation interaction during tension increased.

As discussed in literature, the cellular structure generated as a result of dislocation tangle first transforms to a granular one, which later will be transformed to the UFG by the partial annihilation of dislocations of opposite signs at the cell boundaries when further deformation is applied. Simple models for grain refinement during ECAP were also modeled by researchers considering grain rotation and increase in high angle boundary with increase in number of pass. Hence, the ultrafine grain structure could be obtained only when both the accumulative strain and the strain per each passage imparted to the specimen exceeds certain values. When the specimens were processed through the 120° channel, the accumulative strain level to attain the ultra-fine grains was found to be ≈ 2.4 which corresponds to 4 pass. So this mechanism could possibly be the fact of easy dislocation glide and perfect plastic behavior in the early deformation passes and the strain hardening in the later passes.

4.3.2. Results of X-ray Diffraction Analysis

X-ray analysis had always been a quick check method in the production sequence. For single phase materials microstructural features could be controlled by examining the peak intensities and broadenings. Figure 4.27 showed the comparison of the x-ray peak spectrums of annealed and DCAPed 6061 Al alloy samples. It was observed that the intensities of (200) plane was dominant with (311) plane. According to the ICDD card# 4-0787, aluminum's most intensive diffraction peak should be obtained for the (111) plane. Hence this was the indication of a texture along (200) and (311) remained from the sheet formation history.

Along the deformation history, the intensities and peak broadenings tend to change with DCAP deformation. The changes in the maximum intensities and peak broadening values obtained from curve fitting methods like Lorentz and Gaussian were tabulated in Table 4.4. Generally there was a tendency of intensity decrease and peak broadening for all peaks except the (111) series. When intensities of (200) plane

was compared, it was highest in the annealed case and it started to decrease with DCAP deformation till 2 pass. The intensities for the samples deformed more, seemed to fluctuate between the intensities of annealed and the 2 DCAP passed samples. The variations of (111) intensities were complicated but compared to the annealed sample, it was the only peak whose intensity was increased with deformation being the 3 DCAP passed sample as the highest. This was the indication of texturing and re-arrangement along (111). It was a rule of thumb that for FCC materials the major deformation takes place on the {111} plane family along [110] direction with slip. Crystallographical arrangements during deformation that activates the major slip system by increasing the number of (111) planes should be predicted; hence the deformation mechanism in severe plastic deformation methods like DCAP was pure shear.

As discussed previously the mechanical performance was strongly dependent on the previous deformation history before DCAP. X-ray diffraction profiles for the samples which deformed with the TD-route were presented in the Figure 4.28. In this case, there was a sharp intensity decrease for (200) plane after the third DCAP pass where the intensity for (111) plane was higher than that of (200). After fifth DCAP pass no preferred orientation remained in the sample. When DCAP deformation directions were compared; the TD direction was more effective in activating the slip on (111) plane and maintaining a more uniform structure and isotropic properties. Also it should be noted that this texturing in TD mode was the reason of perfect plastic behavior in the material after 1 and 3 passes.

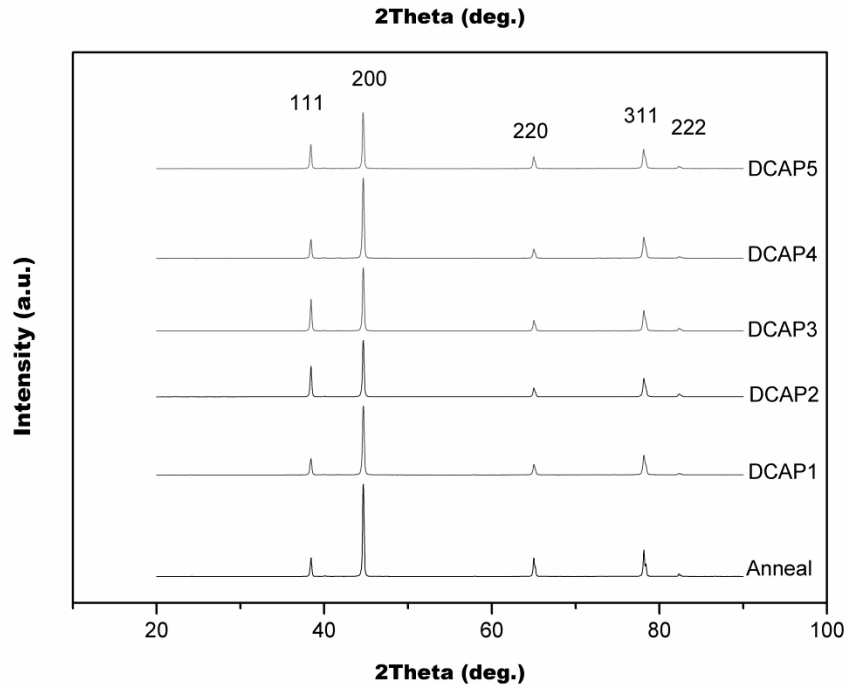


Figure 4.27 XRD patterns of AA-6061 sheet DCAPed along LD after annealing

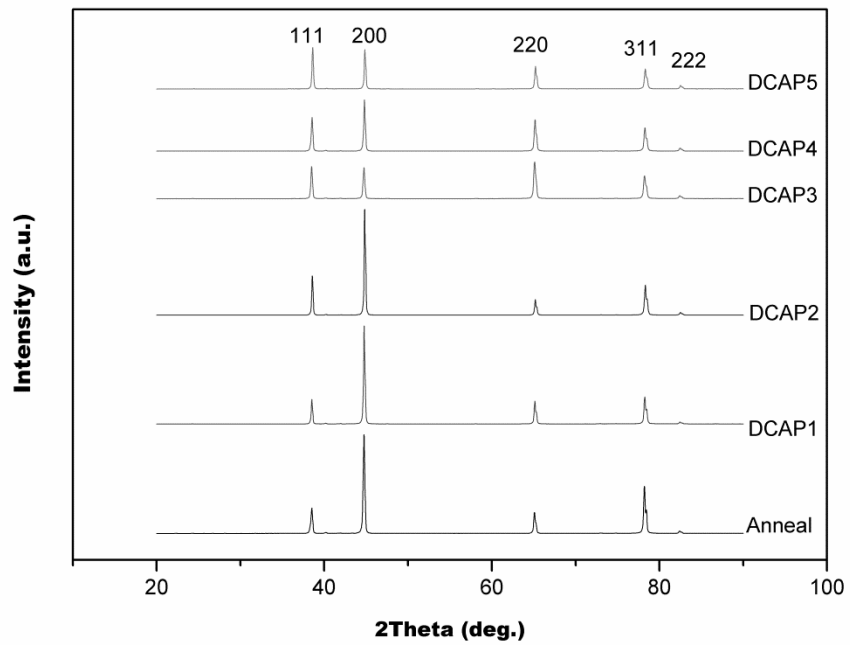


Figure 4.28 XRD patterns of AA-6061 sheet DCAPed along TD after annealing

Table 4.4 Variation of XRD peak intensity and broadening with DCAP processing

DCAP along LD							
		Anneal	DCAP1	DCAP2	DCAP3	DCAP4	DCAP5
(111)	Intensity	7499	6553	12184	12648	7528	9609
	Broadening (deg)	0.18947	0.22253	0.19541	0.18932	0.20188	0.19214
(200)	Intensity	31739	23663	19429	21801	27653	19289
	Broadening (deg)	0.19767	0.22508	0.21597	0.21476	0.22126	0.20867
(220)	Intensity	4520	2607	2166	260	2253	2944
	Broadening (deg)	0.18251	0.23991	0.22094	0.22433	0.23819	0.20376
(311)	Intensity	5524	4082	3814	4280	4383	3938
	Broadening (deg)	0.18757	0.25351	0.24265	0.24174	0.25873	0.23132
(222)	Intensity	590	301	580	538	348	438
	Broadening (deg)	0.14669	0.30704	0.25703	0.24844	0.27009	0.24368
DCAP along TD							
		Anneal	DCAP1	DCAP2	DCAP3	DCAP4	DCAP5
(111)	Intensity	17302	16216	25851	21221	22272	27417
	Broadening (deg)	0.18204	0.17065	0.16564	0.20387	0.20076	0.1739
(200)	Intensity	56600	56099	60195	17805	29443	22199
	Broadening (deg)	0.17494	0.18787	0.18257	0.22722	0.20497	0.19657
(220)	Intensity	8534	9242	6302	14906	12754	9103
	Broadening (deg)	0.15279	0.16632	0.17675	0.22761	0.20161	0.18539
(311)	Intensity	16328	9361	10460	7893	8102	6958
	Broadening (deg)	0.15579	0.19124	0.2045	0.24423	0.22099	0.21395
(222)	Intensity	897	665	948	1088	1089	1225
	Broadening (deg)	0.20249	0.21529	0.22991	0.24114	0.22612	0.21305

In Table 4.4, the variations in peak broadening were also presented. Broadening values were calculated by taking the broadening value of the annealed sample as the reference. Due to texture evolution and reconstruction of (111); some peaks did not broaden and these were excluded from size-strain calculations. It was known that leaving instrumental broadening aside, three main factors affect the peak breath: presence of defect structure, size of substructure and internal micro-strains. As the sheet was deformed by DCAP, the strain imposed to the material increased; but the

increased defect (dislocation) density might be fluctuating by dislocation reactions and annihilation processes to form UFG structure. In the meantime the cell size and micro-strain amount was thought to be fluctuating also. In order to distinguish these two cases from each other, Williamson-Hall plots were drawn and presented at Figure 4.29. The typical anisotropic behavior of deformed FCC metals was clearly seen from this plot. The investigation was performed with the use of 111/222 reflections as the first and second order reflections, from this available data. Size (D_{WH}) and strain (ϵ_{WH}) values were extracted from the ordinate intercept and slope respectively and tabulated in Table 4.5. According to the table it was observed that the main part of broadening was due to strain effect in the early stages of DCAP along LD and as the DCAP pass number increased, the strain was decreased and the size effect was increased by obtaining finer structure. This finding might be the proof of dislocation reactions and arrangements to form UFG during the processing cycle. In the case of DCAP along TD; the peak broadening were less and eventually the micro-strain values were too low and the sub-structure sizes were high. This indicates that DCAP along TD was less effective in UFG formation as compared to DCAP along LD; but it might be preferred due to its texturing effect.

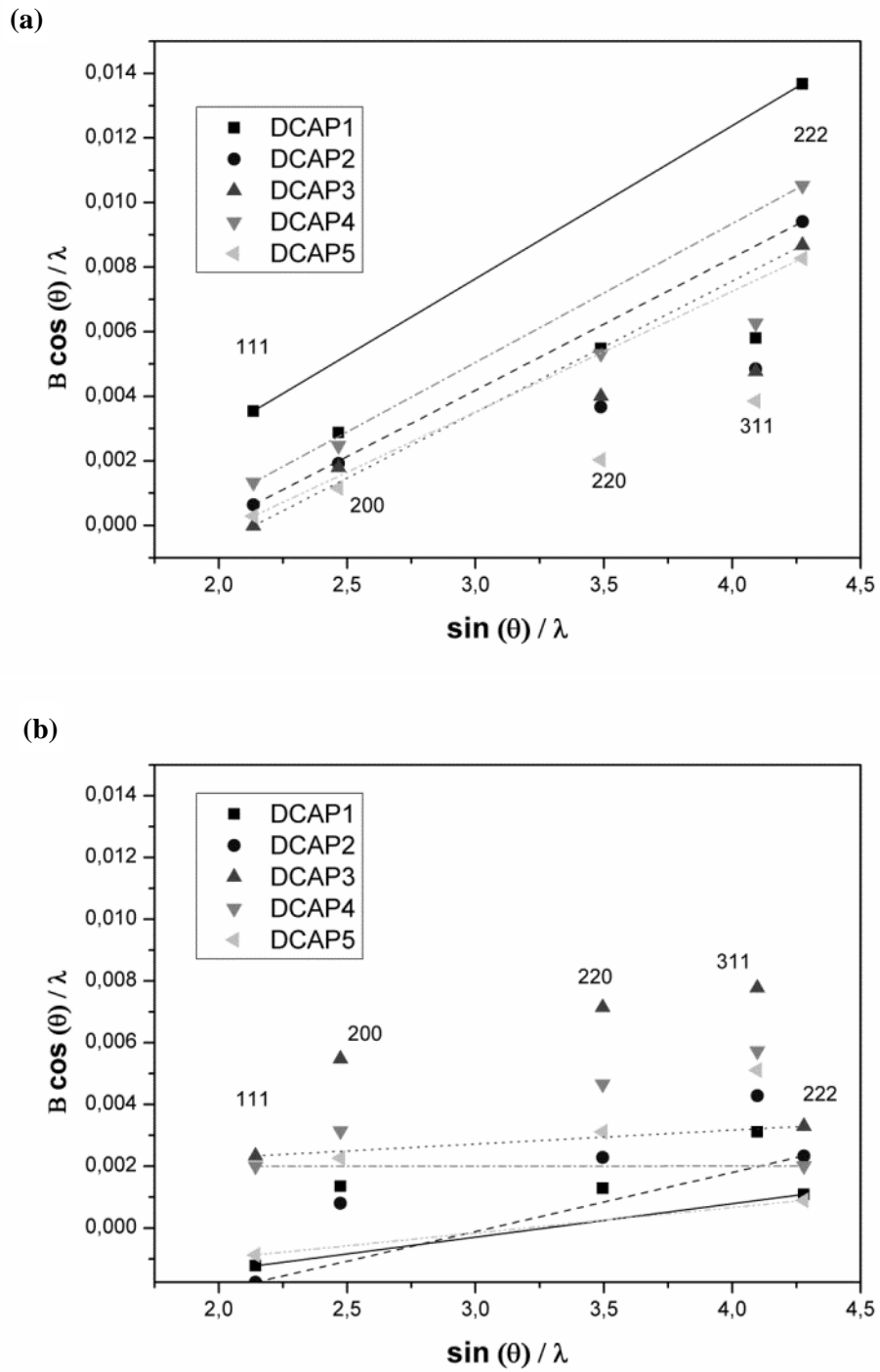


Figure 4.29 Williamson-Hall plots for DCAPed Al-6061 sheet processed with different pass number (a) DCAPed along LD (b) DCAPed along TD

Table 4.5 Size-strain values for DCAPed AA-6061 sheet processed with different pass number and route calculated for <111>

DCAP pass	DCAP along LD		DCAP along TD	
	D _{WH} (nm)	ε _{WH} (%)	D _{WH} (nm)	ε _{WH} (%)
1	151	0.47	-	-
2	123	0.41	-	-
3	126	0.43	714	0.04
4	129	0.37	500	0.0005
5	114	0.41	-	-

Apart from Williamson-Hall analysis; sub-structure size were also calculated with Scherrer formula by just considering the size effect of broadening. For that method (311) peak was used and minimum sub-structure of the LD-DCAPed samples were calculated as 42 nm. This value was 130-135nm for the TD case. When the two methods were compared, there seems a huge difference in the results. The main difficulty in the Williamson-Hall method was that there was a restructuring along (111) and it affected the calculations on the only available data (111/222 pair). Thus, it became meaningless to compare or contrast the results with Scherrer's (311) results. However, by that method; the sizes obtained after deformation along TD was again much higher than that of LD case. But more accurate microstructural feature size information should be obtained by TEM analysis.

4.3.3. Microstructural Investigations

4.3.3.1. Macro and Mezzo-Scale Investigations

Like all visual characterization studies, the work under investigation was conducted starting with macroscale. The visual inspection of the annealed and five pass DCAPed sample was given in Figure 4.30. The photograph was obtained during sample preparation steps. Samples were mounted in same epoxy and cut into slices of 250μm in thickness with a precision saw using same cutting parameters. As seen from Figure 4.30b, 5 pass DCAPed alloy preserved its shape after cutting while annealed sample was curled and removed from the epoxy as chips (Figure 4.30a) due

to internal strain. This finding can be considered as an evidence of texture homogenization after severe plastic deformation as discussed in x-ray analysis.

Leading one step further, optical images were obtained for the annealed and 5-pass DCAPed sheets and they were presented in Figure 4.31. When two micrographs were compared; no drastic difference was observed, slightly equiaxed grains as small as 10-20 μm in size were distributed all along the structure. The effective strain imposed on the material after 5 pass DCAP was about 3 which is equivalent to 90% cold rolling. The predicted structure after that amount of conventional processing would be highly banded grain morphology; but in the case of DCAP, the isotropy was preserved and the mechanical improvements discussed earlier had been reached.

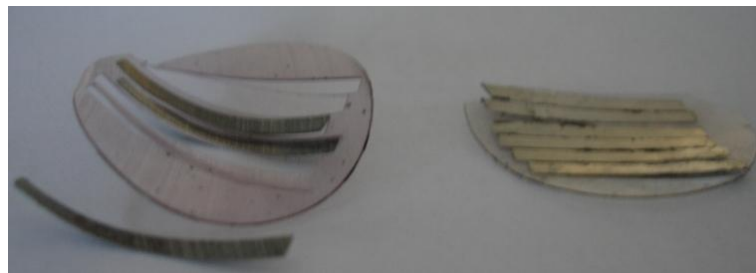


Figure 4.30 Macro-scale observation of the 250 μm thick AA 6061 sample in (a)annealed condition, (b) 5 pass DCAPed condition

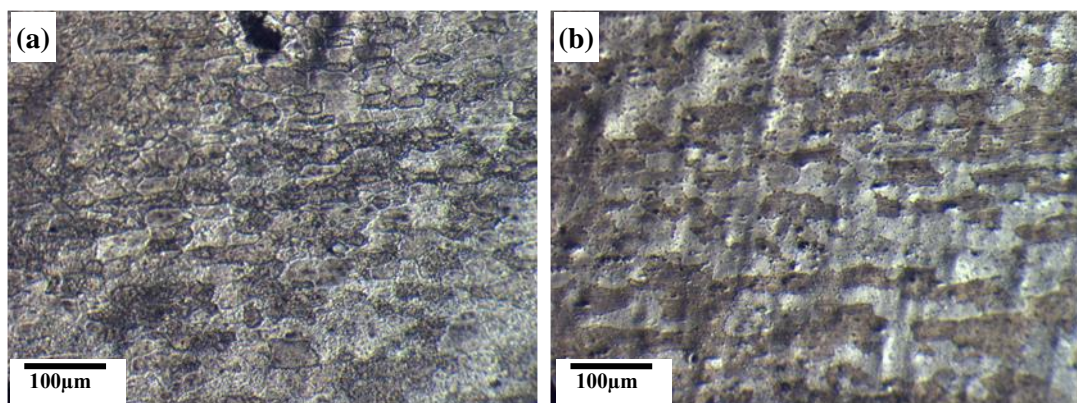


Figure 4.31 Optical micrographs of AA-6061 sheet in (a)annealed condition, (b) 5 pass DCAPed condition

Further investigations using scanning electron microscopy (SEM) clarifies that the average grain sizes are in the vicinity of 9-15 μm . In Figure 4.32 secondary electron image of annealed sample shows that second phase particles are present in the structure which may be the eutectic intermetallic compounds. It is probable that they were formed during casting and broken into pieces of various sizes during sheet making.

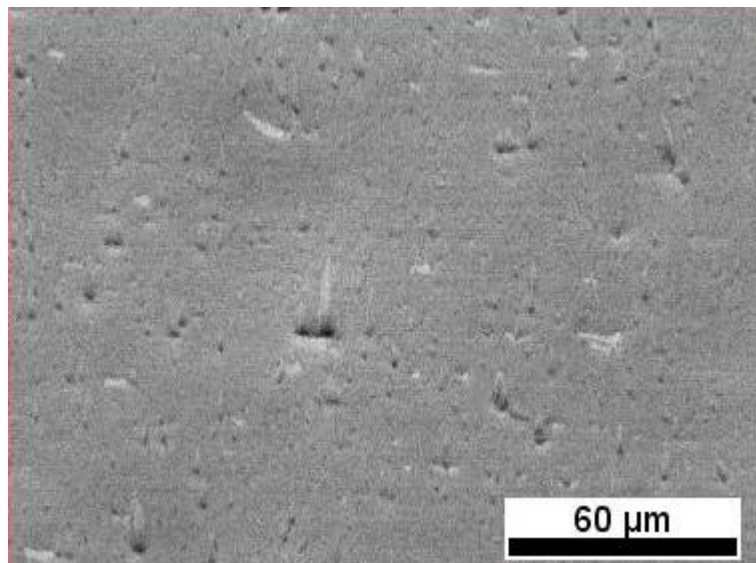


Figure 4.32 Secondary electron image of annealed AA-6061

4.3.3.2. Transmission Electron Microscopy Analysis

The aim in the DCAP type severe plastic deformation was to maintain a UFG structure separated by high angle misorientations. Due to limited resolution of the previous methods, no differential results have been presented yet. Grain and boundary evolution with DCAP deformation was investigated in this section.

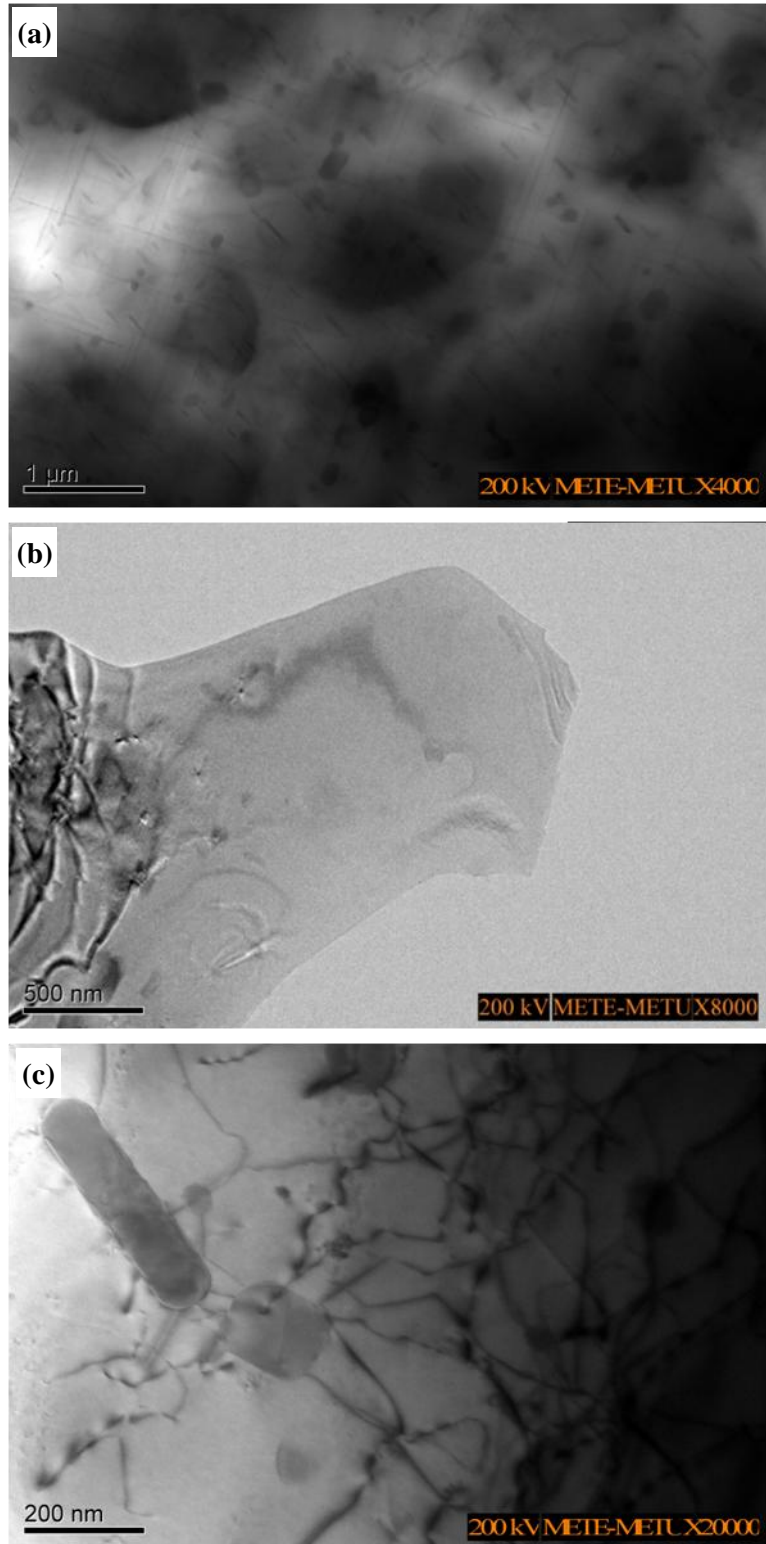


Figure 4.33 Bright field TEM images of annealed AA-6061 sheet

The general appearance of the annealed sample (Figure 4.33) was grains all through the image. From mezzo-scale observations, the grain size of an annealed sheet should be more than 9 μ m. Since TEM is a location sensitive method; photograph an image containing a boundary could not be observed. Low dislocation density (geometrically necessary dislocations) and second phase particles have been the main constituents of the annealed sheet's microstructure (Figure 4.33a&c).

Detected second phase constituents in rod, oval or square shapes were similar to the ones observed in SEM analysis. These particles (Figure 4.34) have been monitored in all levels of deformation with various sizes (100nm - 3 μ m). The EDS analysis (Figure 4.35) carried out in TEM showed that the particles had a complex composition containing Fe, Si, Al, Cr, Mn and Cu. It was known that, virtually all Fe in Al alloys forms a wide variety of Fe-containing intermetallic phases [75] and with the presence of manganese, chromium and copper, a complex phase could be formed as (Fe,Mn,Cu,Cr)₃SiAl₁₂ [76]. It was observed that the number of small intermetallic particles was increased as the DCAP pass number increases; hence the size of these particles were decreased as in Figure 4.34b.

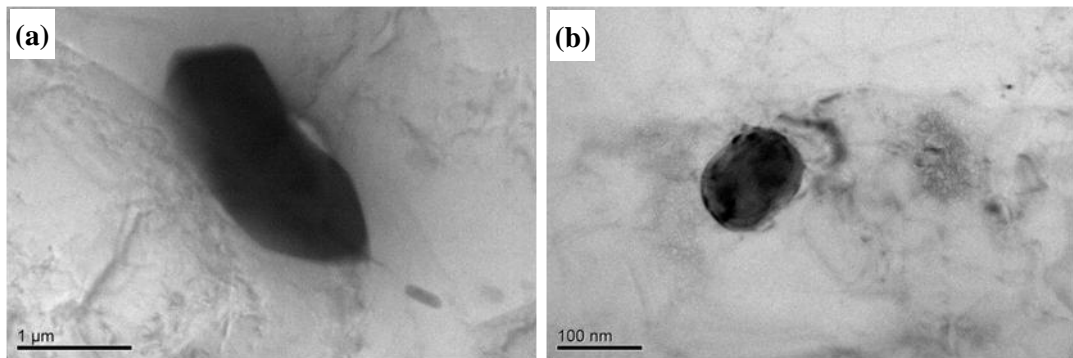


Figure 4.34 Intermetallic particles observed in (a) annealed AA 6061 sheet, (b) 5 pass DCAPed sheet

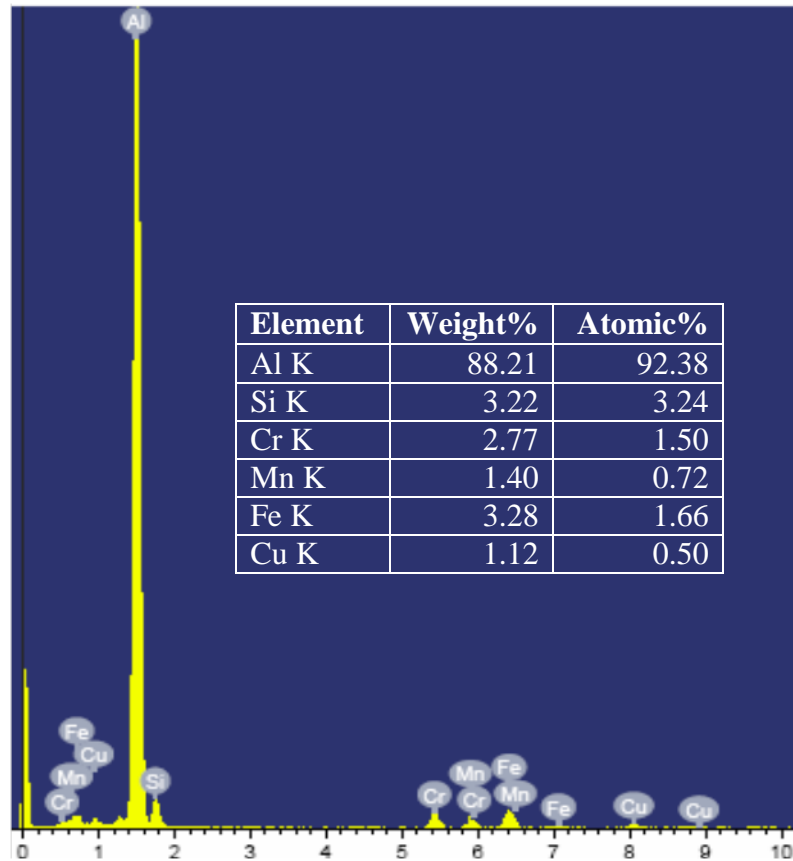


Figure 4.35 EDS analysis of the intermetallic phase under TEM

Other than intermetallics, in some regions of the samples, rod shaped precipitates were observed. A bright field micrograph of annealed sheet was presented in Figure 4.36. According to the aging sequence of 6xxx alloys, equilibrium β precipitate (Mg_2Si) in the shape of rod is expected to form after peak aging. The detection of this kind of precipitates in the annealed state was attributed to over-aging of the sheet during annealing of as-received Al 6061-T6.

Similar findings were run across in the 5 pass DCAPed sample (Figure 4.37), but it was far more difficult to differentiate the morphology from the complicated micrographs caused by high dislocation density. Hence dark field imaging was used as a tool (Figure 4.37c&d). Two spots have been selected from the diffraction pattern (Figure 4.37b) which was obtained by a selected area aperture of $100\mu m$ in size. Rod shaped β precipitates having a width of 25-30nm and length of 500-800nm were detected.

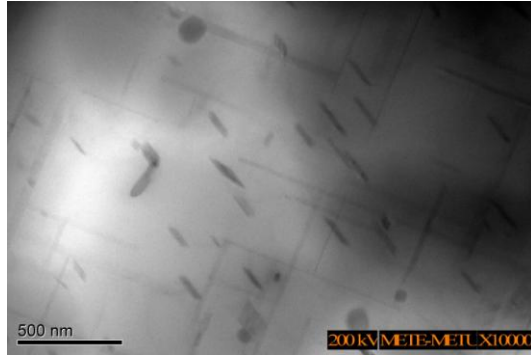


Figure 4.36 TEM micrograph of annealed AA-6061 sheet containing β precipitates

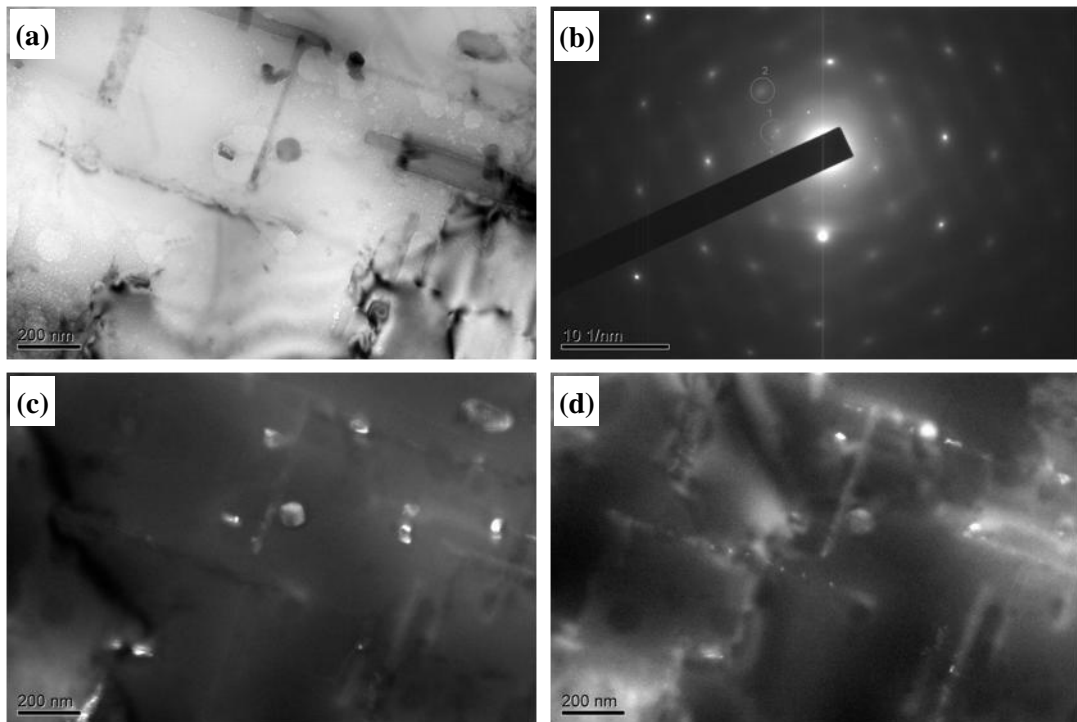


Figure 4.37 TEM micrograph of 5 pass DCAPed AA-6061 sheet containing β precipitates (a) bright field image, (b) selected area diffraction pattern (SA=100 μ m), (c-d) dark field images from the selected spots of 1 & 2 respectively

DCAP has been applied along two different directions as longitudinal (LD) and transverse (TD) and the differences in mechanical performance and X-ray analysis

has been reported previously. Hence TEM analysis of the severely deformed Al 6061 sheet was separately analyzed for the two cases.

Similar to the TEM analysis of ECAPed sample, post DCAP annealing was preferred for the investigations of the samples deformed by DCAP along LD direction. Two different temperatures namely 200°C and 350°C were selected and used. In Figure 4.38 effect of temperature on 2 pass DCAPed structure was presented. High dislocation density in the form of complex tangles and forests was the evidence of as deformed sheet (Figure 4.38a). Due to banded morphology of dislocations, detection of boundary structure (grain or cell) was challenging. However, with the increase of annealing temperature, dislocation arrangement processes took place by annihilation and the accumulated dislocations near boundaries began to be dissolved. Moreover, a slight increase in grain/cell structure size was observed (Figure 4.38b&c). A couple of grains with clear boundaries could be seen in Figure 4.38c; where the grain sizes were in the range of 0.5 – 1.5µm. Due to thermal stability, the investigations to the forefront were carried out on post-DCAP annealed samples where 350°C was the annealing temperature.

The increased number of DCAP passes lead to microstructure evolution and cell size variations. In Figure 4.39, TEM bright field images of DCAPed samples from one to 5-passes were given. The sheets had been DCAP processed along LD were annealed prior to TEM. At first glance, grains/substructures were observed to be surrounded by well-defined boundaries. Although grain size distribution was not uniform; nearly all of them were finer than 600 nm which makes the structure ultra fine. Some examples of dislocation free substructures (UFG) were marked by white arrows and the sizes have been measured as 150-250 nm; a tiny one with 50 nm also existed in the micrograph of 2-pass DCAPed sheet (Figure 4.39b). From the size-strain analysis in the x-ray section the substructure size was calculated to be 110-150 nm which is in good agreement with the observed microstructure. It should also be noted that; although annealing was applied, high dislocation density is observed in some regions of 5-passed sample. The boundaries were observed to be smoother and the number of UFG was increased yet, an overall transformation into a homogeneous ultrafine structure could not be completed.

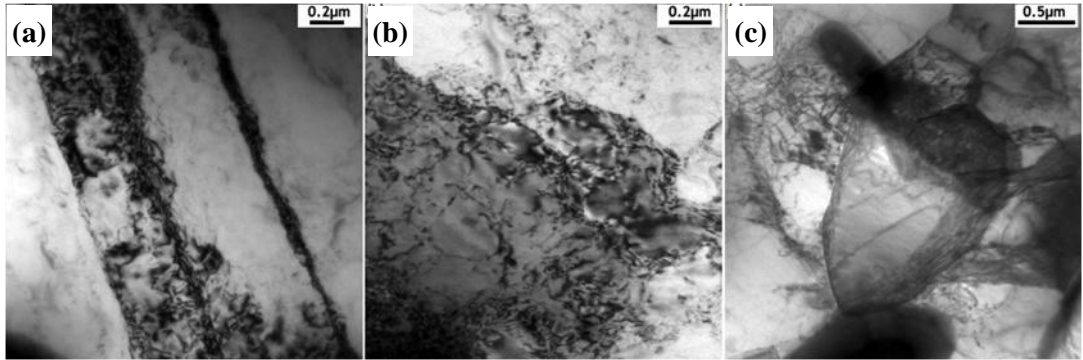


Figure 4.38 TEM images of AA-6061 sheets after 2-pass LD-DCAP (a) as-deformed, (b) annealed at 200°C, (c) annealed at 350°C [77]

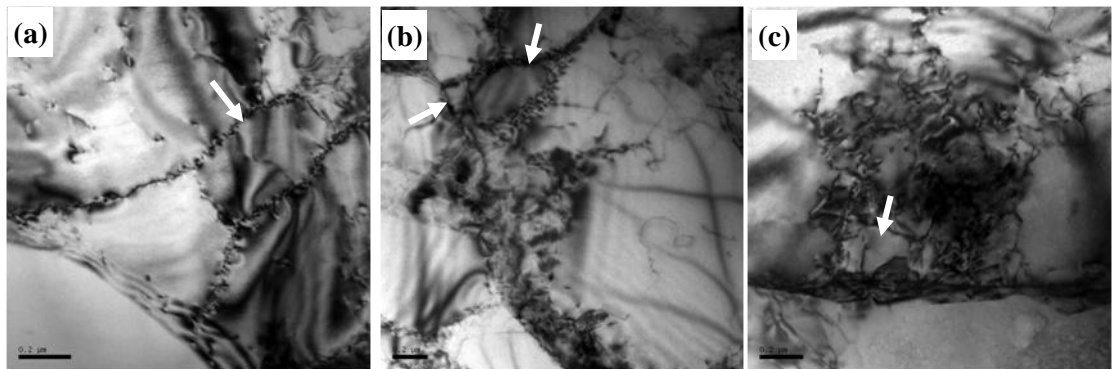


Figure 4.39 TEM micrographs of AA-6061 sheets annealed at 350°C after (a) single pass LD-DCAP, (b) 2-pass LD-DCAP, (c) 5-pass LD-DCAP [77]

Variations in the boundary characteristics at different strain levels have attracted the attention to the UFG formation in the DCAPed samples. In literature, a structural evolution for Al 1050 sequence has been proposed such as dislocation cells → PDWs (polygonized dislocation walls) → PTBs (partially transformed boundaries) → Ultra-fine grains [78]. Similar indications for DCAP passed AA 6061 supporting this proposal were monitored as shown in Figure 4.40. In the single pass DCAPed sheet, complicated shape of PDW type boundaries were dominant; and once the amount of strain level was increased, the number of PTBs were increased as it can be seen from

Figure 4.40b which belongs to 2-pass DCAPed sheet. Thickness fringes were the clue of PTB type boundaries here. In the later stages of deformation, PTBs were replaced with a sharp and distinct grain boundary structure shown in Figure 4.40c. It was reported that misorientation values are less than 1° for PDWs; in the range of 1° to 5° for PTBs and larger than 10° for GBs [78] Hence UFG with high angles of misorientation could have been achieved by examining simple shaped grain boundaries at high levels of strains.

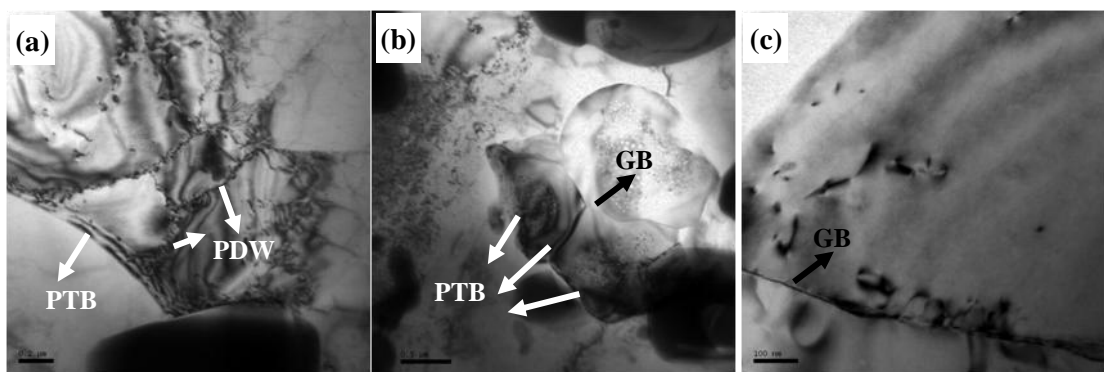


Figure 4.40 Boundary evolution during DCAP of AA-6061 sheets (a) single pass LD-DCAP, (b) 2-pass LD-DCAP, (c) 5-pass LD-DCAP [77]

Previous investigations had shown that material performance was strongly related to the earlier deformation history. In order to correlate the mechanical performance differences; similar TEM analysis was carried on the AA 6061 sheets which were DCAPed along TD. Boundary analysis in the LD-deformed samples shows that fraction of UFG with high angle boundaries increases with strain induced to the sample. So, only 5-pass sheet was investigated; and no post-DCAP annealing was used for that group samples.[†]

[†] It should be noted that observation of grain morphology and clarifying images within complex dislocations was harder in un-annealed condition and low temperature annealing would still preserve its vitality for an easier TEM analysis. Due to the complex nature of severe plastic deformation, tilting the sample to a correct position becomes important. Hence TEM operator should check all possible zones to have an apparent micrograph without post-annealing.

In Figure 4.41; a micrograph of 5-pass TD-DCAPed AA6061 sheet was given. Banded structure with dislocation forests could be observed from Figure 4.41a. Selected area diffraction pattern of the sample was also obtained and presented in Figure 4.41b. According to SADP, a complex system containing more than three grains were observed. The dark field image presented in Figure 4.41c was captured by selecting an arbitrary diffraction spot shown. With the use of reference dark field, positions of grains were predicted and numbered on the bright field image. The average size of the grains was measured to be 600-900nm. Similar to the LD-DCAPed samples; generally two types of grains were detected: the ones containing cellular structure separated by thin boundaries and the ones containing high dislocation density in the form of tangles. The cellular type microstructure was in the size of 150-250nm as the smallest.

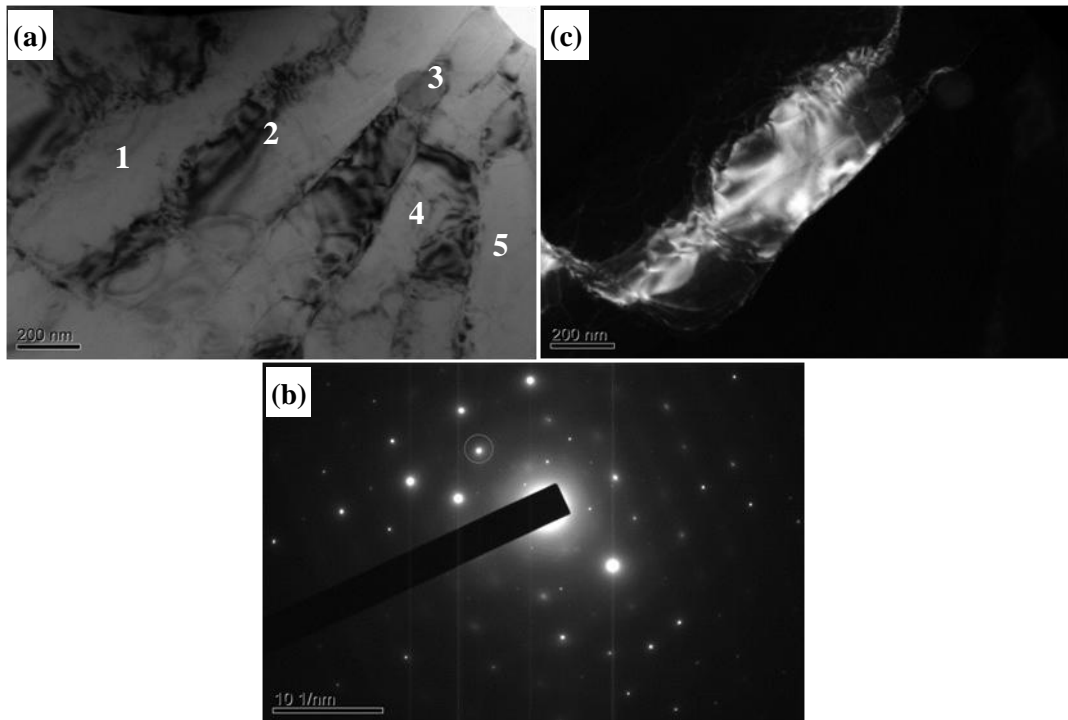


Figure 4.41 TEM micrograph of 5 pass TD-DCAPed AA-6061 sheet (a) Bright field image, (b) SADP, (c) Dark field image

Once the boundaries of 5-pass TD-DCAPed sample (Figure 4.42) were investigated; similar boundary morphologies as in the case of DCAP along LD were observed. The main difference between LD and TD modes was the limited amount of high angle boundaries in the TD case. Main type of boundary in the 5-pass TD-DCAPed sheet was the PTBs. Another difference between LD and TD modes were in the substructure size. As measured from Figure 4.41 and Figure 4.42 the substructure sizes were in the vicinity of 600-900 nm and these were coarser than the ones of LD-DCAPed samples. Actually during Williamson-Hall analysis, the peak broadening was detected to be less in the case of DCAP along TD, which leads to higher substructure sizes. As a result DCAP along TD was less effective in UFG formation as compared to DCAP along LD.

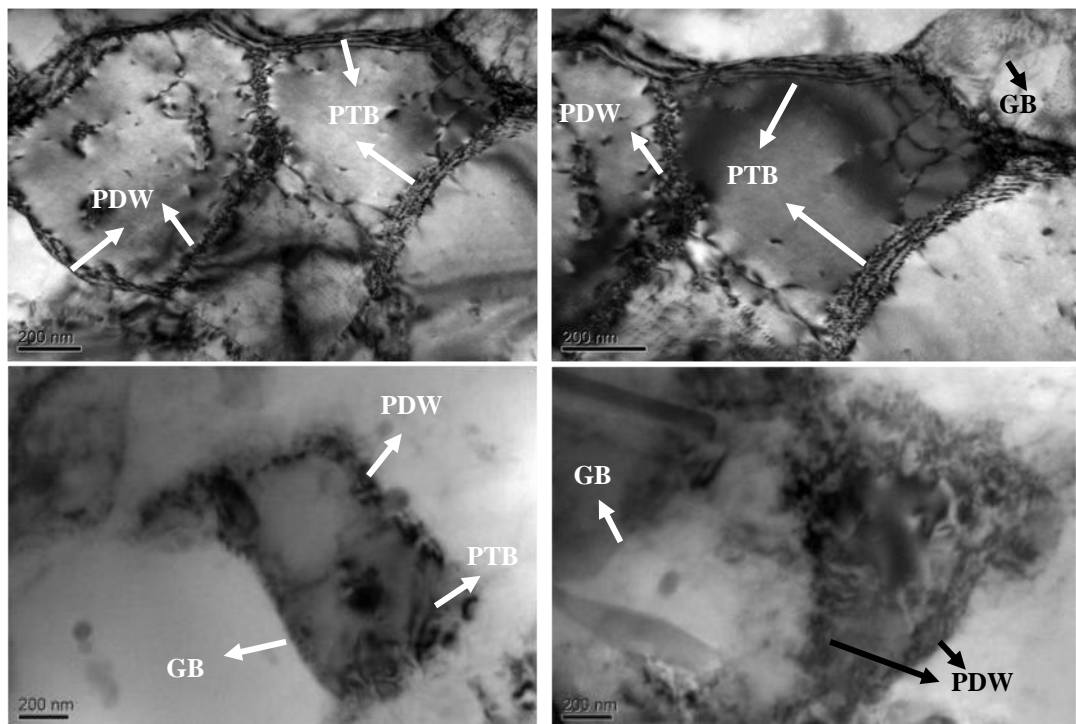


Figure 4.42 Boundaries of 5-pass TD-DCAPed AA-6061 aluminum alloy

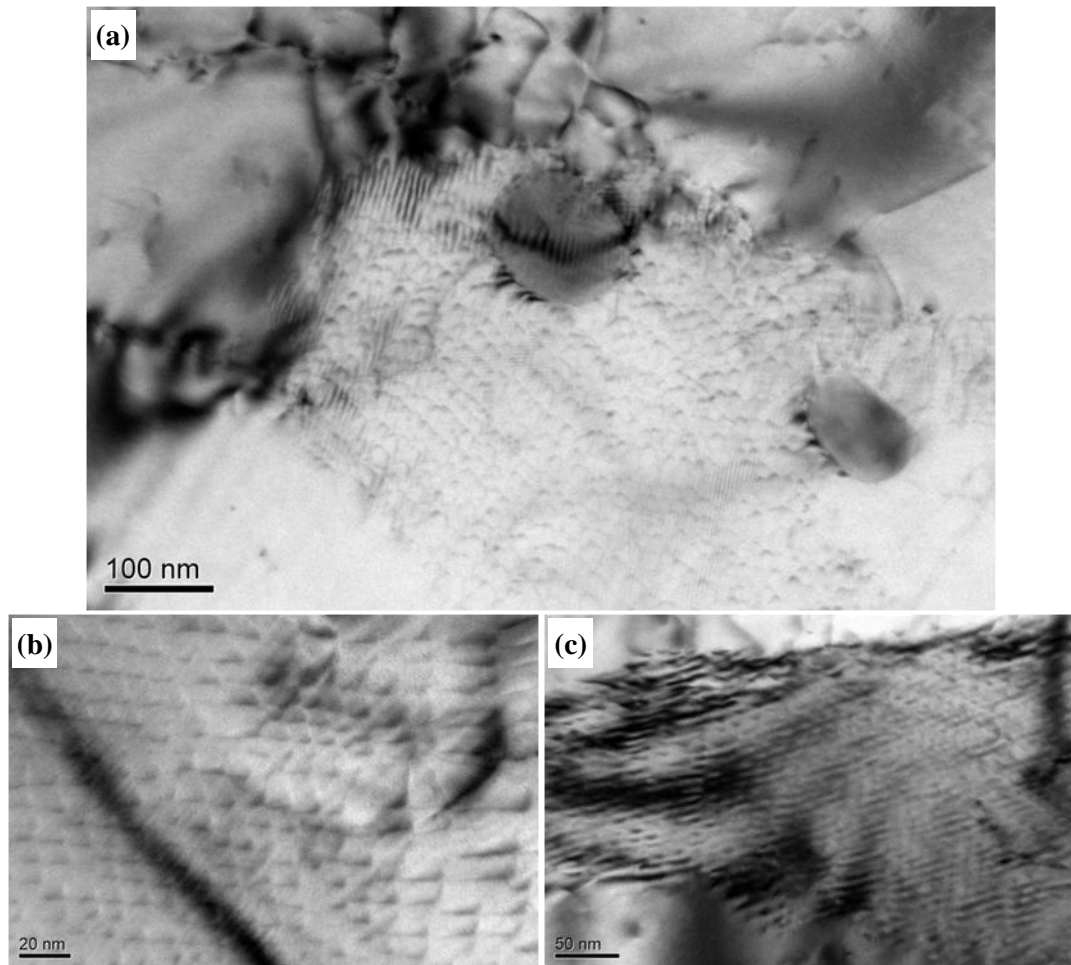


Figure 4.43 Dislocation arrangements in five pass TD-DCAPed AA-6061 sheet (a) ordered structure, (b) zigzag type arrangement when tilt γ was increased 2° , (c) PDW type boundary observation when tilt γ was increased 4°

During analysis of 5-pass DCAPed sample, an interesting area given in Figure 4.43 has been observed. Once selected area diffraction was carried, no evidence of a second phase or orientation was monitored. However by tilting the stage in a single direction, this highly ordered structure turned into a form of PDW type boundary as shown from the series given in Figure 4.43b&c. Polygonized dislocation walls (PDW) type boundaries were observed to be thick boundaries with zigzag shape and the misorientation had been reported to be 1° [78] which explains not observing a difference in diffraction pattern. PDWs were thought to be the first stage of boundary morphology change towards high angle boundaries and they were formed through dislocation arrangement in the first DCAP pass. Consequently it was not surprising

to monitor similar dislocation alignments in single pass TD-DCAPed sheet. In Figure 4.44 the magnified bright field images of PDWs were given for single passed and five passed sheets. It was observed that the number of dislocations was increased in the five passed sample (Figure 4.44b) as compared to the single passed one due to higher amounts of strain induced to the material.

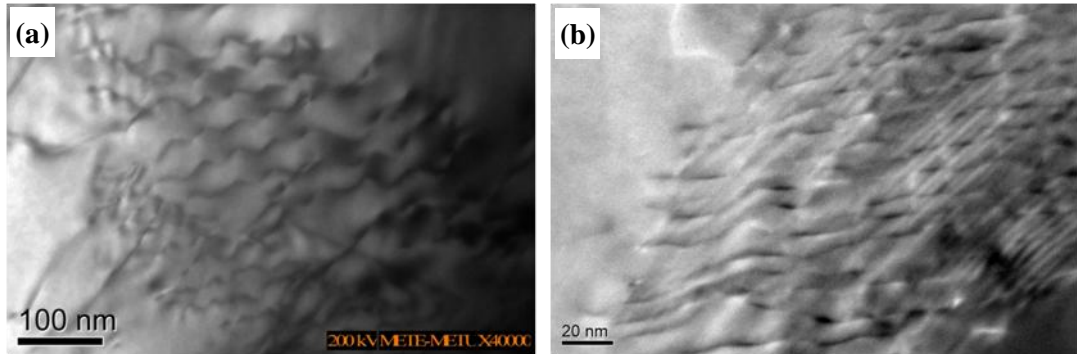


Figure 4.44 Dislocation alignment in the form of zigzag, composing PDW type boundaries within AA-6061 sheet (a) single pass TD-DCAPed, (b) five pass TD-DCAPed

It was discussed previously that due to increase of dislocation density, complex tangles might be observed in structure at a sample tilt. TEM has always been a great tool that; the evidence in UFG structure could also be detected by examining the selected area diffraction patterns. In Figure 4.45 diffraction patterns of annealed sample and five pass DCAPed sample were compared. A coarse single grain of annealed aluminum was given in Figure 4.45a. On the other hand, DCAPed sample in Figure 4.45c contains a grain of $1\mu\text{m}$ in size, in which complex dislocation forests were present that no substructure boundary could be observed. Diffraction patterns were collected from the images selected by $20\mu\text{m}$ region at same magnification. It was observed that different patterns were captured. The single crystal structure was the expected pattern (Figure 4.45b) for the annealed sample. But for the 5 pass DCAPed sample Figure 4.45d was obtained. Spreading of spots was the indication of high internal strain and high dislocation density. And the alignment of diffracted spots along circles in the SADP was also the proof of fine grain structure separated

by high angle boundaries. Hence without imaging, diffraction pattern analysis could be used to prove the existence of UFG.

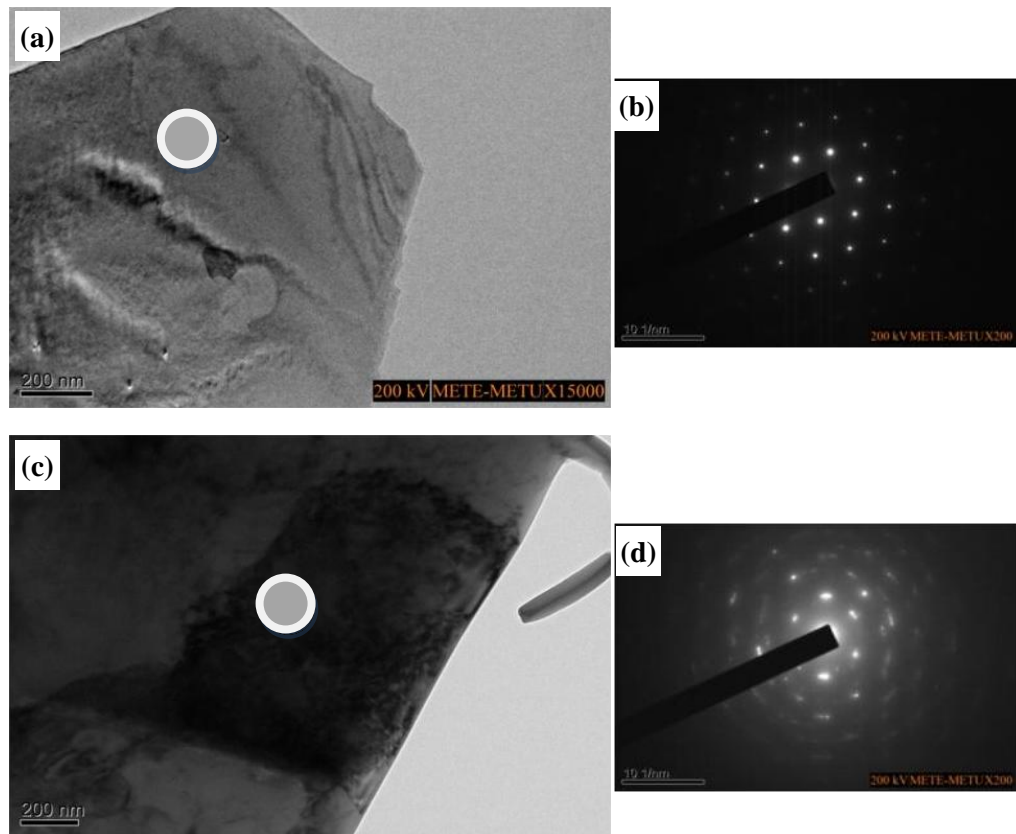


Figure 4.45 Effect of DCAP on microstructure and SADP (a-b) Annealed 6061, (c-d) 5 DCAPed AA-6061 (selected area region was also shown “aperture size:20 μ m”)

TEM investigations used in the characterization step of DCAPed have produced lots of valuable information in terms of structure sizes and structure / boundary evolutions. Due to high dislocation density, different dislocation arrangements in the form of tangles and forests were observed all around the structure. These dislocations were generally collected along boundaries or cell walls and were used up to form structures like PDW, PTB and finally grain boundary with high angle mismatch. The substructure sizes were 150-250nm for the sheets deformed along LD. For some regions of sheets which were deformed along TD, this value was 600-900nm. The

microstructural results were well suited to the ones in x-ray analysis. The formation of UFG structure had initiated by arrangements of dislocations; so it was not surprising to have less homogeneity in the first stages of deformation. During DCAP deformation, excessive strains imposed in the material were used up to generate dislocations during slip. Orowan bowing and dislocation cut mechanisms have been activated by slip to produce a high density of dislocations. The broken intermetallics, remained β precipitates, boundaries and dislocations itself were all used up in the process of creation. Hence the accumulated strains caused by high dislocation density were consumed to form UFG. As a result more homogeneous structures with UFG were formed in the later passes. As the strain imposed to the material increases, the driving force to form UFG has been increased.

In the case of homogenization; TEM might not be a well suitable method due its place sensitive methodology. The region that could be monitored in a single time was about $6\mu\text{m}$. So a need to turn back to the micro-scale from nano-scale was required. For homogenization investigations and boundary-size evaluations over larger distances; a scanning electron microscopy equipped with EBSD camera was used.

4.3.3.3. EBSD Analysis

The EBSD data was collected from the highly polished cross-sectional surface of the annealed and 5 pass DCAPed samples. The basis of the EBSD method is the examination and classification of the surface features according to the crystallographic orientation differences. In Figure 4.46, image quality map for annealed sample was presented. At first sight, the average grain size was not homogenous prior to DCAP deformation as shown from the figure. The image quality map was obtained by collecting data points separated with $0.65\mu\text{m}$ from a $200\times 200\mu\text{m}$ area. The dashed square in the figure was the $45\times 45\mu\text{m}$ region selected for detailed scan with a data interval of $0.2\mu\text{m}$. The inverse pole figure maps for both scans were given in Figure 4.47. According to Figure 4.47a, the annealed sample had a huge grain size distribution with an average size of $33\mu\text{m}$. Tiny grains with $10\mu\text{m}$ in size were present with coarser ones which were as big as $70\mu\text{m}$. The map was mostly composed of grains with red-orange color which was the indication of non-homogeneous grain orientation in the annealed plate. According to the color

map, red color belongs to the (001) and this was well suited to the x-ray analysis results showing the pre-texture in the plate before DCAP deformation.

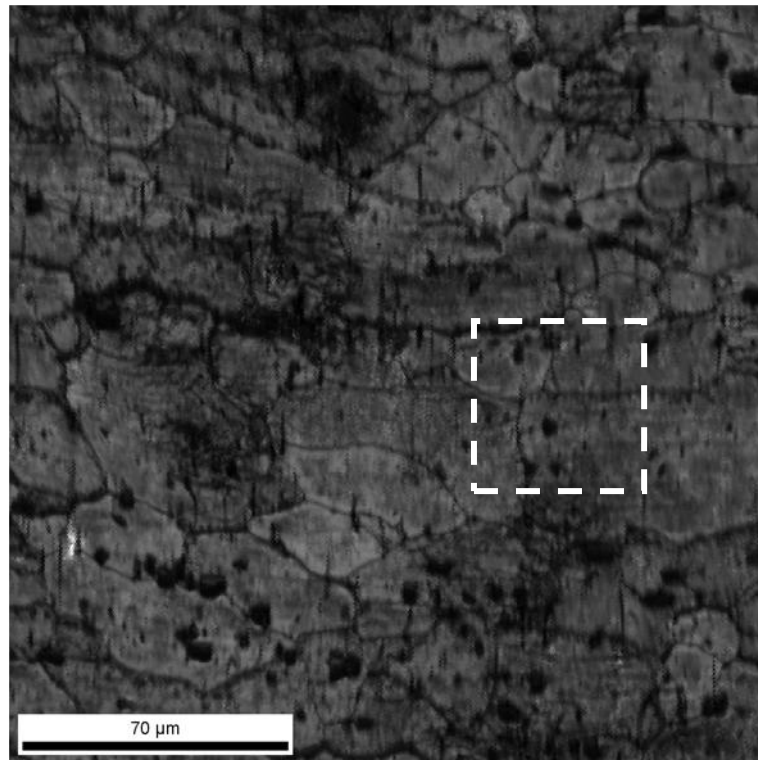
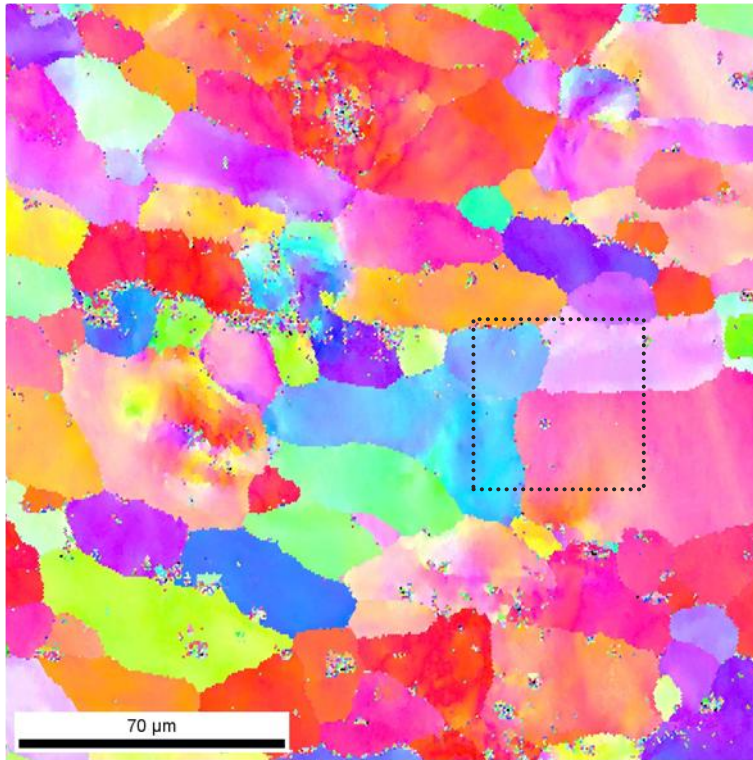
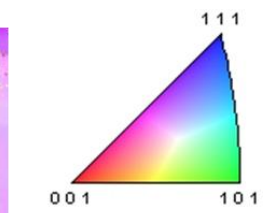
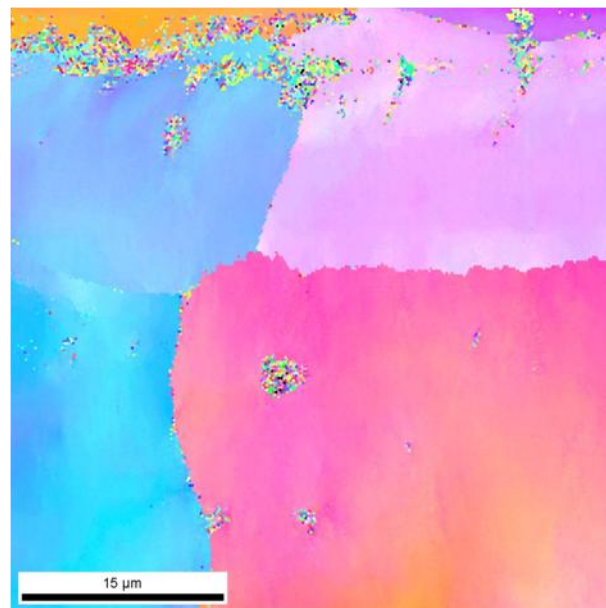


Figure 4.46 Image Quality Maps for annealed AA-6061 sheet

Two types of grains were observed in inverse pole figure (IPF) maps: grains with single color and grains containing two or more color mixed with an arbitrary pattern. This wavy color change in a grain was the indication of high strain imposed in the material. Similar results were gathered from the fine scan of an arbitrarily selected region (Figure 4.47b). Although the resolution was increased; well defined boundaries inside this type of grains were not observed. High strained regions separated by low angle misorientations were the consequence of this analysis.



(a)



Colorful single spots are a sign of improper data collection from the region concerned.

(b)

Figure 4.47 Inverse Pole Figure maps for annealed AA-6061 sheet (a) 200x200 μm area with step size 0.65 μm , (b) 45x45 μm area with step size 0.2 μm

Similar investigations in the annealed case were repeated for the 5 pass DCAPed sample. The image quality map for DCAPed sample was presented in Figure 4.48. The structure became much more complicated and the sizes of features were decreased as compared to Figure 4.46. Similarly an arbitrary region was also selected for fine scan of the DCAPed sample as shown with white dashed square. The inverse pole map belonging to the 200x200 μm scan size was presented in Figure 4.49a. As compared to the annealed sample the grains (separated with HAGB) become much more elongated along the sheet rolling direction of the original plate. The grain sizes were in the vicinity of 27 μm and grain size distribution has been observed to be much steeper. Another difference was the increased number of wavy colored grains. Nearly all the grains became wavy in color which was the indication of high amount of strains distributed all along the structure. Also grains were marked up with all different colors in between red, green and blue; resulting a loss of initial texture of the annealed sample. All these findings were in strong correlation with the x-ray analysis reported previously.

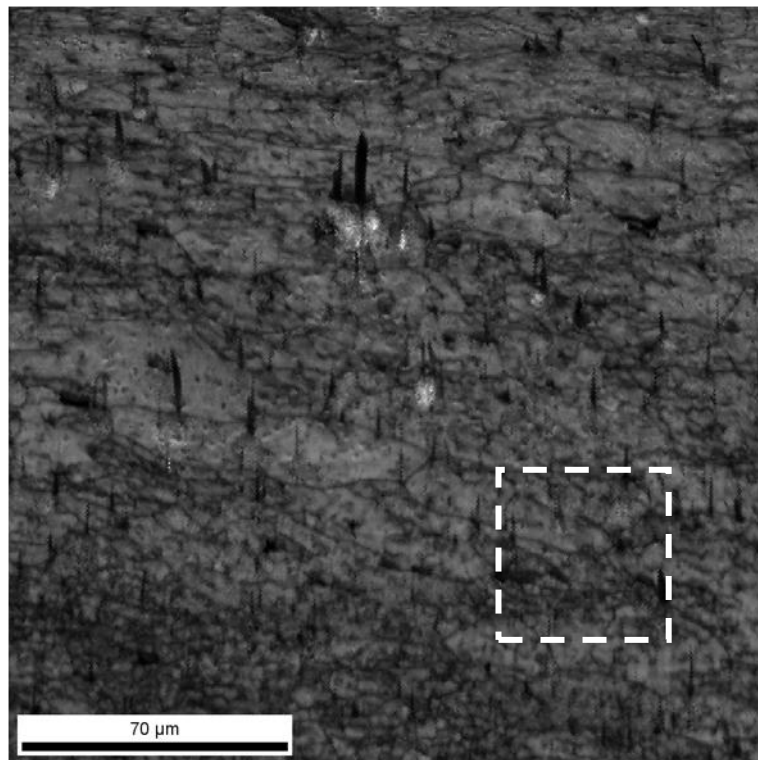
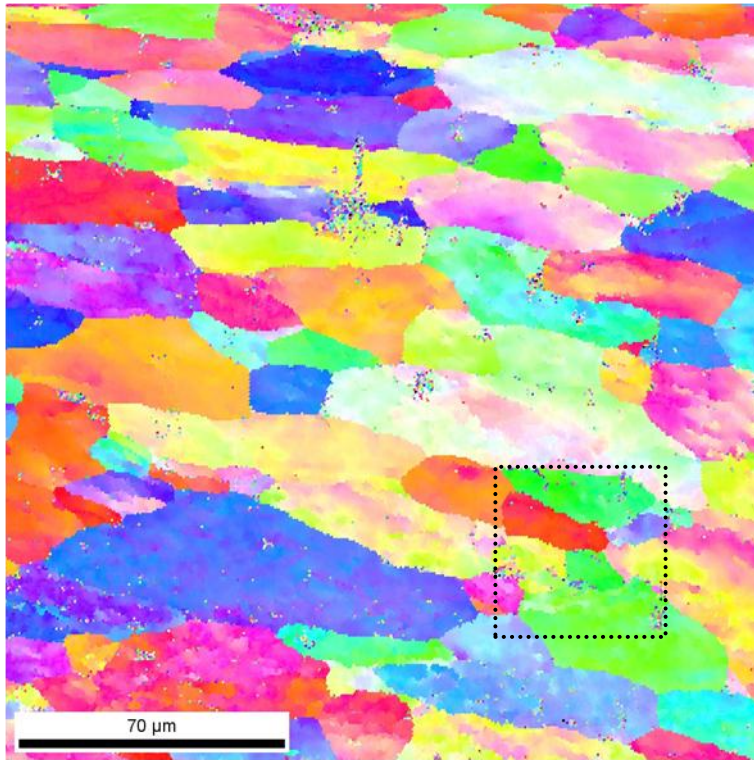


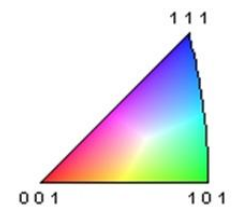
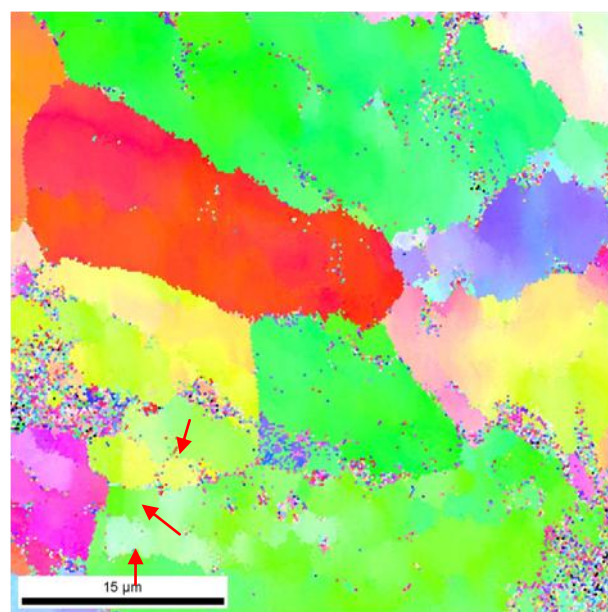
Figure 4.48 Image Quality Maps for 5 pass DCAPed AA-6061 sheet

The detailed scan from 45x45 μm region with 0.2 μm step size was shown in Figure 4.49b. Due to increased resolution, some tiny regions with different color could be differentiated from the wavy structure. Some examples of that kind were shown with red arrows on the map. It was observed that a number of microstructural features tend to form by dislocation arrangements in the high strained wavy regions. But the clarification of this finding should be done by boundary analysis.

As described previously, EBSD method is based on the crystallographic orientations on a surface; hence it could be easier to differentiate a boundary type. Misorientation between two points exceeding 0.75° has been regarded as low angle boundary. In the case of 15° misorientations and above high angle boundary has been introduced. In Figure 4.50; boundary maps for the annealed and 5 pass DCAPed sample was given. Annealed sample had high angle boundaries clearly separating the grains. In some regions the grains had cellular morphology inside which were separated by low angle boundaries. In the high deformed one, the major difference was the increased number of boundaries. Total boundary length was increased from 1.74cm to 2.58 cm with a level of 48%. Also low angle boundaries have been distributed homogeneously all over the structure. This finding was in good agreement with the uniform distribution of wavy colored morphology. As stated earlier, the magic beneath the ultrafine grain formation was the existence of high angle boundary in between. The high amount of strain observed in EBSD maps was the consequence of high dislocation density. Dislocation tangles have been transformed into a granular morphology with low angle boundaries. Due to increased number of passes, in some regions partial dislocation annihilation took place and high angle boundaries have been formed. Boundary map for the DCAPed sample in the fine scan mode was given in Figure 4.51 and these regions were indicated by arrows. Since transformation of UFG has not been completed yet; this constituents had been observed in localized sites. Also note that the size of this UFG structure is about 0.8-2.5 μm which was not the exact case predicted. But it was previously mentioned in the x-ray analysis that the DCAP in the TD case was not good in grain size reduction as its positive texture homogenization effect. Nevertheless these values were below the limits of classical thermo-mechanical processing limits and the clear measurement should be repeated with the use of TEM.



(a)



Colorful single spots are a sign of improper data collection from the region concerned.

(b)

Figure 4.49 Inverse Pole Figure maps for 5 pass DCAPed AA-6061 sheet (a) 200x200μm area with step size 0.65μm, (b) 45x45μm area with step size 0.2μm

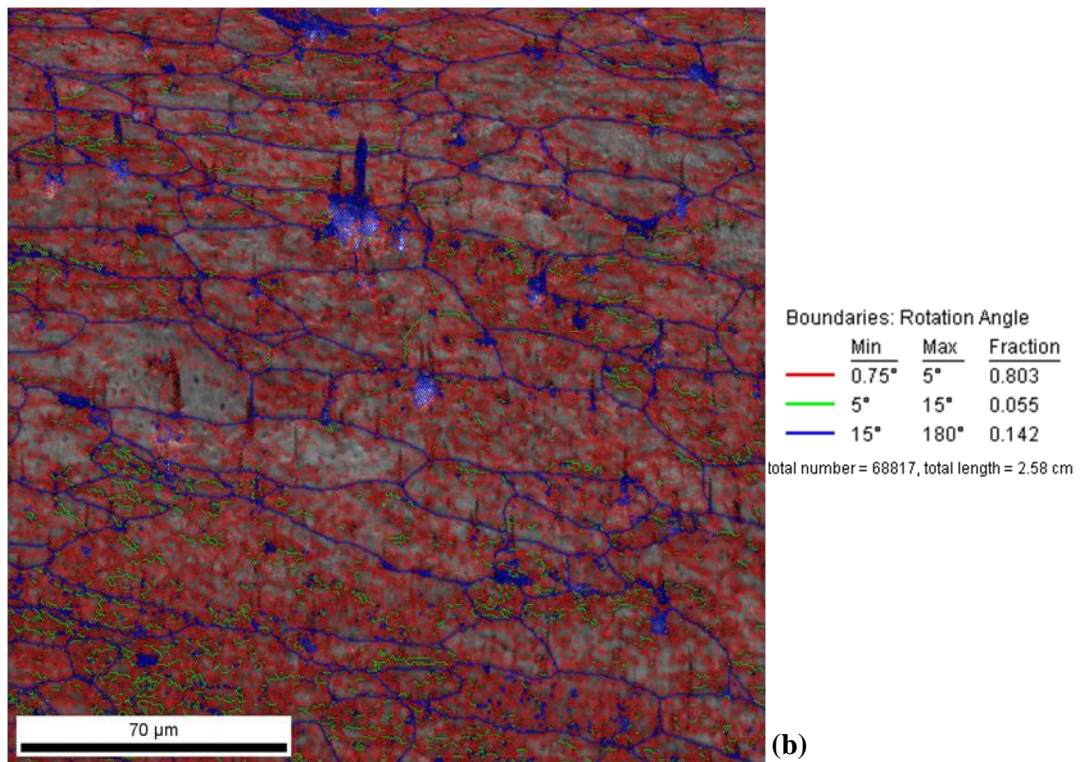
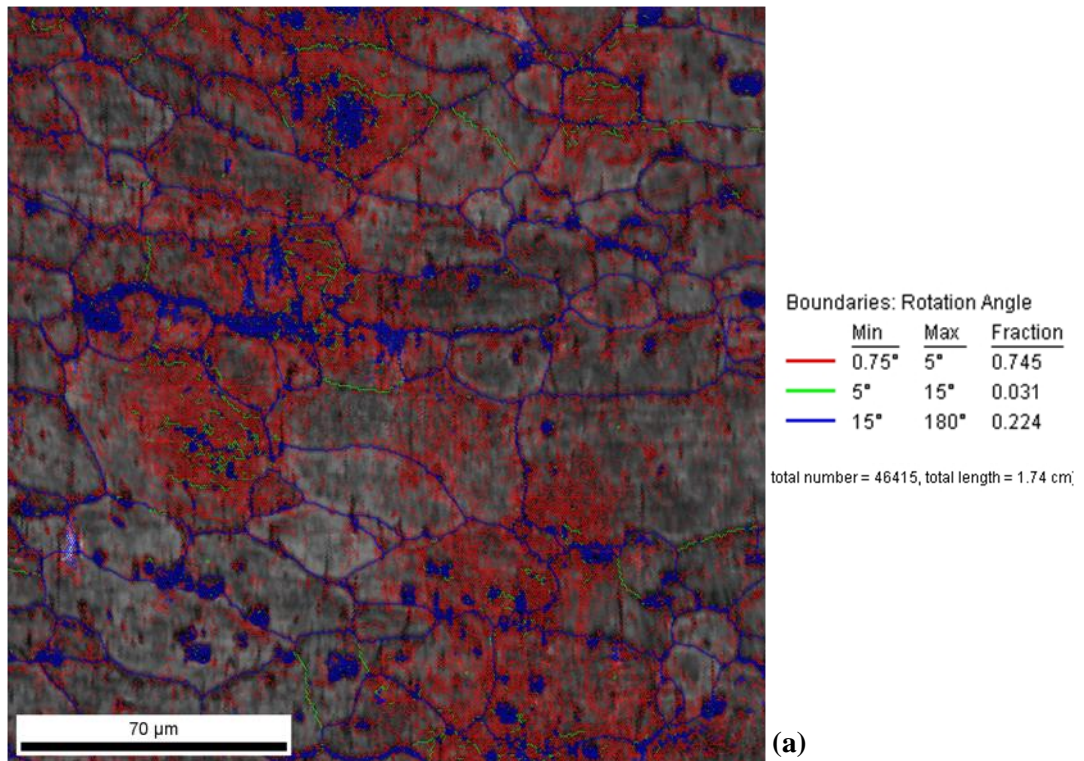


Figure 4.50 Grain boundary maps (0.65μm scan step) (a) Annealed AA-6061 sheet, (b) 5 pass DCAPed AA-6061 sheet

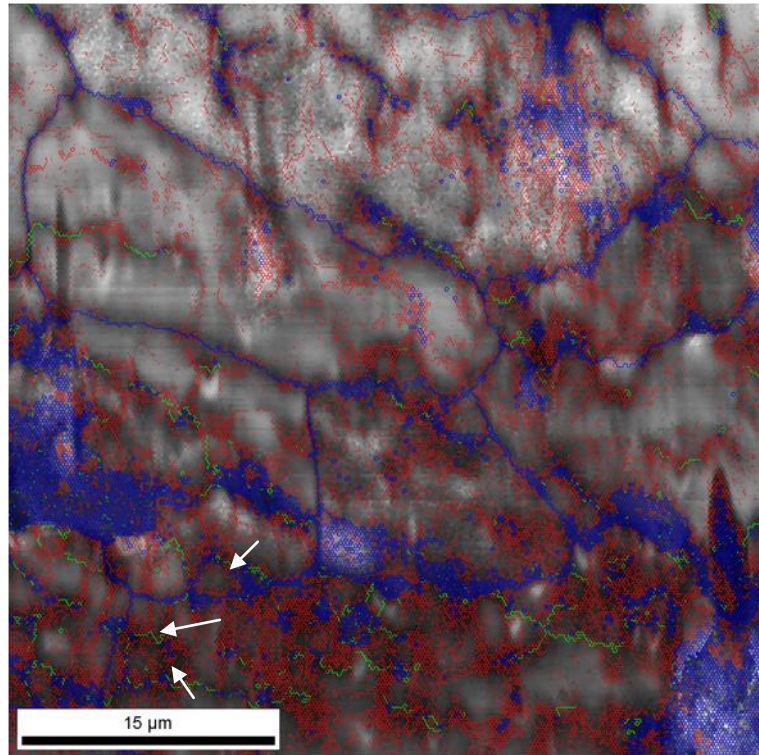


Figure 4.51 Grain boundary map of 5 pass DCAPed AA-6061 sheet (0.2 μ m scan step)

Except from the color maps, grain orientations and textures could be directly investigated with the use of pole figures. Pole figures obtained during EBSD measurements were presented in Figure 4.52. As seen from the Figure 4.52a&b that; grains were primarily oriented in a direction in the annealed case. The previous history of the sample (sheet in this case) was preserved before DCAP deformation. After 5 pass DCAP (Figure 4.52c&d); the selected texture has been eliminated and crystallographically more isotropic material has been obtained. It is a known fact that sheets are anisotropic materials due to cold rolling stage of manufacturing. But in the DCAP deformation of the sheet alloy, high strains were induced and uniform cellular structure has been formed by the annihilation of dislocation tangles in the following passes. Hence DCAP in the TD mode could be possibly used to obtain high strength isotropic sheets.

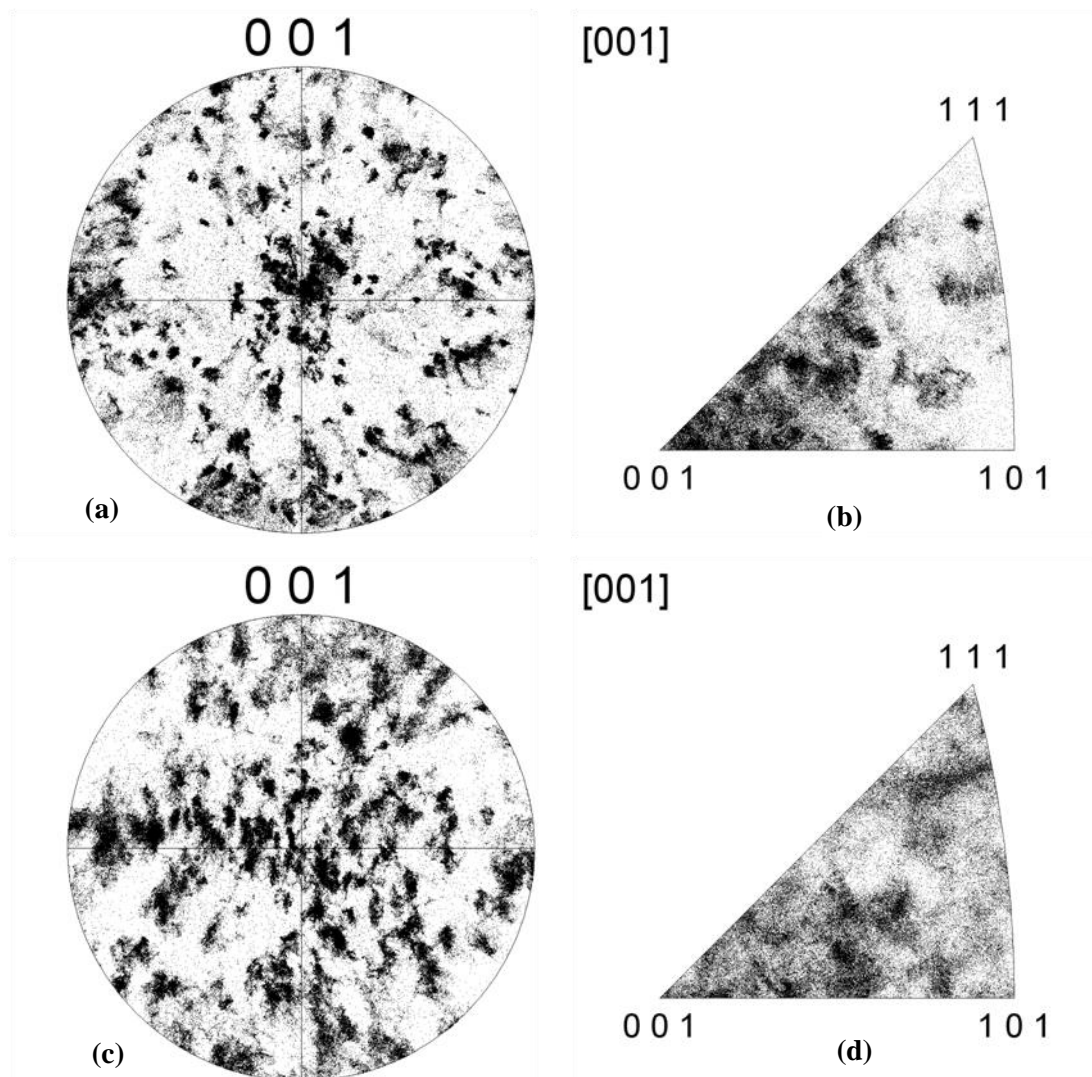


Figure 4.52 Grain orientations (a-b) pole figure and inverse pole figure of annealed AA-6061 sheet, (c-d) pole figure and inverse pole figure of 5 pass DCAPed AA-6061 sheet

4.3.4. Effect of DCAP on Defect Related Properties

4.3.4.1. Ultrasonic Sound Velocity

Ultrasonic sound velocity was measured for the annealed strip and DCAPed strip separately by determining the time of travel between two receiving probes separated by 63mm. For the annealed AA 6061, time was found to be 14.9 μ sec; in the case of single pass DCAPed AA 6061, flight time was 15.7 μ sec. The increased defect

density during DCAP deformation was responsible of this velocity decrease. It could be concluded that system was successful to generate defects in structure.

Similar data collection procedure has been tried for strips deformed more than once. But during experiments it was seen that a setup was required to fix the sending and receiving probes at the predefined positions. More over due to complexity in defect structure and distribution, heterogeneity was present in the DCAPed sample. Hence the values obtained seem to change from position to position. Regarding all these effects, ultrasonic sound velocity measurement was not characterized deeply and it was only used as a method to check the presence of severe plastic deformation.

4.3.4.2. Electrical Conductivity

Four point electrical resistivity measurements were obtained by applying currents in the 0.001 – 0.01A range. The micro-resistance values were converted to resistivity in Ωm and plotted in Figure 4.53. It was observed that for low current values (eg 1mA), there was too much scatter in the resistance due to increased tendency of electron jump in the defect rich structure. The scattering tend to saturate by increasing the current applied. The resistivity of AA6061-O is 3.6 E-8 ohm-m and when the average values were considered; it was obvious that there was no well defined trend as a function of DCAP pass number. It is a known fact that the conductivity decreases with cold deformation for cubic metals because of the lattice distortions hindering the electron motion throughout the sample [79]. This main idea did not worked for the DCAPed sheets.

It was explained in a research by Broom et. al. that; electrical conduction was influenced by vacancies rather than dislocations. Since lattice distortions were mostly dislocation related for a DCAP process; this might be the reason for this observation. In order to clarify this vacancy and dislocation defect morphology difference between cold rolled sheet and DCAP deformed sheet, high resolution electron microscopy (HREM) coupled with scanning transmission electron microscopy (STEM) should be studied.

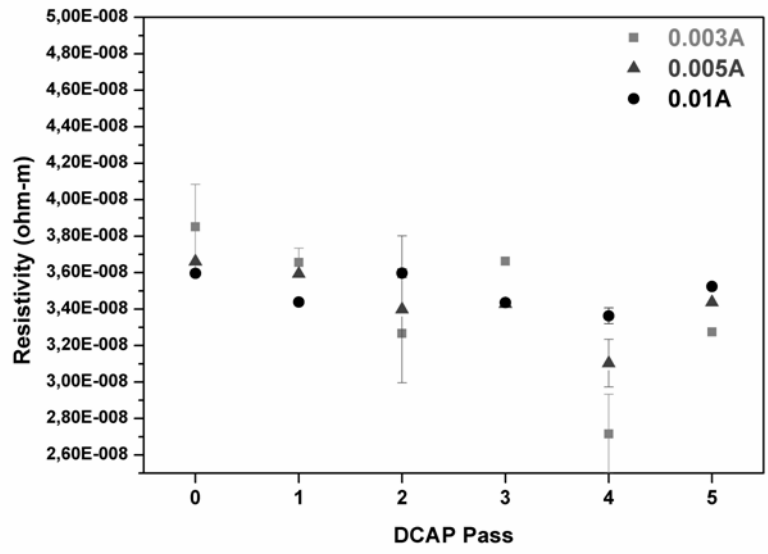
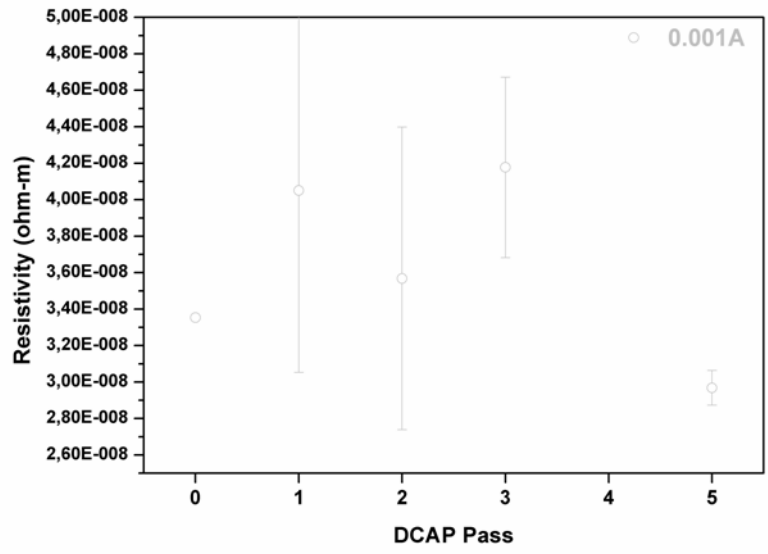


Figure 4.53 Effect of DCAP on four point electrical resistivity of AA-6061 sheets

CHAPTER 5

CONCLUSION

In this study; design and manufacturing steps of laboratory scale set-ups for severe plastic deformation of aluminum alloys were carried out; and the severely deformed samples were characterized by numerous methods. The conclusions withdrawn from the results are listed below:

5.1. Finite Element Modelling

1. Effective plastic strain imposed to the material decreases with increasing die channel angle. Die arc angle is only effective for the 90° die.
2. For frictionless condition, bottom regions of the samples are faced with lower strains at all angles due to corner gap formation.
3. Formation of corner gap could be reduced or even eliminated by increasing the friction between die and the workpiece.
4. 3D strain distribution on a plane section cut along the half depth of the workpiece is similar to 2D analysis results. Thus simulations can be done for the plane strain condition.
5. During ECAP, deformation takes place by simple shear. However the shape of the deformation zone is elliptical due to corner gap formed by strain hardening of the materials. Corner gap can be expressed by a second degree surface where it was related to K linearly and to n in parabolic manner.

5.2. Equal Channel Angular Pressing (ECAP) System

Correlation of FEM with Experimental Data

1. The square meshing on the lateral surface turned to be a parallelogram with a main shearing angle of 57° - 58° ; whereas the main shearing angle were determined as 60° in the simulations.
2. Hardness profiles on vertical cross section predicted by FEM are compatible with the results of the Knoop micro hardness tests. Maximum hardness was obtained in the central regions.

Microstructural Examination and Mechanical Enhancement

3. After single pass ECAP, average hardness value was doubled.
4. From X-ray peak broadening analysis, average cell size was calculated as 50nm which was verified by TEM analysis.
5. TEM micrographs of solutionized AA 2024 show rod shaped T-phase. After ECAP, dislocations tangled around T-phase and took part in hardening.
6. Due to increased dislocation density, detection of boundary seems to be challenging hence post ECAP annealing was performed.
7. S' and S'' precipitates were observed in the post ECAP aged samples.
8. Peak hardness obtained by standard aging procedure (190°C / 24h) can be achieved after 1h aging by applying a single ECAP pass just after solutionizing.

5.3. Dissimilar Channel Angular Pressing (DCAP) of AA 6061 Sheet

Mechanical Performance

1. For one passage, equivalent true strain was found to be changing from 0.3 to 0.6. This high strain might be reached by rolling with extreme reduction (about 40%).
2. After single pass, improvements in yield strengths of the material for the TD and LD cases are 188% and 52%, in sequence.
3. With increasing number of DCAP passes the strength increases without any remarkable loss in ductility (0.25 to 0.195).

X-ray Analysis

4. Annealed sheet shows a texture along (200) and (311).

5. DCAP deformation along TD is more effective in activating the slip on (111) plane and in maintaining a more uniform structure and isotropic properties.
6. According to Williamson-Hall size - strain analysis; the calculated cell sizes are 110-150 nm for the LD-DCAPed; and 500-710 nm for the TD-DCAPed sheets.
7. For UFG formation DCAP along TD is less effective than along LD; but this might be preferred due to its texturing effect.

TEM Investigations

8. Low dislocation density (geometrically necessary dislocations) and second phase particles are the main constituents of annealed sheets.
9. Dislocation free substructures (UFG) observed in the LD-DCAPed sheet in the post annealed condition (350°C) is as fine as 150 – 250 nm.
10. The analysis without prior annealing show that the substructure size of the TD-DCAPed samples is in the vicinity of 600 – 900 nm, which is coarser than those of the LD-DCAPed samples.
11. “Dislocation cells → PDWs → PTBs → UFG” was the boundary evolution whether the structure is deformed along LD or TD. Boundary thickness starts to decrease as DCAP pass number increases to five.
12. There are limited amount of high angle boundaries in the TD case compared to LD case. Main type of boundary in the five-pass TD- DCAPed sheet is the PTBs.
13. PDW type boundaries are formed by the ordering of dislocations in the first pass (zigzag form, wavy alignment, ordered squares).
14. Spreading of spots and the alignment of diffracted spots along circles in the SADP are the proof of fine grain structure separated by high angle boundaries.

EBSD Analysis

15. In the five-pass DCAPed sheet, the number of wavy colored grains increased, which is the indication of high amount of strain.
16. High angle boundaries are dominant in annealed sample. In the DCAPed sample, the increase in the total boundary length is almost 48%, and low angle boundaries are distributed homogeneously all over the structure.
17. The grains are oriented primarily in a direction in the annealed case. The texture of the sheet has been eliminated after five-pass DCAP.

CHAPTER 6

FUTURE DIRECTIONS

This study has been initiated with the aim of suggesting an alternative way to sheet producers in order to shorten the classical thermomechanical processing. Although many results were obtained and published by a number of researchers in the group; the destination still seems to be far away. During the years of work, ECAP being a severe plastic deformation process for bulk materials has been commercialized by some firms to produce implants. But it was a very rare example. Every two years there exists a congress called BNM (Bulk NanoStructured Materials) which was arranged in Russia by the leaders of SPD. Attendance was maintained to the last three one by different researchers from the group. Each year the increase in the number of works presented was clearly observed. But it was thought that the first commercialization of a SPD method for sheet metals (like DCAP) would be possible after decades. Upto that period, these processes would have been attracted by scientists from academia.

It was a known fact that the initial studies were just based on mechanical engineering point of view; observing deformabilities, stress strain, strain rate calculations; the discussion regarding the relation between microstructure was very limited. But within the last years; there was a great effort to thoroughly understand the logic behind this severe plastic deformation. Large groups containing physicists and materials scientists were trying to understand the grain refining mechanism and the structural evidences. Already a number of hypothesis were suggested for grain refinement and boundary evolution; but there were also contradictory thoughts on

them. There still need lots of works as a mechanical metallurgy and physical metallurgy point of view.

Results in this study showed that UFG evolution takes place with boundary variations. Hence a future study on boundaries is required to clarify the unknowns in microstructure evolution. The zigzag arrangements of dislocations forming PDW were presented. Except from this study, some HREM (high resolution imaging) work was established. In Figure 6.1 a high magnification TEM micrograph of the five pass DCAPed sample was presented. Four grains separated by high angle mismatch (122.6°) could be observed. Lattices and grain boundary separation was poor. Details of lattice imaging were checked even at higher magnifications (1.5M) and the results were presented in the Figure 6.2 and Figure 6.3. Fast Fourier Transform (FFT) of the HREM images is the equivalent of selected area diffraction (SADP) of the conventional TEM study by which constituents forming the lattice can be solved. HREM investigations of annealed sample were presented in Figure 6.2. The result of FFT and inverse FFT combination was the aluminum lattice (Figure 6.2d). Similar examination for the 5-pass deformed case was given in Figure 6.3. In the case of DCAPed sheet a complicated FFT was obtained (Figure 6.3b). This FFT was clearly divided into two (Figure 6.3c&e) and the corresponding inverse FFT images were created. According to the analysis the structure was composed of two types of lattices one cubic (most probably (141)) and the other was tetragonal. As a result; when annealed and deformed cases were compared; in the deformed one, a different second structural evolution at the lattice was observed. This finding was clear when FFTs were compared (Figure 6.2b & Figure 6.3b). But in HREM studies, there needs lots of data collection and many modeling studies in the atomic level. Hence all of the HREM analysis in the very beginning level has been forwarded as a future study. Lattice investigations and grain boundary engineering seems to be a critical corner in this type of severe plastic deformation processes and it might be a good topic for future.

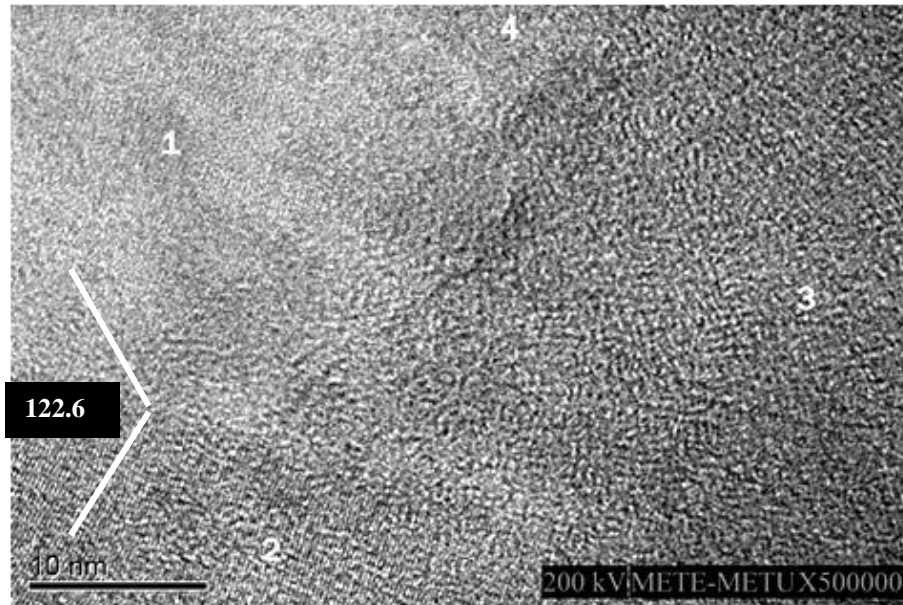


Figure 6.1 High resolution electron image of 5 pass DCAPed AA-6061 sheet

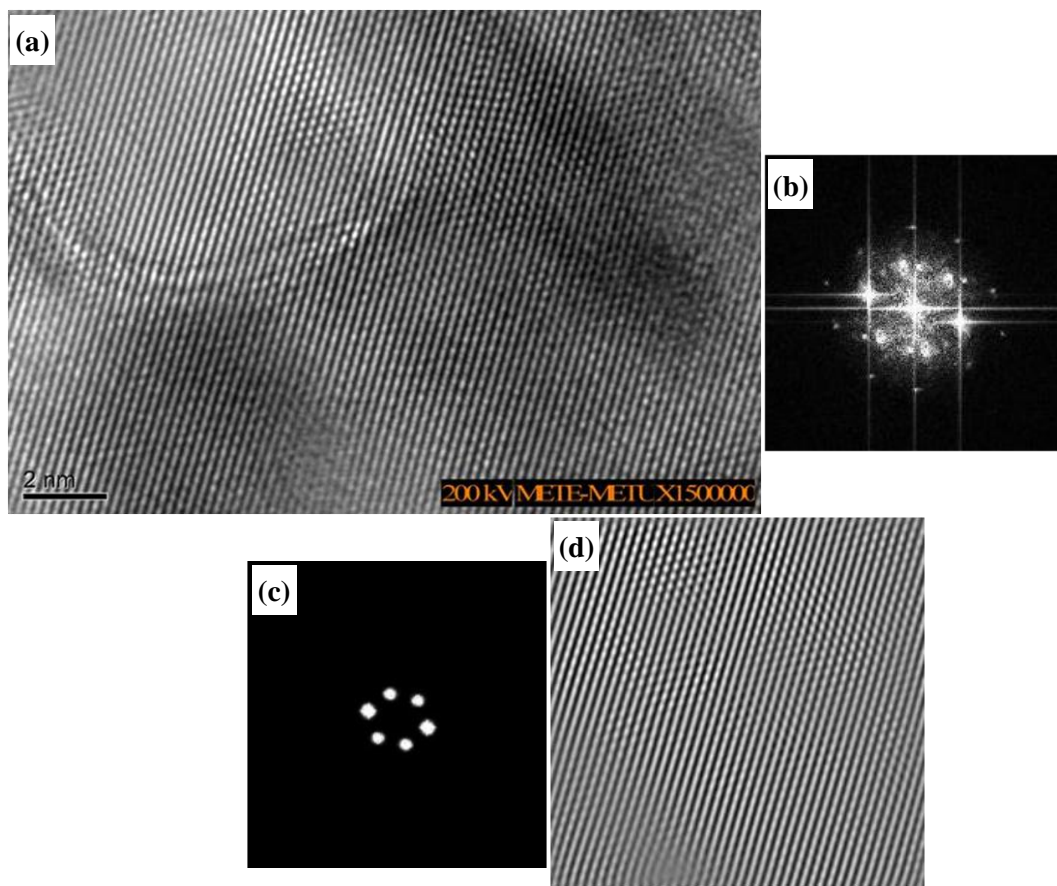


Figure 6.2 HREM investigation of annealed AA-6061 sheet (a) HREM image of annealed single grain, (b) FFT of grain, (c) filtered FFT, (d) Inverse FFT image (single crystal orientation was observed)

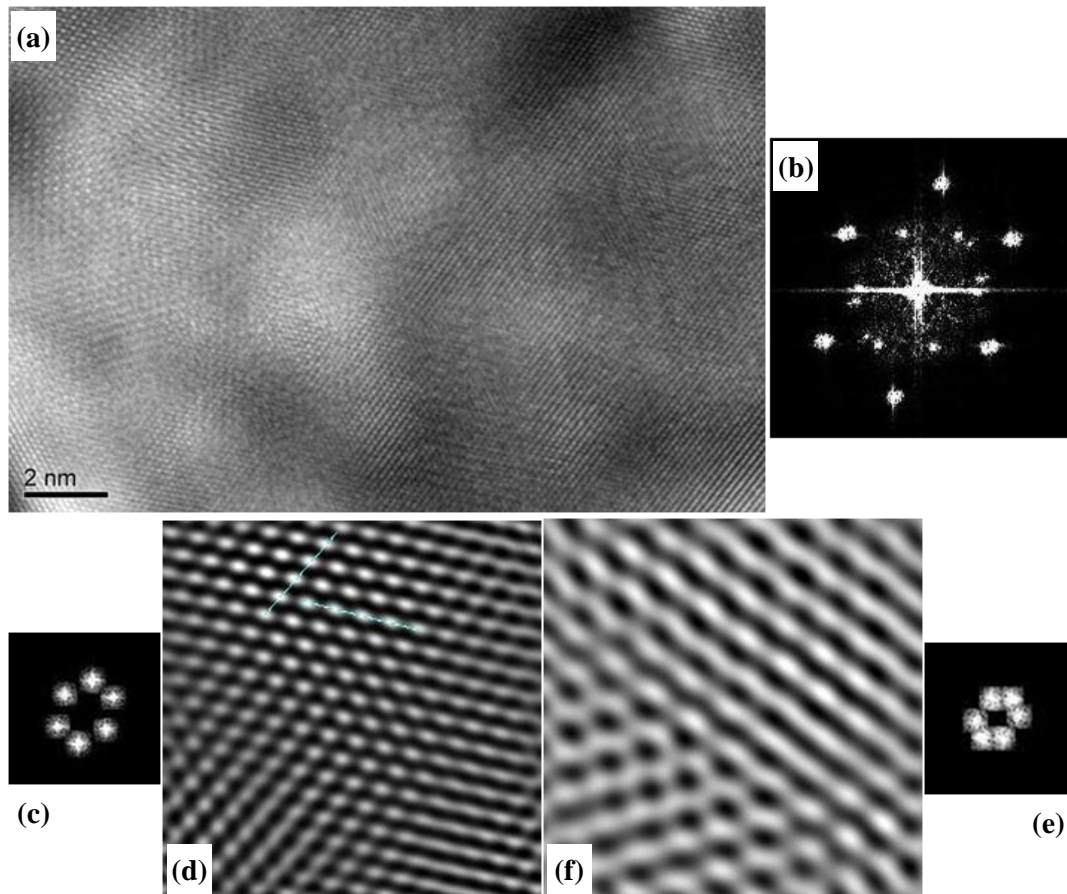


Figure 6.3 HREM investigation of 5 pass DCAPed AA-6061 sheet (a) HREM image of DCAPed single grain, (b) FFT of grain, (c) filtered FFT, (d) Inverse FFT image of c (cubic crystal probably (141)), (e) second filtered FFT, (f) Inverse FFT image of e (tetragonal crystal)

Another future work on the topic might be the effect of temperature on DCAP. The guide plate before the rollers could be replaced by a furnace to heat the samples to a predefined temperature just before SPD. The effect of dynamic recovery and recrystallization effects on the microstructural evolution could be checked. In the case of 6xxx series aluminum sheets combination of aging and deformation might also be challenging. Precipitate, dislocation interactions could be observed; precipitation kinetics might be obtained and compared with the ECAPed sample.

In the ECAP part of this study; a single pass ECAPed AA 2024 was evaluated. It was known that in a single pass; the final substructure size has been fixed; the stability

and texturing would be attained in the following passes. Hence it could be a good opportunity to observe the structural homogeneity in a single passed sample and its thermal stability at various temperatures.

REFERENCES

- 1** Altenpohl, Dietrich G., “Aluminum: Technology, Applications and Environment”, Aluminum Association, 1999.
- 2** Van Horn K. R., “Aluminum, Vol I. Properties, Physical Metallurgy and Phase Diagrams”, American Society for Metals, 1968.
- 3** ASM Specialty Handbook, “Aluminum and Aluminum Alloys”, Materials Information Society, 1996.
- 4** ASM Handbook, “Heat Treating of Aluminum Alloys, Vol 4”, ASM International, 1991.
- 5** De Graeve I. and Hirsch J.;Alumatter;
<http://aluminium.matter.org.uk/content/html/eng/default.asp?pageid=2144417057>.
- 6** Chakrabarti D.J., Peng Y.G., Laughlin D.E.; “Precipitation in Al-Mg-Si Alloys with Cu Additions and the Role of the Q’ and Related Phases”; Materials Science Forum; 396-4; 857-862; 2002.
- 7** Miao W.F., Laughlin D.E.; “Effect of Cu Content and Preaging on Precipitation Characteristics in Aluminum Alloy 6022”; Metallurgical and Materials Transactions A; 31A; 361-371; 2000.
- 8** Staab T.E.M., Krause-Rehberg R., Hornauer U., Zschech E.; “Study of Artificial Aging in AlMgSi (6061) and AlMgSiCu (6013) Alloys by Positron Annihilation”; Journal of Materials Science; 41; 1059-1066; 2006.
- 9** Munitz A., Cotler C., Talianker M.; “Aging Impact on Mechanical Properties and Microstructure of Al-6063”; Journal of Materials Science; 35; 2529-2538; 2000.
- 10** Verhoeven J.D.; “Fundamentals of Physical Metallurgy”; John Wiley & Sons; 1975.
- 11** Hertzberg R.W.; “Deformation and Fracture Mechanics of Engineering Materials”; John Wiley & Sons; 1996.
- 12** Slamova M., Ocenasek V. and Vander Voort G.; “Polarized Light Microscopy: Utilization in the Investigation of the Recrystallization of Aluminum Alloys”; Materials Characterization; 52; 165-177; 2004.

- 13** Starke Jr E.A.; “Encyclopedia of Materials: Science and Technology; Aluminum Alloys: Thermomechanical Processing”; Elsevier Science Ltd.; 118-121; 2001.
- 14** Waldman J., Sulinski H.V. and Markus H.; US Patent No. 3847681; 1974.
- 15** Paton N.E. and Hamilton C.H.; US Patent No. 4092181; 1978.
- 16** Furukawa M., Horita Z., Nemoto M., Langdon T.G.; Materials Science and Engineering; A324; 82–89; 2002.
- 17** Sharnrnazov A.M., Tsenev N.K., Valiev R.Z., Myshlyayev M.M., Bikbulatov, Lebedich S.P.; Physics of Metals and Metallography; 89; 314; 2000.
- 18** Yamashita A., Yamaguchi D., Horita Z., Langdon T.G.; Materials Science and Engineering; A287; 100–106; 2000.
- 19** Matsuki K., Aida T., Takeuchi T., Kusui J., Yokoe K.; Acta Materialia; 48; 2625–2632; 2000.
- 20** Pithan C., Hashimoto T., Kawazoe M., Nagahora J., Higashi K.; Materials Science and Engineering; A280; 62–68; 2000.
- 21** Horita Z., Fujinami T., Langdon T.G.; Materials Science and Engineering; A318; 34; 2001.
- 22** Mabuchi M., Ameyama K., Iwasaki H., Higashi K.; Acta Materialia; 47; 2024; 1999.
- 23** Komura S., Horita Z., Nemoto M., Langdon T.G.; Journal Material Research; 14; 4044; 1999.
- 24** Nakashima K, Horita Z, Nemoto M, Langdon T.G.; Acta Materialia; 46; 1589–1599; 1998
- 25** Nakashima K., Horita Z., Nemoto M., Langdon T.G.; Materials Science and Engineering; A281; 82–87; 2000.
- 26** Furukawa M., Iwahashi Y., Horita Z., Nemoto M., Langdon T.G.; Materials Science and Engineering; A257; 328–332; 1998.
- 27** Lee S., Furukawa M., Horita Z., Langdon T.G.; Materials Science and Engineering; A342; 294–301; 2003.
- 28** Moon B.S., Kim H.S., Hong S.I.; Scripta Materialia; 46; 131–136; 2002.

- 29** Baik S.C., Estrin Y., Kim H.S., Hellmig R.J.; *Materials Science and Engineering*; A351; 86–97; 2003.
- 30** Oh S.J., Kang S.B.; *Materials Science and Engineering*; A343; 107–115; 2003.
- 31** Mao J., Kang S.B., Park J.O.; *Journal of Materials Processing Technology*; 159; 314–320; 2005.
- 32** Kim W.J., Chung C.S., Ma D.S., Hong S.I., Kim H.K.; *Scripta Materialia*; 49; 333–338; 2003.
- 33** Zheng L.J., Chen C.Q., Zhou T.T., Liu P.Y., Zheng M.G.; *Materials Characterization*; 49; 455–461; 2003.
- 34** Horita Z., Fujinami T., Nemoto M., Langdon T.G.; *Journal of Materials Processing Technology*; 117; 288–292; 2001.
- 35** Zao Y.H., Liao X.Z., Jin Z., Valiev R.Z., Zhu Y.T.; *Acta Materialia*; 52; 4589–4599; 2004.
- 36** Xu C., Furukawa M., Horita Z., Langdon T.G.; *Acta Materialia*; 51; 6139–6149; 2003.
- 37** Xu C., Furukawa M., Horita Z., Langdon T.G.; *Acta Materialia*; 53; 749–758; 2005.
- 38** Chang S.Y., Lee K.S., Choi S.H., Shin D.H.; *Journal of Alloys and Compounds*; 354; 216–220; 2003.
- 39** Chang JY, Shan A; *Materials Science and Engineering*; A347; 165–170; 2003.
- 40** Chung C.S., Kim J.K., Kim H.K., Kim W.J.; *Materials Science and Engineering*; A337; 39–44; 2002.
- 41** Kim J.K., Jeong H.G., Hong S.I., Kim Y.S., Kim W.J.; *Scripta Materialia*; 45; 901–907; 2001.
- 42** Segal V.M.; *Materials Science and Engineering*; A197; 157–164; 1995.
- 43** Deformation Mechanics
http://en.wikipedia.org/wiki/File:2D_geometric_strain.svg
- 44** Iwahashi Y., Wang J., Horita Z., Nemoto M., Langdon T.G., *Principle of Equal-Channel Angular Pressing for the Processing of Ultra-Fine Grained Materials*, *Scripta Materialia*, 35, 143–6, 1996.

- 45** Horita Z., Smith D.J., Furukawa M., Nemoto M., Valiev R.Z., Langdon T.G.; *Materials Characterization*; 37; 285; 1996.
- 46** Valiev R.Z., Ivanisenko Y.V., Rauch E.F., Baudelet B.; *Acta Materialia*; 44; 4705; 1997.
- 47** Meyers M.A., Nesterenko V.F., LaSalvia J.C., Xue Q.; *Materials Science and Engineering*; A317; 204–225; 2001.
- 48** Mishra A., Richard V., Gregori F., Asaro R.J., Meyers M.A.; *Materials Science and Engineering*; A410–411; 290–298; 2005.
- 49** Raab G.J., Valiev R.Z., Lowe T.C., Zhue Y.T.; *Materials Science and Engineering*; A382; 30–34; 2004.
- 50** Saito Y., Utsunomiya H., Suzuki H., Sakai H.; *Scripta Materialia*; 42; 1139–1144; 2000.
- 51** Lee J.C., Seok H.K., Suh J.Y.; *Acta Materialia*; 50; 4005–4019; 2002.
- 52** Lee J.C., Seok H.K., Suh J.Y., Han J.H., Chung Y.H.; *Metallurgical and Materials Transactions*; A33; 665–673; 2002.
- 53** Lee J.C., Seok H.K., Han J.H., Chung Y.H.; *Materials Research Bulletin*; 36; 997–1004; 2001.
- 54** Nam C.Y., Han J.H., Chung Y.H., Shin M.C.; *Materials Science and Engineering*; A347; 253–257; 2003.
- 55** Han J.H., Suh J.Y., Oh K.H., Lee J.C.; *Materials Transactions*; 45; 1; 125–130; 2004.
- 56** Han J.H., Suh J.Y., Oh K.H., Lee J.C.; *Acta Materialia*; 52; 4907–4918; 2004.
- 57** Han J.H., Oh K.H., Lee J.C.; *Materials Science and Engineering*; A387–389; 240–243; 2004.
- 58** Han J.H., Yoon J.K., Park J.W., Oh K.H., Lee J.C.; *Materials Transactions*; 46; 1064–1069; 2005.
- 59** Han J.H., Huh M.Y., Suh J.Y., Lee J.C.; *Materials Science and Engineering*; A394; 60–65; 2005.
- 60** Han J.H., Suh J.Y., Jee K.K., Lee J.C.; *Materials Science and Engineering*; A477; 107–120; 2008.

- 61** Lee J.C., Suh J.Y., Ahn J.P.; Metallurgical and Materials Transactions; A34, 625–632; 2003.
- 62** Jining Q., Han J.H., Guoding Z., Lee J.C.; “Characteristic of textures evolution induced by equal channel angular pressing in 6061 aluminum sheets”; Scripta Materialia; 51; 185–189; 2004.
- 63** Suh J.Y.; Han J.H.; Oh K.H. Lee J.C.; “Effect of deformation histories on texture evolution during equal- and dissimilar-channel angular pressing; Scripta Materialia; 49 185–190; 2003.
- 64** Pei Q.X., Hu B.H., Lu C., Wang Y.Y., “A Finite Element Study of the Temperature Rise During Equal Channel Angular Pressing”, Scripta Materialia, 49, 303–8, 2003.
- 65** Gür C.H., Tan E. “Alüminyum Alaşımlarının Aşırı Plastik Deformasyon İşlemleriyle Üretilmesi” TUBİTAK Project No: 105M174 Final Report, 2008, METU, Ankara.
- 66** Uzunçakmak G.E.; “Design and Production of a DCAP System to Obtain High Strength 6061 Aluminum Alloy Sheets”, MSc Thesis, 2009, METU, Ankara.
- 67** Kibar A.A.; “Investigation of the Effect of Dissimilar Channel Angular Pressing Method to the Mechanical and Microstructural Properties of 6061 Aluminum Alloy Sheets”, MSc Thesis, 2010, METU, Ankara.
- 68** ASTM Standard, “B557M Tension Testing Wrought and Cast Aluminum and Magnesium-Alloy Products”, 2002.
- 69** Williamson G.K.and Hall W.H.;Acta Metall. 1, 22-31; 1953.
- 70** Karpuz P.; “Investigation of the Effects of Equal Channel Angular Extrusion on Light Weight Alloys”, PhD Thesis, 2012, METU, Ankara.
- 71** Saraloğlu E.; “Effect of ECAP and Subsequent Heat Treatments on Microstructure and Mechanical Properties of 2024 Aluminum Alloy”, MSc Thesis, 2008, METU, Ankara.
- 72** Saraloglu E., Tan E., Gur C.H.; “Effect of ECAP and Post-Aging Processes on 2024 Aluminum Alloy”; Steel Research International 79/2 467-471; 2008.
- 73** Cheng S., Zhao Y.H., Zhu Y.T., Ma E., Optimizing the Strength and Ductility of Fine Structured 2024 Al Alloy by Nano-precipitation, Acta Materialia, 55, 5822-32, 2007.

74 Tan E., Gür C.H.; “Influence of DCAP process on the Mechanical Properties of 6061 Al-Alloy Sheet”, *Reviews on Advanced Materials Science*, , vol.25, p.189–193; 2010.

75 Sha G., O’Reilly K., Cantor B., Worth J., Hamerton R.; “Growth Related Metastable Phase Selection in 6xxx Series Wrought Aluminum Alloy”; *Materials Science and Engineering A*; A304-306; 612-616; 2001.

76 Tan E.; “The Effect of Hot-Deformation on Mechanical Properties and Age Hardening Characteristics of Al-Mg-Si Based Wrought Aluminum Alloys”, MSc Thesis, 2006, METU, Ankara.

77 Tan E, Kibar AA, Gur CH; “Mechanical and Microstructural Characterization of 6061 Aluminum Alloy Strips Severely Deformed by Dissimilar Channel Angular Pressing”; *Materials Characterization* 62/4, , 391-397; 2011

78 Chang C.P., Sun P.L., Kao P.W., “Deformation induced grain boundaries in commercially pure aluminium”, *Acta Mater.* 48 3377-3385; 2000.

79 Broom T.; “The Effect of Temperature of Deformation on the Electrical Resistivity of Cold-worked Metals and Alloys”, *Proc. Phys. Soc.*, , B 65 p. 871–881; 1952.

VITA

EVREN TAN



PERSONAL INFORMATION

Marital Status : Single
Nationality : T.C.
Date / Place of Birth : 26.09.1981 ANKARA
E- mail : ewrentan@gmail.com
etan@metu.edu.tr
Phone (GSM) : 0 542 488 10 88
(ev) : 0 312 490 10 24

EDUCATION INFORMATION

PhD METU, Metallurgical and Materials Engineering Dept., ANKARA
December 2006 – CGPA: 3,79/4,00

MSc METU, Metallurgical and Materials Engineering Dept., ANKARA
September 2003 – 08.12.2006 CGPA: 3,93/4,00

BSc METU, Metallurgical and Materials Engineering Dept., ANKARA
September 1999 – 29.06.2003 CGPA: 3,52/4,00

HighSchool Çankaya Atatürk Anadolu Lisesi (Atatürk Lisesi), ANKARA
September 1 1992 – 25.06.1999 CGPA: 4,63/5,00

WORK HISTORY

October 2011 –..... Expert Material Design Engineer, ASELSAN, SST, Mechanical Design

December 2004 – September 2010 Research Assistant, METU METE
Electron Microscopes Responsible (sample prep, imaging, microanalysis)
Department Advertising Committee
Alumni Committee
Department Computer Admin
RA of Material Science and Eng lecture and laboratory

June 2002 – July 2002 TUBİTAK – SAGE, Summer Intern, Material Dept.

June 2001 – July 2001 ELROKSAN AŞ, Summer Intern, Mechanical Atelier

EXPERTIES

Structural Hardening, Materials and Metallurgical Technology, Heat Treatment, Forming Treatment, Aluminum and Alloys, Thermomechanical Treatment, Severe Plastic Deformation

Scanning Electron Microscope (SEM) Operator till January 2005
Transmission Electron Microscope (TEM) Operator till April 2009
EBSD attached FEG-SEM Operator till June 2009
X-ray Diffractometer user till 2009

PAPERS IN JOURNALS (SCI/SCIE)

#	PUBLICATION
4	Homogenization of ECAPED Al 2024 Alloy Through Age Hardening Kotan G, Tan E, Kalay YE, Gur CH MATERIALS SCIENCE AND ENG A (Accepted, August 2012)
3	Mechanical and Microstructural Characterization of 6061 Aluminum Alloy Strips Severely Deformed by Dissimilar Channel Angular Pressing Tan E, Kibar AA, Gur CH MATERIALS CHARACTERIZATION 62/4 391-397 (April 2011)
2	INFLUENCE OF DCAP PROCESS ON THE MECHANICAL PROPERTIES OF 6061 Al-ALLOY SHEET Tan E, Gur CH REVIEWS ON ADVANCED MATERIALS SCIENCE 25/2 189-193 (AUG 2010)
1	EFFECT OF ECAP AND POST-AGING PROCESSES ON 2024 ALUMINUM ALLOY Saraloglu E, Tan E, Gur CH STEEL RESEARCH INTERNATIONAL 79/2 467-471 (2008)

OTHER JOURNAL PAPERS

	PUBLICATION	TYPE
2	Aşırı Plastik Deformasyon ve Çökelme Sertleşmesi İşlemlerinin 2024 Alüminyum Alaşımının Özelliklerine Etkisi Tan E, Saraloglu E, Gur CH Metalurji, 155, 33-41, (2010)	TR
1	Influence of Heat Treatment on the Mechanical Properties of AA6066 Alloy Tan E, Ogel B Turkish J. Eng. Env. Sci., 31, 53-60 (2007)	ENG

CONFERENCE PAPERS /ACTIVITIES

	TITLE	CONF	LANG.
13	Investigation of the Precipitation Mechanism in the Severely Deformed and Aged 2024 Al-Alloy Kotan G, Tan E, Kalay YE, Gur CH	16th Int Metallurgy-Materials Cong. 13-15 Sep 2012 İstanbul	ENG
12	Effect of Post ECAP Aging on the Thermal Stability and Subgrain Structure of 2024 Al-Alloy Kotan G, Tan E, Kalay YE, Gur CH (ORAL)	3rd Int. Symp. Bulk Nanostructured Materials (BNM2011) 22-26 Sep 2009 Ufa-Russia	ENG
11	The Investigation of Inhomogeneity in Single Pass ECAP Through Post-ECAP Aging of Al 2024 Kotan G, Tan E, Kalay YE, Gur CH (POSTER)	3rd Int. Symp. Bulk Nanostructured Materials (BNM2011) 22-26 Sep 2009 Ufa-Russia	ENG
10	Investigating the Mcrostructure of Hot Pressed SiC Reinforced AlCu and AlSi Alloy Composites by Ultrasonic Technique Tan E, Gur CH, Simon A, Gacsi Z	6th International Powder Metallurgy Conference 05-09 Oct 2011 Ankara	ENG
9	Severe Plastic Deformation of AL-6061 Sheets by Dissimilar Channel Angular Pressing Tan E, Kibar AA, Gur CH	15th Int Metallurgy-Materials Cong. 11-13 Nov 2010 İstanbul	TR
8	Investigating the Correlation between the Porosity, Wear Resistance and the Production Method of Al-SiCp Composites Simon A, Tan E, Gur CH, Pieczonka T, Gacsi Z	15th Int Metallurgy-Materials Cong. 283-289 11-13 Nov 2010 İstanbul	ENG
7	Improving the Strength of 6061 Aluminum Alloy Thin Sheets by Severe Plastic Deformation Kibar AA, Uzunçakmak GE, Tan E, Gur CH	4th Aluminyum Symp. 15-16 Oct 2009 İstanbul	TR
6	Microstructural Characterization of SiC Reinforced Aluminum Matrix Composites Makszimus A, Gacsi Z, Pieczonka T, Gur H, Tan E	EURO PM2009 Proceedings Vol. 3, pp 335-340 12-14 Oct 2009 Copenhagen-Denmark	ENG
5	Influence Of Dcap Process On The Mechanical Properties Of 6061 Al-Alloy Sheet Tan E, Gur CH	2nd Int. Symp. Bulk Nanostructured Materials (BNM2009) 22-26 Sep 2009	ENG

		Ufa-Russia	
4	Effect of Dcap on the Mechanical Properties of 6061 Al-Alloy Strips Uzunçakmak G, Tan E, Gur CH	14th Int Metallurgy- Materials Cong. 16-18 Oct 2008 İstanbul	TR
3	Effect of Ecap and Subsequent Aging on the Mechanical Properties of 2024 Al-Alloy Saraloglu E, Tan E, Gur CH	14th Int Metallurgy- Materials Cong. 16-18 Oct 2008 İstanbul	TR
2	Effect of ECAP and Post-aging Processes on 2024 Aluminum Alloy Saraloglu E, Tan E, Gur CH	12th International Metalforming Conf. (METALFORMING20 08) 21-24 Sep 2008 Krakow-Poland	ENG
1	Comparison of the Microstructure and the Mechanical Properties of Hot and Cold Pressed Al-SiCp Composites Maksimus A, Gur CH, Pieczonka T, Tan E, Gacsi Z	5th International Powder Metallurgy Conference 8-12 Oct 2008 Ankara	ENG